A patterned human neural tube model using microfluidic gradients

https://doi.org/10.1038/s41586-024-07204-7

Received: 26 January 2022

Accepted: 16 February 2024

Published online: 26 February 2024

Check for updates

Xufeng Xue[1], Yung Su Kim[1], Alfredo-Isaac Ponce-Arias[2,3], Richard O'Laughlin[4], Robin Zhexuan Yan[1], Norio Kobayashi[1], Rami Yair Tshuva[2,3], Yu-Hwai Tsai[5], Shiyu Sun[1], Yi Zheng[1], Yue Liu[1], Frederick C. K. Wong[6], Azim Surani[6,7], Jason R. Spence[5,8,9], Hongjun Song[4,10,11,12], Guo-Li Ming[4,10,11,13], Orly Reiner[2,3] & Jianping Fu[1,8,9] ✉

The human nervous system is a highly complex but organized organ. The foundation of its complexity and organization is laid down during regional patterning of the neural tube, the embryonic precursor to the human nervous system. Historically, studies of neural tube patterning have relied on animal models to uncover underlying principles. Recently, models of neurodevelopment based on human pluripotent stem cells, including neural organoids[1–5] and bioengineered neural tube development models[6–10], have emerged. However, such models fail to recapitulate neural patterning along both rostral–caudal and dorsal–ventral axes in a three-dimensional tubular geometry, a hallmark of neural tube development. Here we report a human pluripotent stem cell-based, microfluidic neural tube-like structure, the development of which recapitulates several crucial aspects of neural patterning in brain and spinal cord regions and along rostral–caudal and dorsal–ventral axes. This structure was utilized for studying neuronal lineage development, which revealed pre-patterning of axial identities of neural crest progenitors and functional roles of neuromesodermal progenitors and the caudal gene *CDX2* in spinal cord and trunk neural crest development. We further developed dorsal–ventral patterned microfluidic forebrain-like structures with spatially segregated dorsal and ventral regions and layered apicobasal cellular organizations that mimic development of the human forebrain pallium and subpallium, respectively. Together, these microfluidics-based neurodevelopment models provide three-dimensional lumenal tissue architectures with in vivo-like spatiotemporal cell differentiation and organization, which will facilitate the study of human neurodevelopment and disease.

Patterning of the neural tube (NT) along the rostral–caudal (R–C) axis establishes the following main subdivisions of the nervous system: the forebrain (FB), the midbrain (MB), the hindbrain (HB) and the spinal cord (SC) (Fig. 1a). During human NT development, neuropores close by Carnegie stage 12 (CS12), which results in a completely closed NT[11]. At CS12, the NT has an R–C length of about 4 mm, with a height of about 200 μm defined by the SC along the dorsal–ventral (D–V) axis[11] (Extended Data Fig. 1a). Classical embryology studies have shown that C-to-R gradients of caudalizing signals, including fibroblast growth factors (FGFs)[12], retinoic acid (RA)[13] and WNTs[14], act synergistically for R–C patterning of the NT.

To develop a microfluidic NT-like structure (μNTLS), we exploited microcontact printing to print an array of Geltrex adhesive islands to guide the formation of human pluripotent stem (PS) cell colonies with prescribed tubular geometries (Extended Data Fig. 1b–e, Methods and Supplementary Note). Geltrex was chosen because of its enrichment for basement membrane proteins surrounding the NT[15]. Positions of human PS cell colonies were aligned with the patterning region inside the central channel of a microfluidic device (Extended Data Fig. 1b,e and Supplementary Note). Controllable chemical gradients were established inside the patterning region of the microfluidic device along the length (designated as the R–C axis) or width (designated as the D–V axis) of human PS cell colonies (Supplementary Fig. 1). Morphogen diffusion in the patterning region was assessed on the basis of passive diffusion of fluorescent dextran as a proxy, which confirmed the establishment of stable chemical gradients (Supplementary Fig. 1).

[1]Department of Mechanical Engineering, University of Michigan, Ann Arbor, MI, USA. [2]Department of Molecular Genetics, Weizmann Institute of Science, Rehovot, Israel. [3]Department of Molecular Neuroscience, Weizmann Institute of Science, Rehovot, Israel. [4]Department of Neuroscience and Mahoney Institute for Neurosciences, Perelman School of Medicine, University of Pennsylvania, Philadelphia, PA, USA. [5]Department of Internal Medicine, Division of Gastroenterology, University of Michigan Medical School, Ann Arbor, MI, USA. [6]Wellcome Trust/Cancer Research UK Gurdon Institute, University of Cambridge, Cambridge, UK. [7]Department of Physiology, Development and Neuroscience, University of Cambridge, Cambridge, UK. [8]Department of Cell and Developmental Biology, University of Michigan Medical School, Ann Arbor, MI, USA. [9]Department of Biomedical Engineering, University of Michigan, Ann Arbor, MI, USA. [10]Department of Cell and Developmental Biology, Perelman School of Medicine, University of Pennsylvania, Philadelphia, PA, USA. [11]Institute for Regenerative Medicine, University of Pennsylvania, Philadelphia, PA, USA. [12]The Epigenetics Institute, Perelman School of Medicine, University of Pennsylvania, Philadelphia, PA, USA. [13]Department of Psychiatry, Perelman School of Medicine, University of Pennsylvania, Philadelphia, PA, USA. ✉e-mail: jpfu@umich.edu

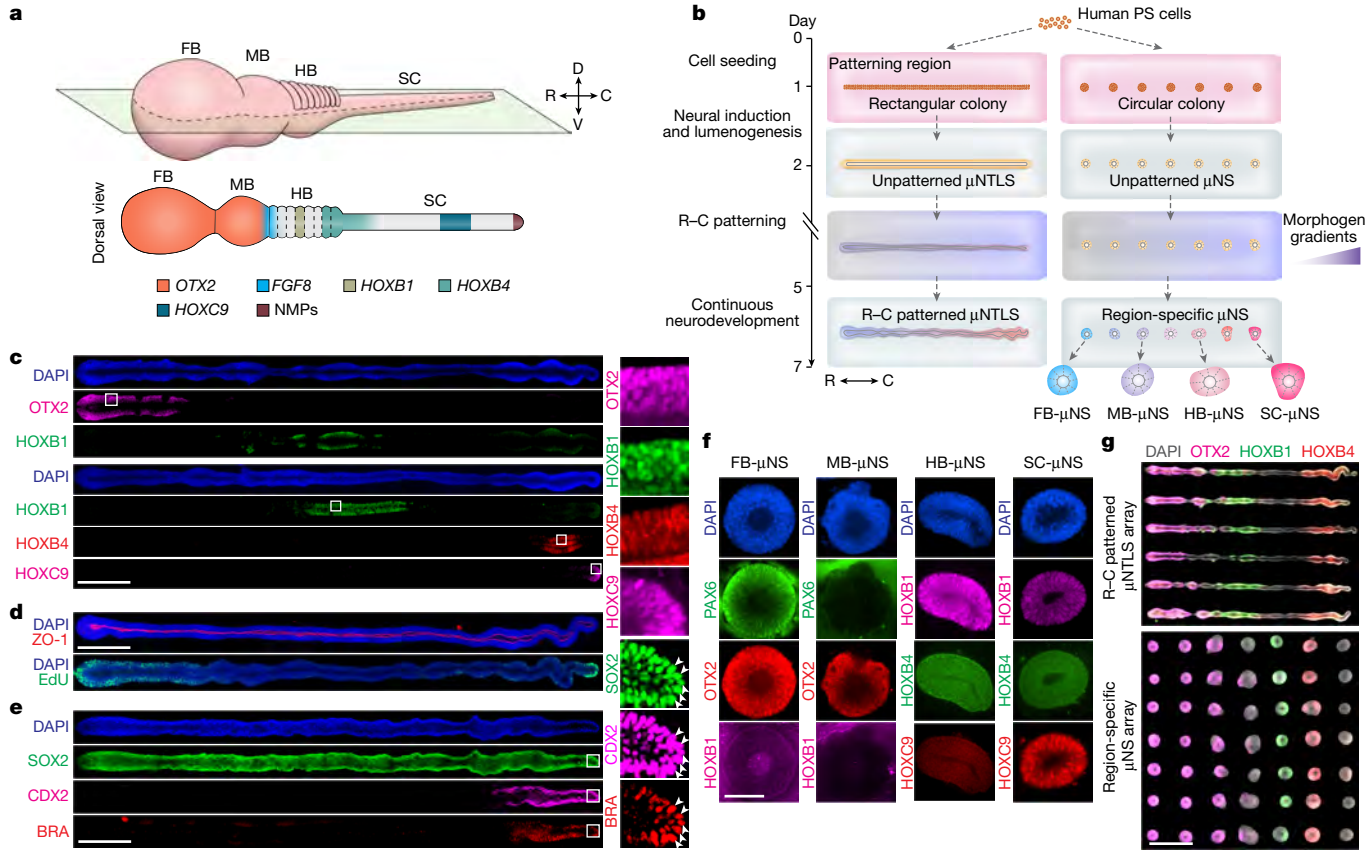

Fig. 1 | An R–C patterned human NT model using microfluidics. a, A 3D and dorsal view of the human NT in vivo patterned along the R–C axis into the FB, MB, HB and SC. NMPs develop at the SC caudal end. Regionalization of the NT leads to patterned gene expression, with upregulated *OTX2* expression in the FB and MB, *FGF8* at the MB–HB boundary and HOX family genes in the HB and SC as indicated. **b**, Schematic of microfluidics protocols for generating R–C patterned µNTLS and region-specific µNS. Human PS cells form tubular or spherical tissues that enclose a single lumen in the patterning region of a microfluidic device and further develop into R–C patterned µNTLS or region-specific µNS, respectively, when exposed to C-to-R gradients of caudalizing signals. See Methods for details. **c**, Left, stitched confocal micrographs showing R–C patterned µNTLS on day 7 immunostained for OTX2, HOXB1, HOXB4 and HOXC9 as indicated. Right, zoom-in views of the boxed regions as indicated. **d**, Stitched confocal micrographs showing R–C patterned µNTLS on day 7, with ZO-1 and EdU staining. **e**, Left, stitched confocal micrographs showing R–C patterned µNTLS on day 4 immunostained for SOX2, CDX2 and BRA. Right, zoom-in views of boxed regions as indicated. $SOX2^+CDX2^+BRA^+$ cells are marked by arrowheads. **f**, Confocal micrographs showing µNS on day 7 immunostained for PAX6, OTX2, HOXB1, HOXB4 and HOXC9 as indicated. **g**, Stitched confocal micrographs showing an array of R–C patterned µNTLS on day 7 from a single microfluidic device (top) and an array of region-specific µNS on day 7 from another device (bottom), both stained for OTX2, HOXB1 and HOXB4. In **c**–**g**, nuclei were counterstained with DAPI. Experiments were repeated three times with similar results. Scale bars, 200 µm (**f**), 400 µm (**c**–**e**) or 800 µm (**g**).

R–C patterned µNTLS

We first sought to develop R–C patterned µNTLS. Single human embryonic stem (ES) cells (from the H9 line) loaded into the central channel on day 0 only attached to Geltrex islands, which then formed rectangular cell colonies (4 mm × 100 µm) with an overall size comparable to that of CS12 human NT (Fig. 1b and Extended Data Fig. 1e). To promote µNTLS formation, a Geltrex solution was loaded into the central channel on day 1. Neural induction medium was added into the two medium reservoirs of the central channel on the same day[16,17] (Extended Data Fig. 1e,f). Colonies of human ES cells self-organized and underwent lumenogenesis in a synchronized manner, with small ZO-1$^+$ apical lumens emerging on day 2 along the R–C axis (Extended Data Fig. 1e,g and Supplementary Video 1). Lumens grew over time and coalesced with each other (Supplementary Video 1). By day 3, each human ES cell colony, although still expressing OCT4, developed into an elongated tubular structure that contained a single continuous apical lumen (Extended Data Fig. 1e). For R–C patterning of µNTLS, CHIR99021 (a WNT pathway activator), FGF8 and RA were supplemented into the right-side reservoir of the central channel from day 2 to day 5, which established C-to-R gradients of these signals in the patterning region (Fig. 1b and Extended Data Fig. 1f). On day 7, spatially ordered expression of OTX2 (a FB and MB marker), HOXB1 (a HB marker), HOXB4 (a HB and SC marker) and HOXC9 (a SC marker) was evident, with OTX2 expression restricted to rostral µNTLS, followed by patterned expression domains of HOXB1, HOXB4 and HOXC9 in a R-to-C order (Fig. 1c and Extended Data Fig. 1h,i). R–C patterned µNTLS on day 7 showed cell proliferation most notably at rostral and caudal regions (Fig. 1d and Supplementary Fig. 2a). By contrast, µNTLS without exposure to caudalizing signal gradients showed uniform OTX2 expression, supporting a default FB identity, and similar cell proliferation along the entire R–C axis (Extended Data Fig. 1j). This result suggests that regional identity-associated mechanisms have a role in the regulation of cell proliferation.

R–C patterned µNTLS on day 7 enclosed a single lumen demarcated by ZO-1 expression at its apical surface (Fig. 1d and Extended Data Fig. 1k), which mimicked the neural canal. Immunofluorescence analysis supported the presence of primary cilia at the µNTLS apical surface and interkinetic nuclear migration in the µNTLS (Extended Data Fig. 1k). No notable cell death was observed in day 7 µNTLS (Supplementary Fig. 2b).

To further examine R–C patterning of μNTLS, μNTLS on day 7 was cut into 4 even segments along the R–C axis (regions 1–4 in an R-to-C order; Extended Data Fig. 1l). Quantitative PCR with reverse transcription (RT–qPCR) analysis of these segments confirmed patterned expression of *HOX1–HOX9* along the R–C axis of day 7 μNTLS and the consistency of such patterns with the 3′-to-5′ orders of the HOX family of genes along the chromosomes[18] (Extended Data Fig. 1m,n). Expression of *HOX10–HOX13* was not detected (Extended Data Fig. 1n), which suggested that the caudal-most regions of μNTLS had a thoracic SC identity.

The effects of WNT, FGF8 and RA signals on R–C patterning of μNTLS were examined by modulating their doses (Extended Data Fig. 2) or inhibiting their activities using pharmacological drugs (Supplementary Fig. 3). The results revealed that WNT was the most essential for caudalizing μNTLS, and RA and FGF8 mainly affected rostral and caudal HOX gene expression, respectively (Supplementary Note).

We next tracked the dynamics of μNTLS patterning (Extended Data Fig. 3). R–C patterning of μNTLS emerged on day 3, before neural conversion completion around day 5 (Extended Data Fig. 3a,b and Supplementary Note), a result consistent with recent findings[19]. Dynamic patterning of HOXB1$^+$ and HOXC9$^+$ domains in μNTLS was consistent with their initiation, expansion and regression in vivo[20,21] (Extended Data Fig. 3a,d and Supplementary Note). However, in μNTLS, HOXB4$^+$ cells appeared later than HOXB9$^+$ cells (Extended Data Fig. 3a,d). With high doses of RA, the co-linearity of HOX genes exhibited in vivo[18] was recapitulated in μNTLS (Extended Data Fig. 3c,d). This observation is consistent with the effect of RA on inducing rostral HOX gene expression and suggests that dynamics of different HOX gene expression might depend on specific morphogen signals and their concentrations, a topic that warrants future investigation.

To examine the role of cell migration in R–C patterning of μNTLS, clonal growths of single H2B–GFP human ES cells spiked in μNTLS were tracked over several days. The centre of mass of H2B–GFP human ES cell colonies did not appreciably shift (Supplementary Fig. 4 and Supplementary Video 2), a result consistent with limited cell migration during NT patterning in vivo[22].

The R–C patterning of μNTLS was highly efficient and reproducible, with a success rate of 90.9 ± 3.7% (mean ± s.e.m.) using multiple human PS cell lines, including a human induced pluripotent stem (iPS) cell line (Supplementary Fig. 5; see Methods for criteria used for identifying successful R–C patterning of μNTLS).

Neuromesodermal progenitors and secondary organizers

In mice, neuromesodermal progenitors (NMPs) emerge at the caudal tailbud on embryonic days 8 to 8.5 (E8–E8.5)[23] (Fig. 1a). NMPs are bipotent and give rise to both SC and paraxial mesoderm derivatives[24,25]. We therefore asked whether NMPs would develop in μNTLS. Putative SOX2$^+$ Brachyury (BRA)-positive NMPs appeared transiently at the μNTLS caudal end from day 3 to day 5 and became undetectable on day 6 (Fig. 1e and Extended Data Fig. 4a,b). These NMPs also expressed CDX2, a caudal marker (Fig. 1e and Extended Data Fig. 4a,b). The transient emergence of NMPs at the μNTLS caudal end was confirmed using a BRA–mNeonGreen human ES cell reporter line (Extended Data Fig. 4c and Supplementary Video 3). Inhibiting either WNT or FGF activity, but not RA activity, blocked NMP development in μNTLS (Supplementary Fig. 3a,c). Caudal-most regions of day 4 μNTLS were able to differentiate into presomitic mesoderm cells[26] or motor neuron progenitors[27] under suitable conditions (Extended Data Fig. 4d–f), supporting the presence of bipotent NMPs in caudal μNTLS.

We further developed a *TBXT*::T2A-Cre lineage tracing human ES cell line to track NMP progenies in μNTLS (Extended Data Fig. 4g,h). Live imaging confirmed NMP progenies at μNTLS caudal ends (Extended Data Fig. 4i and Supplementary Video 4). NMP progenies expanded over time and contributed to HOXC9$^+$ thoracic SC region development (Extended Data Fig. 4i–k and Supplementary Video 4).

Coarse segmental organization of the FB, MB, HB and SC in the NT is followed by progressively refined patterning through formations and activities of secondary organizers, including isthmic organizer (IsO) at the MB–HB boundary[28] (Fig. 1a). RA signalling also has an important role in patterning the HB and the rostral SC, where the greatest RA signalling is located[29,30]. Notably, RT–qPCR analysis of dissected μNTLS segments revealed increased expression of several key IsO markers, including *WNT1*, *FGF8* and *EN1/2*, in regions 2–3, flanked by expression peaks of the FB and MB marker *OTX2* in region 1 and the HB marker *GBX2* in region 3 (Extended Data Fig. 4l,m). This result indicated the presence of an IsO-like domain in μNTLS. Furthermore, RT–qPCR analysis of genes associated with RA synthesis and degradation and RA target genes consistently showed the highest endogenous RA signalling activities in region 3, the μNTLS region that was associated with a putative HB identity (Extended Data Fig. 4m).

In mice, *Cdx2* and *Tbxt* (which encodes Brachyury) interact with WNT and FGF signalling to regulate axial elongation and posterior patterning[31,32]. R–C patterned μNTLS generated from *CDX2* knockout (KO) human ES cells showed few SOX2$^+$BRA$^+$ NMPs at caudal ends on day 4 (Extended Data Fig. 5a,c). Instead of HOXC9$^+$ thoracic SC-like cells, caudal μNTLS on day 7 contained HOXB4$^+$ cells with a caudal HB or rostral SC identity (Extended Data Fig. 5b,c). *CDX2* KO μNTLS further showed decreased contour lengths and defective clonal expansion at their caudal regions (Extended Data Fig. 5d–f). These results indicated defective axial elongation and were consistent with the posterior truncation and disrupted axial patterning observed in *Cdx2* mutant mice[31,32]. Notably, *TBXT* KO did not affect CDX2 expression in caudal μNTLS; nonetheless, *TBXT* KO resulted in fewer HOXC9$^+$ thoracic SC-like cells in caudal μNTLS (Extended Data Fig. 5g–i).

Region-specific neural spheroids

The microfluidic platform can be adapted to generate region-specific, microfluidic neural spheroids (μNS). To this end, an array of circular human ES cell colonies was formed in the patterning region and cultured under a R–C patterning condition with C-to-R gradients of CHIR99021, FGF8 and RA (Fig. 1b and Extended Data Fig. 6a,b). Similar to μNTLS development, as they underwent neural conversion, circular human ES cell colonies self-organized and formed lumenal spheroids (Extended Data Fig. 6b). Based on expression of OTX2, PAX6 (a marker expressed in dorsal FB, HB and SC, but not in MB) and HOX genes, μNS with FB (PAX6$^+$OTX2$^+$), MB (PAX6$^-$OTX2$^+$), HB (HOXB1$^+$), and SC (HOXC9$^+$) identities were developed in prescribed positions in a R-to-C order within the patterning region (Fig. 1f,g and Extended Data Fig. 6c,d).

R–C and D–V patterned μNTLS

D–V patterning of the NT is mediated by morphogen signals secreted from two organizer regions that extend along dorsal and ventral midlines of the embryo: dorsal non-neural ectoderm and roof plate (RP) transmitting BMP[33] and WNT[34] signals, and ventral notochord and floor plate (FP) emanating Sonic hedgehog (SHH)[35]. RA secreted from paraxial mesoderm also has a role in ventralizing the NT[36]. Under these antiparallel morphogen gradients, the FB is partitioned into pallium and subpallium domains along the D–V axis[37]. By contrast, the SC is divided into 11 discrete neural progenitor domains along the D–V axis in addition to the RP and the FP[38] (Fig. 2a). D–V patterning of the NT also leads to migratory neural crest (NC) cells delaminating from the dorsal NT, which give rise to many derivatives, including mesenchymal cells, neurons and glia[39] (Fig. 2a).

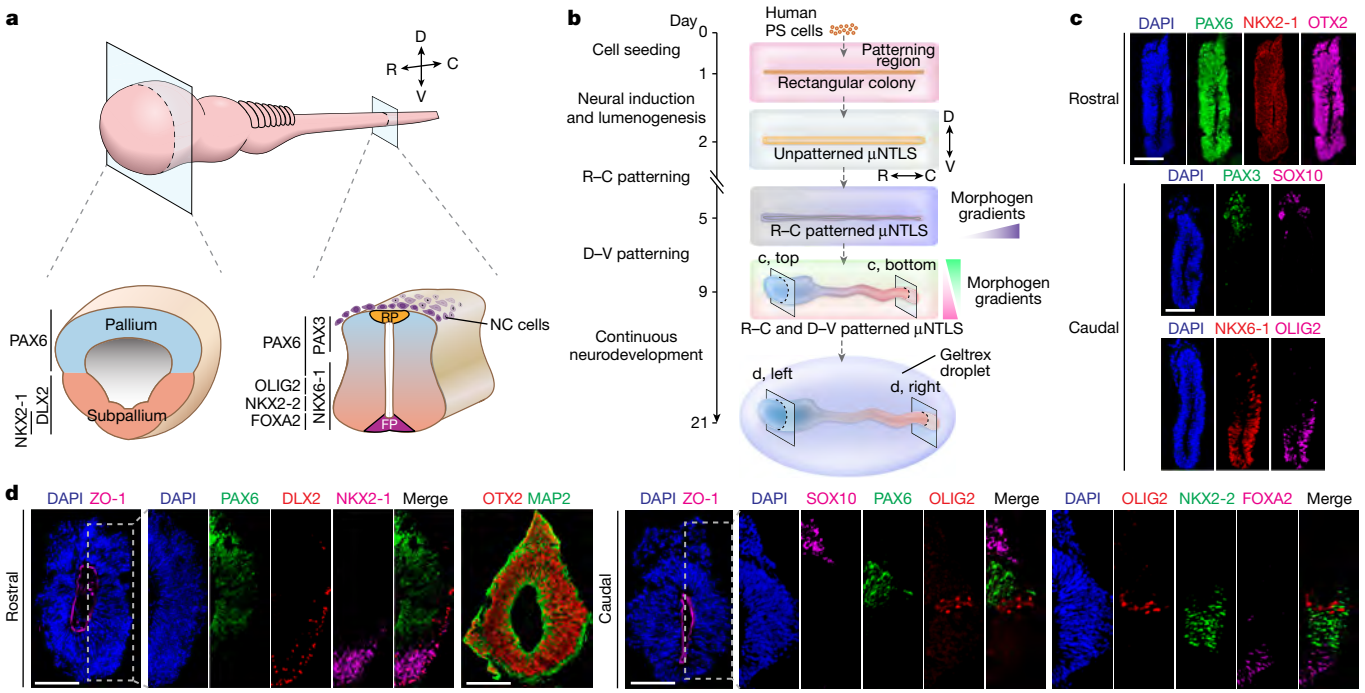

Fig. 2 | R–C and D–V patterning of μNTLS. a, Transverse sections of the FB and the SC in vivo as indicated. D–V patterning of the FB leads to the formation of the pallium and the subpallium. D–V patterning of the SC results in the development of NC cells delaminating from the dorsal SC and the emergence of discrete, non-overlapping progenitor domains along the D–V axis, including the RP and the FP at dorsal and ventral poles, respectively. Different progenitor domains in the FB and SC express distinct combinations of transcription factors as indicated. **b**, Schematic of the microfluidics protocol for generating R–C and D–V patterned μNTLS. After R–C patterning between day 2 and day 5, μNTLS are continuously cultured in the microfluidic patterning region until day 9, exposed to antiparallel gradients of dorsalizing and ventralizing signals established along the width (D–V axis) of the microfluidic patterning region. From day 9 to day 21, μNTLS are released from the device and embedded in Geltrex droplets. Transverse sections of rostral and caudal regions of μNTLS on day 9 and day 21 were analysed using immunocytochemistry as indicated. **c**, Representative confocal micrographs showing transverse sections of rostral (top) and caudal (bottom) regions of R–C and D–V patterned μNTLS on day 9, stained for indicated markers. **d**, Representative confocal micrographs showing transverse sections of rostral (left) and caudal (right) regions of R–C and D–V patterned μNTLS on day 21, stained for indicated markers. Zoom-in views of boxed regions are shown on the right. In **c** and **d**, nuclei were counterstained with DAPI. Experiments were repeated three time with similar results. Scale bars, 100 μm (**c**,**d**).

To achieve a R–C and D–V patterned NT model, a single μNTLS was generated at the centre of the microfluidic patterning region (Extended Data Fig. 7a). Following R–C patterning from day 2 to day 5, μNTLS was exposed to antiparallel gradients of BMP4 versus RA and SHH along the D–V axis (Fig. 2b and Extended Data Fig. 7a). Notably, rostral μNTLS expanded rapidly from day 5 onwards, which led to an increased projected area and greater cell numbers in rostral ends, mimicking the rapid growth of primary brain vesicles (Extended Data Fig. 7b, Supplementary Fig. 6 and Supplementary Video 5). R–C patterning of μNTLS remained evident, with spatial expression domains of OTX2, HOXB1, HOXB4 and HOXC9 in a R-to-C order on day 9 (Extended Data Fig. 7c). Dextran diffusion assays confirmed the establishment of stable chemical gradients along the D–V axis in the patterning region during D–V patterning of μNTLS (Supplementary Fig. 1c,d).

To discern D–V pattering of μNTLS, transverse slices of μNTLS were examined. On day 9, all cells in rostral μNTLS expressed OTX2 and PAX6 (a pallium marker) but not NKX2-1 (a ventral subpallium marker; Fig. 2c). However, caudal μNTLS displayed essential features of D–V patterning in the SC, with SOX10$^+$ NC cells delaminating from the dorsal pole, PAX3$^+$ dorsal NT cells in dorsal regions and NKX6-1$^+$ ventral NT cells and OLIG2$^+$ motor neuron progenitor (pMN) cells in ventral domains (Fig. 2c and Extended Data Fig. 7d). NKX2-2 and FOXA2, two additional markers of the ventral SC, were not detectable in caudal μNTLS on day 9 (Extended Data Fig. 7d).

R–C and D–V patterned μNTLS on day 9 showed a success rate of 86.03 ± 2.93% and were generated from multiple human PS cell lines, including a human iPS cell line (Supplementary Fig. 7; see Methods for criteria used for identifying successful R–C and D–V patterning of μNTLS).

We further prolonged μNTLS development by releasing them from the microfluidic device on day 9 before culturing them in Geltrex droplets until day 21 under a neurodevelopment condition (Fig. 2b and Methods). Between day 9 and day 21, μNTLS grew continuously, with expansion of rostral μNTLS regions most notable (Extended Data Fig. 7b). On day 21, the apical lumen of μNTLS remained open (Fig. 2d and Extended Data Fig. 7e). Notably, rostral and caudal μNTLS exhibited spatially ordered gene expression consistent with D–V regionalization of the FB and SC, respectively. In rostral μNTLS, PAX6$^+$ pallium domain became restricted in dorsal regions, and DLX2$^+$ subpallium domains and NKX2-1$^+$ ventral-most subpallium areas appeared in ventral areas (Fig. 2d and Extended Data Fig. 7f). The post-mitotic neuron marker MAP2 was detectable at basal surfaces of μNTLS, which provided evidence of active neurogenesis in μNTLS (Fig. 2d). Caudal μNTLS also showed distinct neural progenitor domains along the D–V axis on day 21, with SOX10$^+$ NC cells delaminating from dorsal sides, PAX6$^+$ dorsal domains in dorsal regions and discrete OLIG2$^+$ pMN, NKX2-2$^+$ p3 and FOXA2$^+$ FP domains in ventral regions (Fig. 2d and Extended Data Fig. 7f). Thus, the FP and p3 progenitor cells develop later than pMN cells in μNTLS, a finding consistent with data from mouse SC[40]. D–V patterning of μNTLS depended on dosages of exogenous morphogens, with increased RA and SHH signals leading to dorsal expansion of ventral domains, results consistent with in vivo[35] and in vitro[8] findings (Extended Data Fig. 7f).

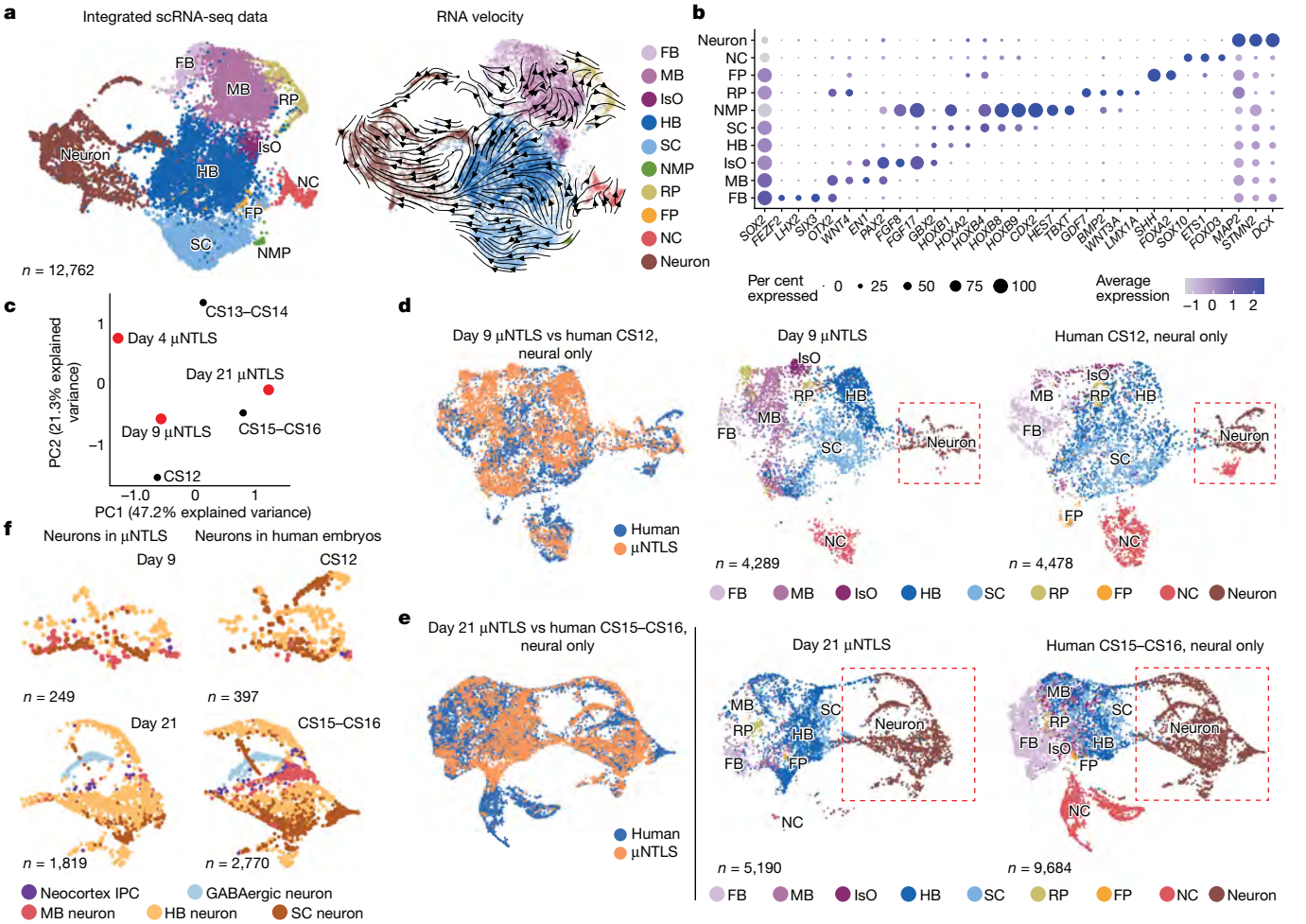

Fig. 3 | Single-cell transcriptome analysis of μNTLS. a, Left, UMAP of integrated single-cell transcriptome datasets of μNTLS on day 4, day 9 and day 21, colour-coded according to cell identity annotations. Right, RNA velocity vectors projected onto UMAP-based embeddings show major cell progression directions in transcriptional space. **b**, Dot plot showing the expression of key marker genes across cell clusters as indicated. Dot sizes and colours indicate proportions of cells expressing corresponding genes and their averaged scaled values of log-transformed expression, respectively. **c**, PCA of day 4, day 9 and day 21 μNTLS relative to neural cells in human embryonic tissues at different Carnegie stages as indicated[42]. **d**, Left, UMAP projection of integrated scRNA-seq datasets from day 9 μNTLS and neural cells of a CS12 human embryo[42]. Middle and right, UMAP projections of datasets from day 9 μNTLS and neural cells of a CS12 human embryo, separated from the integrated UMAP plot on the left, with cell identity annotations indicated. **e**, Left, UMAP projection of integrated scRNA-seq datasets from day 21 μNTLS and neural cells of a CS15–CS16 human embryo[42]. Middle and right, UMAP projections of datasets from day 21 μNTLS and neural cells of a CS15–CS16 human embryo, separated from the integrated UMAP plot on the left, with cell identity annotations indicated. **f**, Top, UMAP projections of neuron clusters from day 9 μNTLS and CS12 human embryos, with cell identity annotations indicated. Bottom, UMAP projections of neuron clusters from day 21 μNTLS and CS15–CS16 human embryos, with cell identity annotations indicated. In **d**–**f**, original annotations of human neural cells from ref. 42 are used (Methods). *n* indicates cell numbers.

Transcriptome analysis of μNTLS

We next applied single-cell RNA-sequencing (scRNA-seq) for transcriptome analysis of day 4 R–C patterned μNTLS and of day 9 and day 21 R–C and D–V patterned μNTLS. Unbiased clustering of cells from all three μNTLS samples revealed ten distinct populations annotated as FB, MB, IsO, HB, SC, NMP, RP, FP, NC and neuron, based on lineage marker expression (Fig. 3a,b, Extended Data Fig. 8 and Supplementary Note). Notably, the NMP cluster existed only in day 4 μNTLS (Extended Data Fig. 8c,d), a result consistent with their transient presence. The neuron cluster emerged in day 9 μNTLS, and the proportion of cells in the neuron cluster rapidly increased between day 9 and day 21 μNTLS, results consistent with active neurogenesis in μNTLS (Extended Data Fig. 8c,d). The RP and FP clusters appeared in day 9 and day 21 μNTLS datasets, respectively (Extended Data Fig. 8c,d), findings consistent with the D–V patterning dynamics of μNTLS shown in Fig. 2 and Extended Data Fig. 7. RNA velocity analysis, which predicts the directions of cells moving in transcriptional space, showed that progenitor cells in the FB, MB, HB and SC clusters all contribute to neurogenesis in μNTLS (Fig. 3a). Opposing RNA velocity trajectories were evident at the boundary of MB and HB clusters, where the IsO cluster was located. This result provides support for the notion that lineage restriction prevents the transition between MB and HB cell fates[41] (Fig. 3a). RNA velocity trajectories for the SC cluster were rooted in the NMP cluster, thereby supporting a role of NMPs in SC development (Fig. 3a).

We next compared the μNTLS transcriptome with scRNA-seq datasets of human embryos at early organogenesis stages (CS12–CS16)[42]. Principal component analysis (PCA) revealed that μNTLS on day 9 and on day 21 showed closest transcriptome similarities with human neural cells at CS12 and at CS15–CS16, respectively (Fig. 3c). When day 9 and day 21 μNTLS data were integrated with those of human neural cells at CS12 and at CS15–CS16, respectively, high concordance was evident between μNTLS and human cells at the corresponding stages (Fig. 3d–f and Extended Data Fig. 9a–d). Cell clusters of day 9 and day 21

μNTLS overlapped with their counterparts from CS12 and CS15–CS16 human embryos, respectively (Fig. 3d–f and Extended Data Fig. 9a–d). Moreover, expression patterns of key markers in uniform manifold approximation and projection (UMAP) analyses showed notable similarities between μNTLS and corresponding human neural cells (Extended Data Fig. 9a–d). Additional correlation analysis between annotated neural cell clusters from μNTLS and human embryos further supported transcriptome similarities between day 9 and day 21 μNTLS and CS12 and CS15–CS16 human neural cells, respectively (Extended Data Fig. 9e,f). Consistent with that, the proportion of cells in the neuron cluster increased between day 9 and day 21 μNTLS, as well as between CS12 and CS15–CS16 human embryos, findings that support the presence of active neurogenesis in μNTLS between day 9 and day 21 (Extended Data Fig. 9g).

Transcriptomes of day 4, day 9 and day 21 μNTLS also showed similarities with neural cells from E8.25, E10.5 and E11.5 mouse embryos[43,44], respectively (Supplementary Figs. 8–10 and Supplementary Note). This result provides support for conserved overall gene expression programs between mouse and human early NT development[42]. Altogether, μNTLS on day 4, day 9 and day 21 showed the closest transcriptome similarities with human neural cells at CS8–CS9 (days 17–20), CS12 (days 26–30) and CS15–CS16 (days 35–42), respectively (Extended Data Fig. 9h).

We further analysed the FB, SC and neuron clusters from μNTLS and compared them with their counterparts from human embryos. Even though transcripts associated with metabolic and cell cycle processes were downregulated in the day 21 μNTLS FB cluster compared with their expression in FB cells in CS15–CS16 human embryos, key markers associated with dorsal and ventral FB, including *FOXG1*, *EMX2* and *NKX2-1*, were clearly evident in the day 21 μNTLS FB cluster (Extended Data Fig. 10a–f and Supplementary Note). Subclustering analysis of SC-related cells provided additional evidence of D–V patterning of caudal μNTLS (Extended Data Fig. 10g–k and Supplementary Note). Comparisons between the neuron clusters from day 9 and day 21 μNTLS and CS12 and CS15–CS16 human neuron cells, respectively, confirmed their transcriptome similarity (Fig. 3f, Extended Data Fig. 9b,d,f, and Supplementary Note). The results also supported the presence of FB, MB, HB and SC neurons and therefore neurogenesis along the entire R–C axis in day 21 μNTLS (Fig. 3f, Extended Data Fig. 9b,d,f, Supplementary Fig. 11 and Supplementary Note). The presence of neocortex intermediate progenitor cells (IPCs) and GABAergic neurons in day 21 μNTLS further supported the successful D–V patterning in rostral μNTLS (Fig. 3f, Extended Data Fig. 9b,d,f, Supplementary Fig. 11 and Supplementary Note).

CellChat analysis, which is useful for inference of ligand–receptor interactions between pairs of cell clusters, was conducted using integrated μNTLS transcriptome data. The results revealed that IsO, NMP, RP and FP clusters are notable sources of endogenous morphogen signals, findings consistent with in vivo knowledge[28,33,35] (Supplementary Fig. 12a,b and Supplementary Note). We further performed gene regulatory network analysis for each cell cluster of μNTLS and identified their regulons (Supplementary Fig. 12c,d and Supplementary Note).

The reproducibility of μNTLS production was analysed on the basis of scRNA-seq data of day 9 μNTLS from two different batches. The results showed that μNTLS had greater reproducibility than those of brain organoids[4] (Supplementary Fig. 13 and Supplementary Note).

NC development

The μNTLS platform offers a promising system to study neuronal lineage development. To demonstrate this, we sought to investigate NC lineage development. In vivo, NC cells arise from the neural plate border and undergo epithelial-to-mesenchymal transition to delaminate from the dorsal NT before giving rise to both ectodermal-like and mesodermal-like derivatives[39] (Fig. 4a). Depending on their axial level of origin, NC cells display distinct developmental potentials. Cranial NC cells, but not trunk NC cells, give rise to mesenchymal cells, whereas trunk NC cells are biased for neuronal lineages such as sympathetic neurons, which do not arise from cranial NC cells[45,46] (Fig. 4a). Consistently, dispersed single migratory SOX10$^+$ NC cells were evident dorsal to the dorsal pole of μNTLS, with those abutting μNTLS expressing SNAI2, an epithelial-to-mesenchymal transition marker (Extended Data Fig. 11a). Notably, TWIST1$^+$ mesenchymal cells were evident adjacent to SOX10$^+$ NC cells only in the rostral half but not in the caudal half of μNTLS (Fig. 4b,c,g and Extended Data Fig. 11b). Conversely, PHOX2B$^+$ sympathetic neurons were evident adjacent to SOX10$^+$ NC cells only in the caudal half but not in the rostral half of μNTLS (Fig. 4b,d,g and Extended Data Fig. 11b). ISL1$^+$ sensory neurons and S100B$^+$ Schwann cells, which are also progenies of NC cells in vivo, were detectable along the entire R–C axis of μNTLS (Extended Data Fig. 11b).

SOX10$^+$ NC cells only emerged during the D–V patterning step of R–C patterned μNTLS (Extended Data Fig. 11d,e), during which NC cells along the R–C axis were exposed to similar chemical environments. To examine when axial identities of NC progenitors were specified, after initial R–C patterning of μNTLS, gradients of caudalizing WNT, FGF8 and RA signals were reversed to establish their R-to-C gradients during D–V patterning of μNTLS (Fig. 4b and Extended Data Fig. 11d). Such ectopic caudalizing environments at μNTLS rostral regions did not affect the rostral preference of TWIST1$^+$ mesenchymal cell development (Fig. 4e–g). This result provides support for the pre-patterning of axial identities of NC progenitors during R–C patterning of μNTLS.

NMPs derived from human PS cells can differentiate into trunk NC cells in vitro, which indicates a possible developmental origin of trunk NC cells from NMPs[47]. Thus, we generated R–C and D–V patterned μNTLS using the *TBXT*::T2A-Cre lineage tracer and followed the development of NMP progenies (Extended Data Fig. 11f and Supplementary Video 6). NMP progenies were clearly evident in HOXC9$^+$ trunk NC cells, and notable proportions of ISL1$^+$ sensory and PHOX2B$^+$ sympathetic neurons at caudal μNTLS regions were NMP progenies (Fig. 4h and Extended Data Fig. 11g,h). These data indicate that NMPs have a role in caudal SC and trunk NC development.

Subclustering analysis of the NC cluster from integrated day 4, day 9 and day 11 μNTLS transcriptome datasets revealed 7 subclusters annotated as premigratory NC, delaminating NC, Schwann cell, mesenchymal cell, sensory neuron, sympathetic neuron and melanoblast (Fig. 4i, Extended Data Fig. 12a–d and Supplementary Note). Based on HOX gene expression, the NC cluster was further subdivided into '*HOX*$^-$' and '*HOX*$^+$' cranial NC, vagal NC (*HOX3–HOX5*) and trunk NC (*HOX6–HOX9*) (Fig. 4j and Extended Data Fig. 12e). Consistent with that, the mesenchymal cell subcluster existed only in cranial and vagal NC populations but not in the trunk NC population (Fig. 4j and Extended Data Fig. 12f). Conversely, the sympathetic neuron subcluster existed only in vagal and trunk NC populations but not in the cranial NC population (Fig. 4j and Extended Data Fig. 12f). Lineage marker expression in different NC subclusters depended on their axial identities (Extended Data Fig. 12g). Notably, in the premigratory NC cluster, *CDX2* showed the highest expression in trunk NC cells but was almost undetectable in cranial NC cells (Fig. 4k), which suggested that *CDX2* might have a role in trunk NC development. To test this, R–C and D–V patterned μNTLS were generated from *CDX2* KO human ES cells. *CDX2* KO completely blocked trunk NC or sympathetic neuron development in μNTLS, and caudal-most NC cells were HOXB4$^+$ vagal NC cells (Fig. 4l,m and Extended Data Fig. 11i).

Developmental trajectories of *HOX*$^-$ cranial NC lineages in μNTLS were inferred on the basis of pseudotime analysis, which revealed lineage diversification of *HOX*$^-$ cranial NC cells into Schwann cells, mesenchymal cells, sensory neurons and melanoblasts (Extended Data Fig. 12h–j). All four lineages underwent premigration and delamination stages, followed by lineage specification towards Schwann cells, mesenchymal cells, sensory neurons or melanoblast fates, respectively (Extended Data Fig. 12h–j and Supplementary Note).

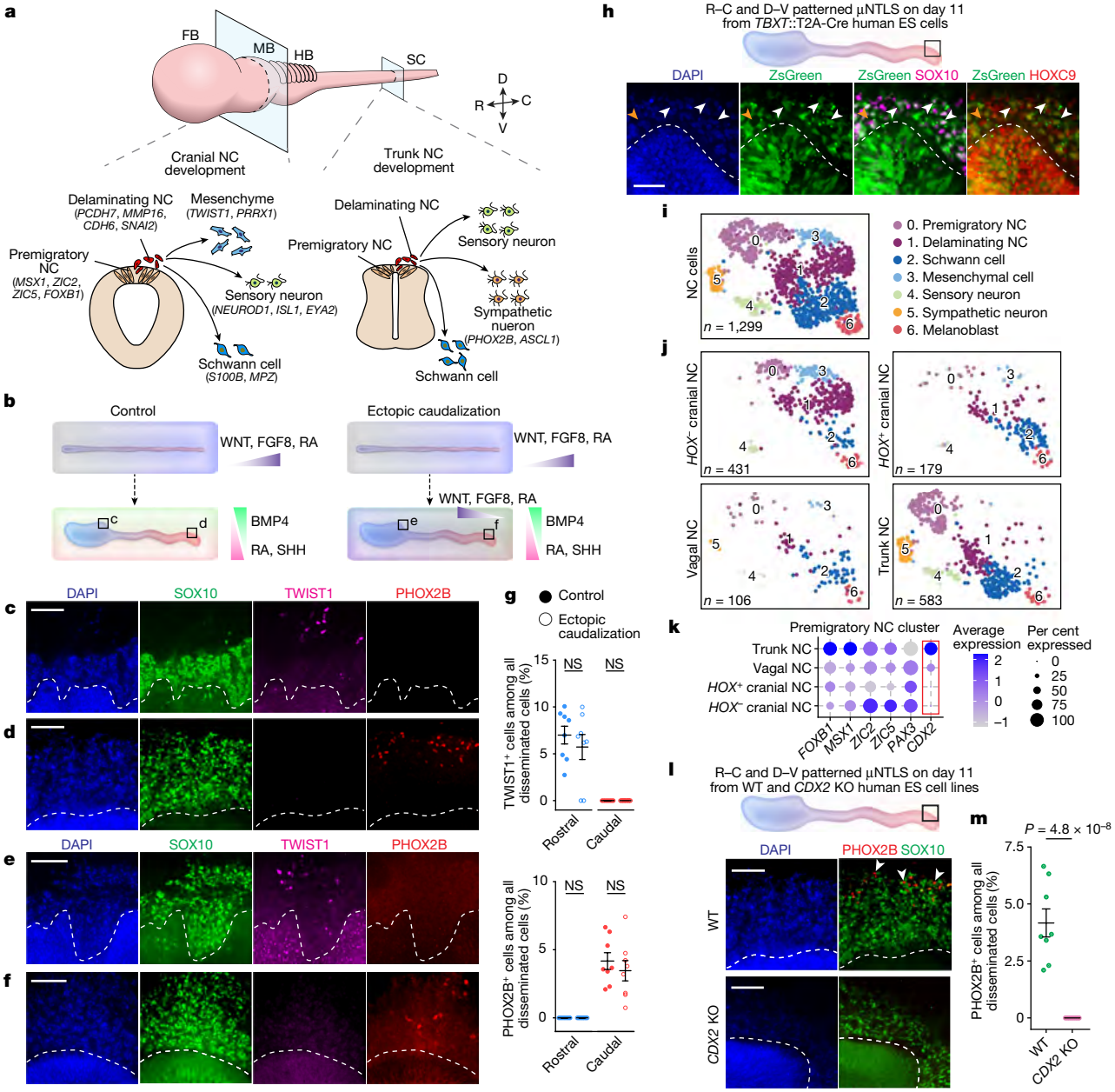

Fig. 4 | NC development in μNTLS. a, Schematic of cranial and trunk NC development in vivo. **b**, R–C and D–V patterned μNTLS (left) and ectopic caudalization of μNTLS (right). **c**–**f**, Micrographs showing rostral and caudal regions of day 11 R–C and D–V patterned μNTLS without (**c**,**d**) or with (**e**,**f**) ectopic caudalization, stained for indicated markers. **g**, Percentages of TWIST1$^+$ cells (top) and PHOX2B$^+$ cells (bottom) among all disseminated cells in rostral or caudal halves of μNTLS with or without ectopic caudalization. $n_{colony} = 8$ and $n_{experiment} = 2$. **h**, Schematic (top) and micrographs (bottom) showing caudal ends of day 11 R–C and D–V patterned μNTLS generated from the *TBXT*::T2A-Cre lineage tracer, stained for indicated markers. White and orange arrowheads mark ZsGreen$^+$ and ZsGreen$^-$ NC cells, respectively. **i**, UMAP of NC clusters isolated from integrated transcriptome datasets of day 4, day 9 and day 11 μNTLS, colour-coded according to cell identity annotations. **j**, UMAP of transcriptome data of *HOX*$^-$ and *HOX*$^+$ cranial NC cells, vagal NC cells and trunk NC cells isolated from the UMAP plot in **i**. **k**, Dot plot showing the expression of selected markers in premigratory NC cells from four NC lineages. **l**, Schematic (top) and micrographs (bottom) showing caudal regions of day 11 R–C and D–V patterned μNTLS generated from wild-type (WT) and *CDX2* KO human ES cells, stained for indicated markers. Arrowheads mark PHOX2B$^+$ cells. **m**, Percentage of PHOX2B$^+$ cells among all disseminated cells at caudal regions of μNTLS generated from WT and *CDX2* KO human ES cells. $n_{PHOX2B} = 8$ and $n_{experiment} = 2$. In **c**–**f**, **h** and **l**, nuclei were counterstained with DAPI, dashed lines mark dorsal μNTLS boundaries and experiments were repeated three times with similar results. In **g** and **m**, error bars represent the mean ± s.e.m., and two-sided Student's *t*-tests were performed. In **i** and **j**, *n* indicate cell numbers. Scale bars, 50 μm (**h**) or 100 μm (**c**–**f**,**l**).

D–V patterned FB-like structures

We next sought to use μNS to generate D–V patterned, microfluidic FB-like structures (μFBLS). During FB development, dorsal pallium and ventral subpallium regions give rise to glutamatergic excitatory neurons and GABAergic inhibitory neurons, respectively (Extended Data Fig. 13a). Regionalization of μNS with uniform treatments of two SMAD inhibitors or a smoothened agonist (SAG), followed by continuous neuronal differentiation culture, led to the formation of dorsal or ventral μFBLS, respectively (Extended Data Fig. 13b–d and Methods). On day 40, 66.4 ± 4.1% dorsal μFBLS and 60.0 ± 4.8% ventral μFBLS contained a single central apical lumen, and they both expressed the FB

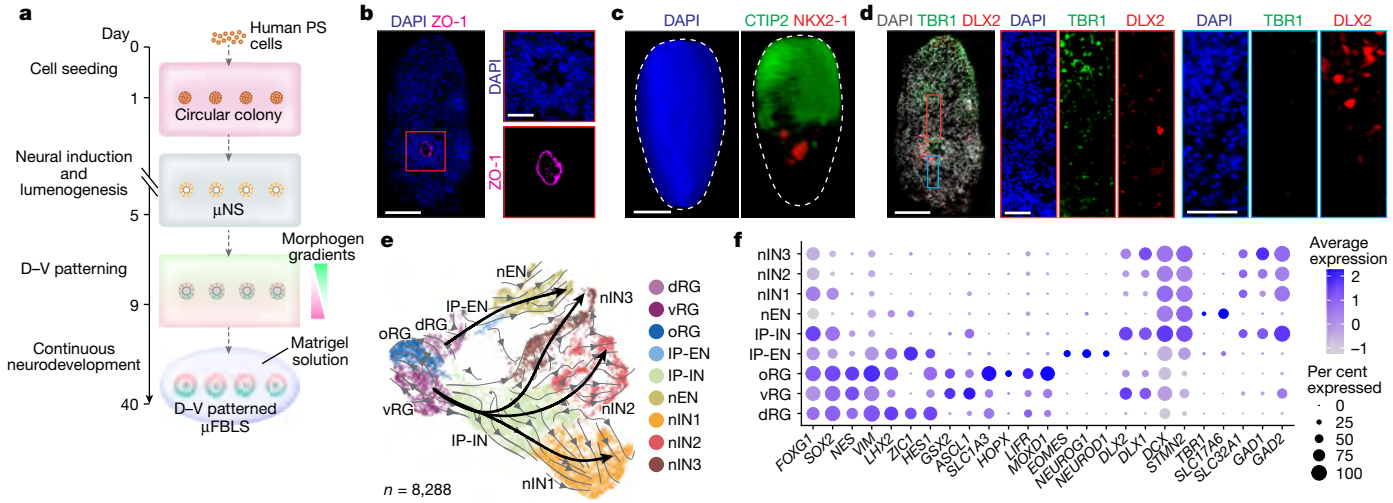

Fig. 5 | Development of D–V patterned μFBLS. a, Protocol for generating D–V patterned μFBLS. μNS are exposed to antiparallel gradients of dorsalizing and ventralizing signals in the microfluidic patterning region until day 9, after which they are released from the device and cultured in Matrigel solutions. **b**, Representative confocal micrographs showing sections of D–V patterned μFBLS on day 40 stained for ZO-1. Right, zoom-in views of the boxed region. **c**, 3D view of representative whole-mount staining images showing D–V patterned μFBLS on day 40 stained for CTIP2 and NKX2-1 (Supplementary Video 7). Dashed line marks the boundary of μFBLS. **d**, Representative confocal micrographs showing sections of D–V patterned μFBLS on day 40 stained for TBR1 and DLX2. Right, zoom-in views of the boxed regions. **e**, UMAP of single-cell transcriptome data of day 40 D–V patterned μFBLS, colour-coded according to cell identity annotations. Grey arrows indicate RNA velocity vectors predicting future cell states. Black arrows indicate inferred lineage trajectories. One excitatory neuron trajectory (dRG → IP-EN → nEN) and three inhibitory neuron trajectories (vRG → P-IN → nIN1, nIN2 and nIN3) are constructed. *n* indicates cell number. **f**, Dot plot showing the expression of key marker genes across all cell clusters as indicated. Dot sizes and colours indicate proportions of cells expressing corresponding genes and their averaged scaled values of log-transformed expression, respectively. In **b**–**d**, nuclei were counterstained with DAPI, and experiments were repeated three times with similar results. Scale bars, 50 μm (zoom-in views in **b** and **d**) or 200 μm (all other images).

marker FOXG1 (Extended Data Fig. 13d,e,g and Supplementary Note). Reelin$^+$ Cajal–Retzius cells were evident in the outer regions of dorsal μFBLS (Extended Data Fig. 13e). Dorsal μFBLS expressed the dorsal FB neural progenitor cell (NPC) marker PAX6, but not the ventral FB marker DLX2 (Extended Data Fig. 13e,f). Along the apical–basal axis of dorsal μFBLS, PAX6$^+$ dorsal NPCs, TBR2$^+$ IPCs and CTIP2$^+$, TBR1$^+$ and SATB2$^+$ cortical neurons exhibit layered organizations (Extended Data Fig. 13f), thereby mimicking cortical patterning in vivo[48]. Similarly, layered apicobasal organizations of ventral NPCs (GSX2$^+$), IPCs (ASCL1$^+$) and neurons (DLX2$^+$, MEIS2$^+$ and CTIP2$^+$) were also evident in ventral μFBLS (Extended Data Fig. 13g,h), thereby resembling the developing ventral FB in vivo[49].

We next induced D–V patterning of μFBLS. To this end, μNS were exposed to antiparallel gradients of BMP4 and SAG along the D–V axis, followed by long-term neuronal differentiation culture (Fig. 5a and Extended Data Fig. 13b,c). On day 40, 54.9 ± 2.1% D–V patterned μFBLS contained a single central apical lumen, demarcated by ZO-1 (Fig. 5b and Extended Data Fig. 13c,d,i). Notably, the cortical and lateral ganglionic eminence (LGE) neuron marker CTIP2 was evident only in one side of D–V patterned μFBLS, whereas the medial ganglionic eminence (MGE) marker NKX2-1 was restricted to the opposite side, which recapitulated the D–V patterning in the FB (Fig. 5c and Supplementary Video 7). D–V patterned μFBLS further showed spatial separation of TBR1$^+$ cortical neurons in dorsal regions and DLX2$^+$ subpallium neurons in ventral regions (Fig. 5d and Extended Data Fig. 13i). Dorsal and ventral regions of D–V patterned μFBLS also exhibited layered apicobasal organizations of neural progenitor and neuron domains, as revealed by the patterned expression of PAX6, TBR1 and CTIP2 in dorsal regions and ASCL1, DLX2, CTIP2 and MEIS2 in ventral domains, respectively (Extended Data Fig. 13i and Supplementary Note). D–V patterning of μFBLS showed a success rate of 75.5 ± 3.2% (see Methods for criteria used for identifying successful D–V patterning of μFBLS).

Identities of cells in D–V patterned μFBLS on day 40 were further characterized using scRNA-seq. Unbiased clustering analysis revealed nine distinct cell clusters, annotated as dorsal radial glia (dRG), ventral radial glia (vRG), outer radial glia (oRG), excitatory intermediate progenitor (IP-EN), inhibitory intermediate progenitor (IP-IN), newborn excitatory neuron (nEN) and newborn inhibitory neuron 1 (nIN1), nIN2 and nIN3 (Fig. 5e,f, Extended Data Fig. 14a,b and Supplementary Note). We compared the transcriptome of day 40 μFBLS with scRNA-seq data of human embryonic brains at 5–14 post-conceptional weeks (p.c.w.)[50] (Extended Data Fig. 14c–j and Supplementary Note). PCA revealed transcriptome similarities between day 40 μFBLS and 11.5–12 p.c.w. human FB (Extended Data Fig. 14c,g). Pallium-related cell clusters (dRG, IP-EN and nEN) in day 40 μFBLS showed substantial molecular similarities with their counterparts in 11.5 p.c.w. human FB (Extended Data Fig. 14d–f). Comparison of nIN1, nIN2 and nIN3 clusters and inhibitory neurons in human FB revealed the presence of inhibitory neurons associated with the LGE, MGE and caudal ganglionic eminence (CGE) in μFBLS (Extended Data Fig. 14h–j). RNA velocity and pseudotime analyses supported lineage development trajectories from RG clusters to excitatory and inhibitory neuron clusters, respectively (dRG → IP-EN → nEN and vRG → IP-IN → nIN) (Fig. 5e, Extended Data Fig. 14k–m).

Summary

In this study, we reported the development of μNTLS and μFBLS using microfluidic gradients. The μNTLS represents a promising in vitro neurodevelopment model that recapitulates several crucial aspects of neural patterning in brain and SC regions and along R–C and D–V axes. In addition to exhibiting patterned expression of canonical regional markers, including HOX genes, μNTLS showed dynamic development of NMPs and NC cells. NC cells in μNTLS exhibited axial position-dependent developmental potentials, mimicking NC development in vivo. Our study further provided new knowledge about pre-patterning of axial identities of NC progenitors in the NT and the roles of NMPs and *CDX2* in thoracic SC and trunk NC development, all in the context of human development. We also developed D–V patterned

μFBLS with spatially segregated dorsal and ventral regions and layered apicobasal cellular organizations that mimic human forebrain pallium and subpallium development, respectively.

It should be noted that the complexity of spatiotemporal patterning signals in the developing NT might not be fully recapitulated in current μNTLS or μFBLS protocols. This might have resulted in tissue patterning and cellular organizations in μNTLS and μFBLS being less organized than they are in vivo. In addition, human caudal SC development might involve mechanisms different from what are recapitulated in current μNTLS protocols. This might have led to the caudal-most regions of μNTLS currently having a thoracic SC identity. It remains a future goal to leverage microfluidics to control dynamic biochemical and biophysical environments of μNTLS and μFBLS development, thereby enabling them to better mimic patterning of different brain and SC regions, as well as to prolong their development while maintaining in vivo-like tissue organization and a single central open lumen. The μNTLS might not be suitable for modelling NT closure defects. Nonetheless, in its current form, it already offers a useful experimental system to study some long-standing questions in developmental biology, including the regulation of HOX gene expression, the molecular basis of NC axial identity and the functional role of NMPs in SC and NC development. Continuous developments of μNTLS and μFBLS might provide advanced neurodevelopment models that facilitate inter-regional and long-range cellular interactions to promote neurodevelopment and complex network functions. Altogether, both μNTLS and μFBLS offer 3D lumenal tissue architectures with in vivo-like spatiotemporal cell differentiation and organization, and they are promising for studying human neurodevelopment and disease.

Online content

Any methods, additional references, Nature Portfolio reporting summaries, source data, extended data, supplementary information, acknowledgements, peer review information; details of author contributions and competing interests; and statements of data and code availability are available at https://doi.org/10.1038/s41586-024-07204-7.

1. Lancaster, M. A. et al. Cerebral organoids model human brain development and microcephaly. *Nature* **501**, 373–379 (2013).
2. Qian, X. et al. Brain-region-specific organoids using mini-bioreactors for modeling ZIKV exposure. *Cell* **165**, 1238–1254 (2016).
3. ctipBirey, F. et al. Assembly of functionally integrated human forebrain spheroids. *Nature* **545**, 54–59 (2017).
4. Velasco, S. et al. Individual brain organoids reproducibly form cell diversity of the human cerebral cortex. *Nature* **570**, 523–527 (2019).
5. Faustino Martins, J.-M. et al. Self-organizing 3D human trunk neuromuscular organoids. *Cell Stem Cell* **26**, 172–186.e176 (2020).
6. Meinhardt, A. et al. 3D reconstitution of the patterned neural tube from embryonic stem cells. *Stem Cell Reports* **3**, 987–999 (2014).
7. Haremaki, T. et al. Self-organizing neuruloids model developmental aspects of Huntington's disease in the ectodermal compartment. *Nat. Biotechnol.* **37**, 1198–1208 (2019).
8. Zheng, Y. et al. Dorsal–ventral patterned neural cyst from human pluripotent stem cells in a neurogenic niche. *Sci. Adv.* **5**, eaax5933 (2019).
9. Rifes, P. et al. Modeling neural tube development by differentiation of human embryonic stem cells in a microfluidic WNT gradient. *Nat. Biotechnol.* **38**, 1265–1273 (2020).
10. Karzbrun, E. et al. Human neural tube morphogenesis in vitro by geometric constraints. *Nature* **599**, 268–272 (2021).
11. Müller, F. & O'Rahilly, R. The development of the human brain, the closure of the caudal neuropore, and the beginning of secondary neurulation at stage 12. *Anat. Embryol.* **176**, 413–430 (1987).
12. Storey, K. G. et al. Early posterior neural tissue is induced by FGF in the chick embryo. *Development* **125**, 473–484 (1998).
13. Niederreither, K., Subbarayan, V., Dollé, P. & Chambon, P. Embryonic retinoic acid synthesis is essential for early mouse post-implantation development. *Nat. Genet.* **21**, 444–448 (1999).
14. Nordström, U., Jessell, T. M. & Edlund, T. Progressive induction of caudal neural character by graded Wnt signaling. *Nat. Neurosci.* **5**, 525–532 (2002).
15. O'Shea, K. S. Differential deposition of basement membrane components during formation of the caudal neural tube in the mouse embryo. *Development* **99**, 509–519 (1987).
16. Chambers, S. M. et al. Highly efficient neural conversion of human ES and iPS cells by dual inhibition of SMAD signaling. *Nat. Biotechnol.* **27**, 275–280 (2009).
17. Xue, X. et al. Mechanics-guided embryonic patterning of neuroectoderm tissue from human pluripotent stem cells. *Nat. Mater.* **17**, 633–641 (2018).
18. Philippidou, P. & Dasen, J. S. *Hox* genes: choreographers in neural development, architects of circuit organization. *Neuron* **80**, 12–34 (2013).
19. Metzis, V. et al. Nervous system regionalization entails axial allocation before neural differentiation. *Cell* **175**, 1105–1118.e17 (2018).
20. Deschamps, J. et al. Initiation, establishment and maintenance of *Hox* gene expression patterns in the mouse. *Int. J. Dev. Biol.* **43**, 635–650 (1999).
21. Bel-Vialar, S., Itasaki, N. & Krumlauf, R. Initiating *Hox* gene expression: in the early chick neural tube differential sensitivity to FGF and RA signaling subdivides the *HoxB* genes in two distinct groups. *Development* **129**, 5103–5115 (2002).
22. Duband, J.-L., Blavet, C., Jarov, A. & Fournier-Thibault, C. Spatio-temporal control of neural epithelial cell migration and epithelium-to-mesenchyme transition during avian neural tube development. *Dev. Growth Differ.* **51**, 25–44 (2009).
23. Wymeersch, F. J. et al. Position-dependent plasticity of distinct progenitor types in the primitive streak. *eLife* **5**, e10042 (2016).
24. Tzouanacou, E., Wegener, A., Wymeersch, F. J., Wilson, V. & Nicolas, J.-F. Redefining the progression of lineage segregations during mammalian embryogenesis by clonal analysis. *Dev. Cell* **17**, 365–376 (2009).
25. Henrique, D., Abranches, E., Verrier, L. & Storey, K. G. Neuromesodermal progenitors and the making of the spinal cord. *Development* **142**, 2864–2875 (2015).
26. Diaz-Cuadros, M. et al. In vitro characterization of the human segmentation clock. *Nature* **580**, 113–118 (2020).
27. Gouti, M. et al. In vitro generation of neuromesodermal progenitors reveals distinct roles for Wnt signalling in the specification of spinal cord and paraxial mesoderm identity. *PLoS Biol.* **12**, e1001937 (2014).
28. Wurst, W. & Bally-Cuif, L. Neural plate patterning: upstream and downstream of the isthmic organizer. *Nat. Rev. Neurosci.* **2**, 99–108 (2001).
29. Duester, G. Retinoic acid synthesis and signaling during early organogenesis. *Cell* **134**, 921–931 (2008).
30. Sakai, Y. et al. The retinoic acid-inactivating enzyme CYP26 is essential for establishing an uneven distribution of retinoic acid along the anterio-posterior axis within the mouse embryo. *Genes Dev.* **15**, 213–225 (2001).
31. Chawengsaksophak, K., de Graaff, W., Rossant, J., Deschamps, J. & Beck, F. *Cdx2* is essential for axial elongation in mouse development. *Proc. Natl Acad. Sci. USA* **101**, 7641–7645 (2004).
32. Amin, S. et al. Cdx and T brachyury co-activate growth signaling in the embryonic axial progenitor niche. *Cell Rep.* **17**, 3165–3177 (2016).
33. Liem, K. F., Tremml, G. & Jessell, T. M. A role for the roof plate and its resident TGFβ-related proteins in neuronal patterning in the dorsal spinal cord. *Cell* **91**, 127–138 (1997).
34. Muroyama, Y., Fujihara, M., Ikeya, M., Kondoh, H. & Takada, S. Wnt signaling plays an essential role in neuronal specification of the dorsal spinal cord. *Genes Dev.* **16**, 548–553 (2002).
35. Dessaud, E. et al. Interpretation of the sonic hedgehog morphogen gradient by a temporal adaptation mechanism. *Nature* **450**, 717–720 (2007).
36. Wilson, L., Gale, E., Chambers, D. & Maden, M. Retinoic acid and the control of dorsoventral patterning in the avian spinal cord. *Dev. Biol.* **269**, 433–446 (2004).
37. Wilson, S. W. & Rubenstein, J. L. R. Induction and dorsoventral patterning of the telencephalon. *Neuron* **28**, 641–651 (2000).
38. Sagner, A. & Briscoe, J. Establishing neuronal diversity in the spinal cord: a time and a place. *Development* **146**, dev182154 (2019).
39. Sauka-Spengler, T. & Bronner-Fraser, M. A gene regulatory network orchestrates neural crest formation. *Nat. Rev. Mol. Cell Biol.* **9**, 557–568 (2008).
40. Jeong, J. & McMahon, A. P. Growth and pattern of the mammalian neural tube are governed by partially overlapping feedback activities of the hedgehog antagonists patched 1 and Hhip1. *Development* **132**, 143–154 (2005).
41. Kiecker, C. & Lumsden, A. Compartments and their boundaries in vertebrate brain development. *Nat. Rev. Neurosci.* **6**, 553–564 (2005).
42. Xu, Y. et al. A single-cell transcriptome atlas profiles early organogenesis in human embryos. *Nat. Cell Biol.* **25**, 604–615 (2023).
43. Cao, J. et al. The single-cell transcriptional landscape of mammalian organogenesis. *Nature* **566**, 496–502 (2019).
44. Pijuan-Sala, B. et al. A single-cell molecular map of mouse gastrulation and early organogenesis. *Nature* **566**, 490–495 (2019).
45. Le Douarin, N. M., Creuzet, S., Couly, G. R. & Dupin, E. Neural crest cell plasticity and its limits. *Development* **131**, 4637–4650 (2004).
46. Soldatov, R. et al. Spatiotemporal structure of cell fate decisions in murine neural crest. *Science* **364**, eaas9536 (2019).
47. Frith, T. J. R. et al. Human axial progenitors generate trunk neural crest cells in vitro. *eLife* **7**, e35786 (2018).
48. Eze, U. C., Bhaduri, A., Haeussler, M., Nowakowski, T. J. & Kriegstein, A. R. Single-cell atlas of early human brain development highlights heterogeneity of human neuroepithelial cells and early radial glia. *Nat. Neurosci.* **24**, 584–594 (2021).
49. Onorati, M. et al. Molecular and functional definition of the developing human striatum. *Nat. Neurosci.* **17**, 1804–1815 (2014).
50. Braun, E. et al. Comprehensive cell atlas of the first-trimester developing human brain. *Science* **382**, eadf1226 (2023).

Methods

Cell lines

Human PS cell lines used in this study included H1 human ES cell (WA01, WiCell; NIH registration number: 0043), H9 human ES cell (WA09, WiCell; NIH registration number: 0062), WIBR3 human ES cell (NIH registration number: 0079) and 1196a (human iPS cell) lines from the University of Michigan Pluripotent Stem Cell Core. A Brachyury–mNeonGreen H9 human ES cell reporter line[51], a *CDX2* KO H9 human ES cell line[52], a *TBXT* KO WIBR3 human ES cell line and a *TBXT*::T2A-Cre lineage tracer H9 human ES cell line were also used. All human PS cell lines were authenticated by original sources and in-house by immunostaining for pluripotency markers and successful differentiation to three definitive germ layers. All human PS cell lines were maintained in a feeder-free culture system for at least ten passages and were authenticated as karyotypically normal by Cell Line Genetics. All human PS cell lines tested negative for mycoplasma contamination (LookOut Mycoplasma PCR Detection kit; Sigma-Aldrich). All protocols used in this work with human PS cells were approved by the Human Pluripotent Stem Cell Research Oversight Committee at the University of Michigan. The research conforms to the 2021 Guidelines for Stem Cell Research and Clinical Translation recommended by the International Society for Stem Cell Research.

Cell culture

Human PS cells were maintained in a standard feeder-free culture system using mTeSR medium (mTeSR; StemCell Technologies) and lactate dehydrogenase-elevating virus (LDEV)-free, human ES cell-qualified reduced growth factor basement membrane matrix Geltrex (Thermo Fisher Scientific; derived from Engelbreth–Holm–Swarm tumours, similar to Matrigel). Cell culture was visually examined during each passage to ensure the absence of spontaneously differentiated, mesenchymal-like cells in culture. All human PS cells were used between passages 50 and 70.

TBXT KO human ES cells

WIBR3 human ES cells were grown on gamma-irradiated primary mouse embryonic fibroblasts in HENSM medium[53]. Cells were chemically passaged at 70% confluency with 0.05% Trypsin and 0.02% EDTA (Sartorius). WIBR3 human ES cells were transfected with two plasmids, a gRNA targeting coding exon 3 of *TBXT* (5′-TGCATAAGTATGAGCCTCGA-3′) cloned into pX330-U6-Chimeric_BB-CBh-hSpCas9 (Addgene, plasmid 42230)[54] and pPGKpuro, a gift from A. Bradly. In brief, 5×10^6 cells were collected and washed twice with OptiMEM (Gibco) and resuspended in 300 µl OptiMEM. Next, 100 µl cells were electroporated with 5 µg of each plasmid (NEPA21 Electroporator, Nepagene) before immediately seeding onto pre-warmed culture plates seeded with gamma-irradiated primary mouse embryonic fibroblasts in HENSM medium supplemented with 5 µM Y-27632 for 24 h. Puromycin selection was performed 48 h after cell seeding, with 1 µg ml^{-1} puromycin added to the culture medium for 3 days. After antibiotic selection, surviving colonies were grown in puromycin-free medium for an addition 10 days. A total of 192 colonies were mechanically isolated and further expanded. Genotyping of the 192 colonies was conducted first by high-resolution melting analysis (MeltDoctor, Thermo Fisher) with primers amplifying the targeted region of *TBXT* (forward: 5′-GAGAAGCCTCCCCTGGTGGA-3′; reverse: 5′-CCTCTCAGTGCGGGTTAGCG-3′). Clones that showed a ≥1.5 °C shift in the melting profile were selected for Sanger sequencing to identify mutations. Cell lines with homologous *TBXT* KO were used. The cell line was then maintained in the feeder-free culture system before experiments.

TBXT::T2A-Cre lineage tracer

The *TBXT*::T2A-Cre lineage tracer human ES cell line was generated through two sequential steps using CRISPR–Cas9-mediated genome editing: (1) knock-in of a Cre-responsive ZsGreen cassette into the safe-harbour *AAVS1* locus; and (2) knock-in of P2A-Cre before the stop codon of the *TBXT* locus.

To generate the knock-in plasmid encoding the Cre-responsive ZsGreen cassette, three individual fragments (left homologous arm/T2A-Neomycin-PolyA, Addgene, plasmid 68460 (ref. 55); CAG promoter/loxP-3×PolyA-ZsGreen-PolyA signal, Addgene, plasmid 51269 (ref. 56); and right homologous arm, Addgene, plasmid 68460 (ref. 55)) were amplified by PCR and sequentially inserted into a pU19 plasmid using an in-fusion cloning kit (Takara Bio) according to the manufacturer's instructions. To generate the knock-in plasmid encoding P2A-Cre, three individual fragments (left homologous arm-P2A, Addgene, plasmid 83344 (ref. 57); NlsCre, Addgene, plasmid 12265 (ref. 58); and right homologous arm, Addgene, plasmid 83344 (ref. 57)) were amplified by PCR and sequentially inserted into a pU19 plasmid using an in-fusion cloning kit (Takara Bio) according to the manufacturer's instructions. To generate a CRISPR–Cas9 plasmid targeting the safe-harbour *AAVS1* or *TBXT* locus, gRNAs targeting these loci were cloned into PX459-2A-Venus.

Knock-in plasmids and corresponding CRISPR plasmids were transfected into H9 human ES cells and after 48 h, and Venus-positive cells were sorted by FACS. Sorted cells were grown in the presence of neomycin (50 µg ml^{-1}) for 7 days. Individual human ES cell colonies were genotyped and checked for successful knock-in.

All cloning primers and gRNAs used are listed in Supplementary Table 2.

Device fabrication

The microfluidic device consists of a polydimethylsiloxane (PDMS) structural layer attached to a coverslip. The PDMS structural layer was generated by mixing PDMS curing agent and base polymer (Sylgard 184; Dow Corning) at a ratio of 1:10 before casting the PDMS prepolymer onto a microfabricated silicon mould and baking at 110 °C for 1 h. Reservoirs for medium (6 mm in diameter) and a loading port (1 mm in diameter) were punched into the PDMS structural layer using Harris Uni-Core punch tools (Ted Pella). In parallel, PDMS stamps containing rectangular or circular micropatterns were fabricated by casting PDMS prepolymer (with the ratio of curing agent to base polymer of 1:20) onto a microfabricated silicon mould and baking at 110 °C for 1 h. PDMS stamps were peeled off from the mould before immersing in a 1% Geltrex solution (v/v) at 4 °C overnight. The next day, glass coverslips (Thermo Fisher Scientific) were sonicated in 100% ethanol for 30 min and treated with ultraviolet ozone (Ozone cleaner; Jelight) for 7 min. PDMS stamps coated with Geltrex were then blown dry under nitrogen and placed in conformal contact with ultraviolet ozone-treated coverslips to transfer Geltrex adhesive patterns onto the coverslips. PDMS structural layers were then attached to coverslips, with the microcontact-printed Geltrex islands aligned at the centre of the patterning region of the central channel using a desktop aligner[59].

Generation of µNTLS, µNS and µFBLS

Colonies of human PS cells in tissue culture plates were dissociated using Accutase (Sigma-Aldrich) at 37 °C for 8 min before being suspended in DMEM/F12 (Gibco) as single cells. Cells were centrifuged and resuspended in mTeSR containing 10 µM Y27632 (Tocris), a ROCK inhibitor that prevents dissociation-induced apoptosis of human PS cells[60], at a concentration of 12×10^6 cells per ml. Next, 10 µl human PS cell suspension was introduced into the central channel through the loading port on the microfluidic device (day 0). Two reservoirs of the central channel were immediately filled with fresh mTeSR containing 10 µM Y27632. On day 1, after aspirating mTeSR medium from the central channel, 100% Geltrex was introduced into the central channel to establish a 3D culture environment for human PS cells. On day 2, the culture medium in the left and right reservoirs of the central channel was switched to a neural induction medium (NIM) comprising basal

medium and two SMAD inhibitors (the TGFβ inhibitor SB431542 (10 μM, StemCell Technologies) and the BMP4 inhibitor LDN193189 (500 nM, StemCell Technologies)) to induce neural differentiation. The basal medium comprised 1:1 mixture of DMEM/F12 and neurobasal medium (Gibco), 1% N2 supplement (Gibco), 2% B-27 supplement (without vitamin A, Gibco), 2 mM Glutamax, 1% non-essential amino acids and 1% antibiotic–antimycotic (Gibco).

To generate μNTLS with a default dorsal FB identity, an array of 7 rectangular Geltrex islands (length of 4 mm and width of 100 μm) were first printed onto glass coverslips using microcontact printing before assembling the PDMS structural layer and glass coverslip under proper alignment. NIM was added into two reservoirs of the central channel to induce neural differentiation from day 1 to day 7. The culture medium was replenished daily.

To generate R–C patterned μNTLS, an array of 7 rectangular Geltrex islands (length of 4 mm and width of 100 μm) was first printed onto glass coverslips using microcontact printing before assembling the PDMS structural layer and glass coverslip under proper alignment. CHIR99021 (CHIR, 3 μM, StemCell Technologies), FGF8 (200 ng ml^{-1}, Peprotech) and RA (500 nM, StemCell Technologies) were supplemented into NIM in the right-side medium reservoir of the central channel from day 2 to day 5. Culture medium in the left-side and right-side medium reservoirs of the central channel was switched to fresh NIM from day 5 to day 7. The culture medium was replenished daily.

To generate R–C and D–V patterned μNTLS, a single rectangular Geltrex island (length of 4 mm and width of 200 μm) was first printed onto glass coverslips using microcontact printing before assembling the PDMS structural layer and glass coverslip under proper alignment. CHIR (3 μM), FGF8 (200 ng ml^{-1}) and RA (500 nM) were supplemented into NIM in the right-side medium reservoir of the central channel from day 2 to day 5. From day 5 to day 9, culture medium in the left-side and right-side reservoirs of the central channel was switched back to fresh basal medium, whereas the top channel was filled with new basal medium supplemented with BMP4 (25 ng ml^{-1}, R&D Systems) and the bottom channel was filled with new basal medium supplemented with RA (500 nM) and SAG (500 nM, StemCell Technologies). For assays in Fig. 2d, doses of RA and SAG were both increased to 2,000 nM from day 5 to day 9. For assays in Fig. 4 and Extended Data Figs. 11 and 12, the culture medium in all reservoirs was switched to fresh basal medium from day 9 to day 11 to allow continuous NC development. The culture medium was replenished daily.

To prolong the development of R–C and D–V patterned μNTLS, PDMS structural layers were detached manually from coverslips on day 9, with μNTLS embedded in Geltrex and attached on PDMS structural layers. PDMS structure layers containing μNTLS were cultured in 24-well plates in basal medium from day 9 to day 21, with the edges of the PDMS structural layers trimmed using a razor blade to fit into 24-well plates. The basal medium was replenished every other day.

To generate region-specific μNS, a 7 × 7 array of circular adhesive islands (with a diameter of 200 μm) was first printed onto glass coverslips using microcontact printing before assembling PDMS structural layers and glass coverslips under proper alignment. From day 2 to day 5, CHIR (3 μM), FGF8 (200 ng ml^{-1}) and RA (500 nM) were supplemented into NIM in the right-side medium reservoir of the central channel. The culture medium in both the left-side and right-side medium reservoirs of the central channel was switched to fresh NIM from day 5 to day 7. The culture medium was replenished daily.

To generate μFBLS, a 1 × 4 array of circular adhesive islands (with a diameter of 200 μm) was first printed onto glass coverslips using microcontact printing before assembling PDMS structural layers and glass coverslips under proper alignment. NIM was added into all medium reservoirs from day 1 to day 5. From day 5 to day 9, to generate dorsal μFBLS, all reservoirs were filled with NIM. To generate ventral μFBLS, SAG (500 nM) was supplemented into NIM in all reservoirs. To generate D–V patterned μFBLS, culture medium in the left-side and right-side reservoirs of the central channel was switched to basal medium, whereas the top and bottom channels were filled with basal medium supplemented with BMP4 (25 ng ml^{-1}) and SAG (500 nM), respectively. On day 9, PDMS structural layers were detached manually from coverslips, with μFBLS remaining on PDMS structural layers. PDMS structure layers containing μFBLS were then cultured in 24-well plates in basal medium (without vitamin A) supplemented with CHIR (3 μM) after the edges of the PDMS structural layers were trimmed using a razor blade to fit into 24-well plates. On day 11, medium was switched to basal medium (with vitamin A) supplemented with insulin (2.5 μg ml^{-1}, Thermo Fisher Scientific) and 1% Matrigel (Corning) solution (v/v). On day 30, μFBLS were cultured on an orbital shaker (Fisher Scientific) at a speed of 110 r.p.m. The medium was replenished every other day.

μNTLS patterning efficiency

Quantification of μNTLS patterning efficiency was based on visual examination of brightfield images of μNTLS. μNTLS with an elongated tubular structure, a relatively expanded rostral region and a curly caudal end were counted as R–C patterned μNTLS. The success rate of R–C patterned μNTLS was calculated as the ratio between the number of R–C patterned μNTLS and the total number of cell colonies. Similarly, μNTLS with a tubular structure, an expanded rostral region and delaminated single cells (putative NC cells) adjacent to dorsal poles of μNTLS were counted as R–C and D–V patterned μNTLS. The success rate of R–C and D–V patterned μNTLS was calculated as the ratio between the number of R–C and D–V patterned μNTLS and the total number of cell colonies. μFBLS with spatially patterned expressions of the cortical neuron marker TBR1 and the subpallium marker DLX2, revealed by immunostaining of tissue sections, were counted as D–V patterned μFBLS. The success rate of D–V patterned μFBLS was calculated as the ratio between the number of D–V patterned μFBLS and the total number of stained tissues. Note that only the μFBLS with a visible single lumen were processed for immunostaining.

Dextran diffusion assay

Morphogen diffusion in the microfluidic device was characterized using Texas Red-labelled dextran (70 kDa, with a hydrodynamic radius of 5.8 nm, Invitrogen). In brief, to assess dextran diffusion along the R–C axis, 10 μM Texas Red-labelled dextran was supplemented into the right-side reservoir of the central channel from day 2 to day 5 during R–C patterning of μNTLS. To assess dextran diffusion along the D–V axis, 10 μM Texas Red-labelled dextran was supplemented into the top channel from day 5 to day 9 during D–V patterning of μNTLS. During this period, 100 (10 × 10) fluorescence images with 50% spatial overlap were recorded every 8 h during R–C patterning or every 2 h during D–V patterning using an inverted epifluorescence microscope (Zeiss Axio Observer Z1; Carl Zeiss MicroImaging) equipped with a monochrome charge-coupled device camera to cover the entire patterning region (4 × 4 mm^2) in the central channel of the microfluidic device. Images were then stitched together using the ImageJ plugin Microscopy Image Stitching Tool (MIST; https://pages.nist.gov/MIST/) to obtain fluorescence intensity profiles of the entire patterning region of the microfluidic device. Average fluorescence intensities across the width (for characterizing R–C patterning) or length (for characterizing D–V patterning) of the patterning region were calculated and plotted against their relative R–C or D–V positions in the patterning region.

Clonal growth assay

H2B–GFP human ES cells were mixed with non-fluorescent human ES cells at a ratio of 1:200 before cell seeding into the microfluidic device on day 0. Clonal growth of single H2B–GFP human ES cells was monitored using epifluorescence microscopy from day 2 to day 6 during R–C patterning of μNTLS. The length, width and centre of mass of each H2B–GFP human ES cell colony that grew from a single H2B–GFP cell were quantified as a function of culture time. Using ImageJ, the centre

of mass of each H2B–GFP human ES cell colony was calculated as the GFP intensity-weighted average of *x* and *y* coordinates of all pixels in each H2B–GFP cell colony.

Drug inhibition assays

To inhibit WNT signalling, IWP2 (1 μM, StemCell Technologies) was supplemented into the right-side reservoir of the central channel together with RA (500 nM) and FGF8 (200 ng ml^{-1}) from day 2 to day 5. To inhibit RA signalling, BMS493(2.5 μM, StemCell Technologies) was supplemented into the right-side reservoir of the central channel together with CHIR (3 μM) and FGF8 (200 ng ml^{-1}) from day 2 to day 5. To inhibit FGF signalling, PD173072 (400 nM, Tocris Bioscience) was supplemented into the right-side reservoir of the central channel together with CHIR (3 μM) and RA (500 nM) from day 2 to day 5. R–C patterned μNTLS were fixed on day 4 or day 7.

RNA isolation and RT–qPCR analysis

On day 7, R–C patterned μNTLS were released from the microfluidic device by detaching the PDMS structural layers from coverslips. R–C patterned μNTLS were cut into four even segments using a surgical scissor. RNA from each piece was extracted using a RNeasy mini kit (Qiagen) per the manufacturer's instructions. A CFX Connect SYBR Green PCR master mix system (Bio-Rad) was used for RT–qPCR. An arbitrary *Ct* value of 40 was assigned to samples in which no expression was detected. Relative expression levels were determined by calculating $2^{-\Delta\Delta Ct}$ values with corresponding s.e.m. Human *GAPDH* primer was used as an endogenous control. All fold changes were calculated as fold changes relative to undifferentiated human ES cells unless noted otherwise. All analyses were performed with at least three biological replicates and two technical replicates. All primers are listed in Supplementary Table 3.

Whole-mount immunocytochemistry of μNTLS

PDMS structural layers were first manually detached from glass coverslips to expose μNTLS that remain attached on PDMS structural layers. μNTLS were fixed in 4% paraformaldehyde (PFA; buffered in 1× PBS) at room temperature for 1 h before permeabilizing in 0.1% SDS solution (SDS dissolved in PBS) at room temperature for another 3 h. μNTLS were blocked in 4% donkey serum (Sigma-Aldrich) at 4 °C for 24 h followed by incubation with primary antibody solutions at 4 °C for another 24 h. μNTLS were then labelled with donkey-raised secondary antibodies (1:400 dilution, Fisher Scientific) at 4 °C for 24 h. Both primary and secondary antibodies were prepared in 4% donkey serum supplemented with 0.1% NaN_3. DAPI (Thermo Fisher Scientific) was used for counterstaining cell nuclei. All antibodies are listed in Supplementary Table 4.

Tissue clearing

To optically clear μNTLS after whole-mount immunofluorescence staining, μNTLS were incubated for 30 min in a refractive index (RI)-matching solution comprising 6.3 ml ddH_2O, 9.2 ml OptiPrep Density Gradient medium (MilliporeSigma), 4 g *N*-methyl-D-glucamine (MilliporeSigma) and 5 g diatrizoic acid (MilliporeSigma)[61]. For each PDMS device, 50 μl of RI-matching solution was used. PDMS structure layers containing μNTLS were then attached onto glass coverslips for imaging in IR-matching solution.

Whole-mount immunostaining of μFBLS

The iDISCO protocol was used for whole-mount immunostaining of day 40 μFBLS (https://idisco.info/idisco-protocol/). In brief, μFBLS were fixed in 4% PFA at 4 °C overnight on a rocker (Labnet International). The next day, tissues were incubated in 4% PFA for 45 min at room temperature and washed with Dulbecco's PBS (DPBS) 3 times on a rocker. For tissue pretreatment, μFBLS were washed in PTx.2 (DPBS with 0.2% Triton X-100) twice with rocking before incubating in DPBS with 0.2% Triton X-100 and 20% DMSO at 37 °C overnight on a rocker. All subsequent steps were performed on a rocker at 37 °C. μFBLS were first incubated in DPBS supplemented with 0.1% Tween-20 (Sigma-Aldrich), 0.1% Triton X-100, 0.1% deoxycholate (Sigma-Aldrich), 0.1% NP40 (Sigma-Aldrich) and 20% DMSO overnight and washed in PTx.2 twice the next day. Pretreated μFBLS were then incubated in a permeabilization solution (PTx.2 with 20% DMSO and 2.3% (w/v) glycine (Sigma-Aldrich)) for 1.5 days, before switching to a blocking solution (PTx.2 with 6% donkey serum and 10% DMSO) for 1.5 days followed by incubation with primary antibodies diluted into PTwH (DPBS with 0.2% Tween-20 and 10 mg l^{-1} heparin (Sigma-Aldrich)) with 5% DMSO and 3% donkey serum for 3 days. μFBLS were then washed with PTwH for 1 day and incubated with secondary antibodies and DAPI at 1:500 dilution in PTwH with 3% donkey serum for another 3 days. After washing with PTwH for 1 day, μFBLS underwent a 6-step methanol and water dehydration process (20%, 40%, 60%, 80% and 100% methanol; Fisher Scientific) before incubating in 66% dichloromethane (Sigma) and 33% methanol for another 3 h, followed by two 15-min incubations in 100% dichloromethane (Sigma). μFBLS were finally incubated in dibenzyl ether (Sigma) until imaging by confocal microscopy (Zeiss).

Cryosection and immunohistochemistry

μNTLS were fixed in 4% PFA for 1 h after PDMS structural layers were detached from glass coverslips. μNTLS were then incubated in 30% sucrose overnight before manual transfer into cryomolds (Thermo Fisher Scientific) containing Tissue-Plus OCT compound (Thermo Fisher Scientific) under a stereomicroscope. μNTLS were frozen in OCT medium on dry ice. Tissue sections with a thickness of 10 μm were obtained using cryostat and placed on Superfrost Plus microscope slides (Thermo Fisher Scientific). After drying at room temperature for 2 h, tissue sections were washed with PBS 3 times to remove OCT medium. After permeabilization with 0.2% Triton X-100 at room temperature for 20 min, tissue sections were blocked in 4% donkey serum at room temperature for 1 h followed by incubation with primary antibody solutions at room temperature for another 1 h. Tissue sections were labelled with donkey-raised secondary antibodies (1:400 dilution) at room temperature for 1 h. Both primary and secondary antibodies were prepared in 4% donkey serum supplemented with 0.1% NaN_3. DAPI was used for counterstaining cell nuclei. Superfrost slides with the μNTLS sections were further mounted onto coverslips using Fluoromount-G (Southern Biotech) before imaging.

EdU cell-proliferation assay

A Click-iT EdU Alexa Fluor 488 Imaging kit (Thermo Fisher Scientific) was used to determine cell proliferation according to the manufacturer's instructions. In brief, on day 7, PDMS structural layers were manually detached from glass coverslips to expose μNTLS that remain attached on PDMS structural layers. R–C patterned μNTLS were incubated with basal medium supplemented with EdU (20 μM) for 45 min or 2 h, as indicated, before being fixed, permeabilized and incubated with Click-iT reaction cocktail for 30 min. Cell nuclei were counterstained with DAPI. μNTLS were examined under a confocal microscope to detect EdU-stained cell nuclei.

Cell viability assay

Cell viability was determined using a Live/Dead, Viability/Cytotoxicity kit (Thermo Fisher Scientific) according to the manufacturer's instructions. On day 7, PDMS structural layers were manually detached from glass coverslips to expose μNTLS that remain attached on PDMS structural layers. R–C patterned μNTLS were incubated with basal medium supplemented ethidium homodimer (EthD-1, 4 μM) for 30 min. After incubation, *z* stack (*z* step, 0.5 μm) fluorescence images were recorded using a Nikon X1 Yokogawa spinning-disc confocal microscope. The number of dead cells was quantified using maximum intensity projection images generated from *z* stack images. μNTLS were then fixed and stained for nuclei with DAPI. *z* stack fluorescence images in the DAPI

channel were recorded to generate maximum intensity projection images for quantifying the total number of cells. The percentage of dead cells was quantified as the ratio of the number of dead cells and the total number of cells.

Microscopy

Whole-mount immunostained μNTLS were imaged using an Olympus DSUIX81 spinning-disc confocal microscope or a Nikon X1 Yokogawa spinning-disc confocal microscope. An array of partially overlapping images (50% overlap) were taken to cover the entire μNTLS area. Images were stitched together using the ImageJ plugin MIST after the background and shade of each image were corrected using the ImageJ plugin BaSiC (https://github.com/marrlab/BaSiC). Cryosectioned samples were imaged using a Nikon A1SI point scanning confocal microscope. For 3D reconstruction, *z* stack images were acquired with a slice thickness of 0.5 μm. Low-magnification brightfield images were acquired using a Labomed TCM 400 inverted microscope equipped with a UCMOS eyepiece camera (Thermo Fisher Scientific). Live imaging was conducted using an inverted epifluorescence microscope (Zeiss Axio Observer Z1; Carl Zeiss MicroImaging) enclosed in an environmental incubator (XL S1 incubator, Carl Zeiss MicroImaging), maintaining the cell culture conditions at 37 °C and 5% CO_2.

Fluorescence intensity maps

Stitched whole-mount immunostaining images of μNTLS were manually rotated to ensure their R–C axes is along the horizontal direction. Transverse images showing D–V patterning of μNTLS were also manually rotated to ensure their D–V axes along the vertical direction.

A custom Matlab script was developed to process fluorescence images of various lineage markers to generate fluorescence intensity maps. In brief, DAPI images were first used to generate binary masks by only selecting pixels in the images for which intensities exceeded 15% of the maximum intensity to outline μNTLS contours. The intensity of cell lineage markers in each pixel within μNTLS contours was then divided by corresponding DAPI intensity. The intensity of pixels outside μNTLS contours was automatically set to 0. The pixel intensity in DAPI-normalized intensity maps was further normalized by the maximum intensity identified in each intensity map.

Normalized fluorescence intensity maps were further converted to rectangular heatmaps. In brief, normalized fluorescence intensity maps were divided into 500 zones with equal lengths along either the R–C or D–V axis. The average pixel intensity in each zone was calculated and displayed in a rectangular region of the same size. In total, 500 rectangular regions displaying the average intensity of each zone were then juxtaposed to form normalized intensity heatmaps. Normalized intensity heatmaps from different μNTLS samples were stacked together to obtain average normalized intensity heatmaps.

NMP differentiation assays

To assess the differentiation potential of NMPs, caudal ends of day 4 μNTLS (approximately 500 μm long) were manually dissected using a surgical scissor and seeded on Geltrex-coated tissue culture plates. To differentiate NMPs into presomitic mesoderm cells, cells from dissected μNTLS tissues were cultured in basal medium supplemented with CHIR (3 μM) and LDN (500 nM) for 4 days[26]. To differentiate NMPs into pMN cells, cells from dissected μNTLS tissues were cultured in basal medium supplemented with SAG (1 μM) and RA (1 μM) for 4 days[27]. The culture medium was replenished every other day.

Validation of the *TBXT*::T2A-Cre human ES cell line

TBXT::T2A-Cre lineage tracer cells were seeded as single cells onto tissue culture plates at a density of 1.5×10^4 cells per cm in mTeSR medium containing Y27632 (10 μM). The culture medium was switched to basal medium supplemented with CHIR (3 μM) and FGF8 (200 ng ml^{-1}) from day 1 to day 3 to promote NMP differentiation. The culture medium was then switched to basal medium supplemented with RA (500 nM) and SAG (500 nM) from day 3 to day 5 to differentiate NMPs into pMN cells. Cells were fixed and immunostained on day 3 and day 5 to examine lineage marker expression.

Ectopic caudalization assay

Following the protocol to generate R–C and D–V patterned μNTLS, from day 5 to day 9, in addition to adding BMP4 (25 ng ml^{-1}) into the top channel and RA (500 nM) and SAG (500 nM) into the bottom channel, the caudalizing factors CHIR (3 μM), FGF8 (200 ng ml^{-1}) and RA (500 nM) were added into the left-side reservoir of the centre channel for ectopic caudalization. From day 9 to day 11, the culture medium in all reservoirs was switched to basal medium to allow continuous NC development. All μNTLS tissues were analysed on day 11.

scRNA-seq

To dissociate μNTLS into single cells, PDMS structural layers were manually detached from glass coverslips to release μNTLS. μNTLS were first cut into small pieces (approximately 500 μm long) using a surgical knife and then incubated with Accutase for 2 h to obtain single cells. To dissociate D–V patterned μFBLS, μFBLS were first detached from PDMS layers before being cut into small pieces (approximately 200 μm long) and incubated with Accutase on an orbital shaker at a speed of 110 r.p.m. for 3 h. For scRNA-seq analysis of μNTLS at different time points, dissociated single cells were collected from the following μNTLS: day 4 μNTLS from 4 microfluidic devices; day 9 μNTLS from 1 microfluidic device; day 11 μNTLS from 1 microfluidic device; and day 21 μNTLS from 1 microfluidic device. For scRNA-seq analysis of day 40 μFBLS, dissociated single cells from 1 microfluidic device was collected. Dissociated single cells were collected into PBS containing 0.5% BSA before centrifuging at 300*g* for 5 min. Resultant cell pellets were re-suspended into single cells in PBS containing 0.5% BSA. Within 1 h after cell dissociation, cells were loaded into a 10x Genomics Chromium system (10x Genomics). 10x Genomics v.3 libraries were prepared according to the manufacturer's instructions. Libraries were then sequenced using paired-end sequencing with a minimum coverage of 20,000 raw reads per cell using an Illumina NovaSeq-6000. scRNA-seq data were aligned and quantified using Cell Ranger Single-Cell software suite (v.3.1.0, 10x Genomics) against *Homo sapiens* (human) genome assembly GRCh38.p13 from ENSEMBL.

Data integration, dimensionality reduction and clustering

Integration and analysis of scRNA-seq data were conducted using the R package Seurat (v.3.0.0.0, https://satijalab.org/seurat/)[62]. Default setups in Seurat were used unless noted otherwise. In brief, each scRNA-seq dataset was filtered based on the total number of genes detected and the percentage of mitochondrial genes. Gene expression was calculated by normalizing raw counts with total counts before multiplying by 10,000 and log-transformed. The top 2,000 highly variable genes were identified for each dataset using FindVariableFeatures. Cell cycle was regressed out based on cell cycle scores using CellCycleScoring during the data-scaling process using ScaleData. PCA analysis (RunPCA) was then performed on filtered data followed by embedding into low-dimensional space with UMAP using RunUMAP. Identification of cell clusters by a shared nearest neighbour modularity optimization-based clustering algorithm was achieved using FindClusters. To integrate multiple scRNA-seq data, count matrices of different data were first filtered and normalized separately before integrating using IntegrateData. The integrated scRNA-seq dataset was then analysed following the standard Seurat pipeline. Annotation of cell clusters was based on the expression of canonical lineage marker genes.

Differentially expressed genes (DEGs) were identified using FindAllMarkers, with a minimal fold difference of 0.25 in the logarithmic scale and >10% detection rate in either of the two cell types under comparison. Dot plots and feature plots were generated using DotPlot and

FeaturePlot in Seurat, respectively. Heatmaps were plotted based on the relative expression (*Z* score) of the top 20 gene signatures to distinguish each cell cluster under comparison. Gene ontology analysis was performed using DAVID Bioinformatics Resources 6.8 based on DEGs referencing the GOTERM_BP_FAT database (Supplementary Table 1).

RNA velocity analysis

FASTQ files generated using the Cell Ranger pipeline were used for RNA velocity analysis. Genome annotations from GRCh38 were used for counting spliced and unspliced mRNA in each single cell. Specifically, loompy fromfq was applied with default arguments, with human genome assembly GRCh38 passed as an annotation. Output loom files comprise both spliced and unspliced mRNA counts. Python package scVelo (v.0.2.2, https://scvelo.readthedocs.io) was then used to perform RNA velocity analysis using dynamical modelling (scv.tl.velocity)[63]. The function 'scv.pl.velocity_embedding_stream' was used to project RNA velocities onto UMAP plots. All default parameters were used unless noted otherwise.

Cell–cell communication analysis

The R package CellChat was used to perform cell–cell communication analysis (http://www.cellchat.org/)[64]. Based on manually curated databases that consider known structural compositions of ligand–receptor interactions, CellChat infers and analyses intercellular communication networks from scRNA-seq data using network analysis and pattern recognition. Specifically, the Seurat object including count matrix and clustering results from integrated scRNA-seq data of day 4, day 9 and day 21 μNTLS was imported to CellChat, with default human database and only secreted signalling pathways from Kyoto Encyclopedia of Genes and Genomes used. Default values were used for all parameters, except that the truncated mean was lowered to 5% to increase algorithm sensitivity.

Gene regulatory network analysis

The regulatory activity of transcription factors associated with specific cell types was assessed using the R package SCENIC (single cell regulatory network inference and clustering, v.1.1.2-2; https://github.com/aertslab/SCENIC), except runGenie3 (ref. 65), with filtered counts of integrated Seurat object used as the input of SCENIC. GRNBoost2 in the Python package Arboreto (https://arboreto.readthedocs.io/en/latest/index.html) was used instead of runGenie3 to infer co-expression modules between transcription factors and candidate target genes. Each co-expression module was then analysed using *cis*-regulatory motif analyses (RcisTarget). Modules with significant motif enrichment of correct upstream regulators were retained. Human motif collection v.9 and cisTarget databases for hg38 were used in the pipeline (https://resources.aertslab.org/cistarget/). All default parameters were used in SCENIC unless noted otherwise.

Comparison with human embryo data

To compare scRNA-seq data of day 4, day 9 and day 21 μNTLS with those of human embryos at CS12–CS16, the development systems 'neural progenitor', 'neuron' and 'neural crest', including the cell clusters 'forebrain', 'midbrain', 'hindbrain', 'spinal cord', 'neocortex intermediate progenitor', 'midbrain Pitx2 neuron', 'GABAergic neuron', 'hindbrain neuron' and 'spinal cord neuron', were isolated from human embryo datasets[42]. In Fig. 3c and Extended Data Fig. 9e, scRNA-seq data of neural cells from human CS12–CS16 datasets were integrated with day 4, day 9 and day 21 μNTLS data using a reciprocal PCA approach based on 30 dimensions and 2,000 anchor features (IntegrateData, Seurat). The top 1,000 variable genes in human CS12–CS16 datasets were then identified, with their average expression among all cells in each Carnegie stage (for PCA analysis) or in each related cell cluster (for correlation analysis) calculated. PCA plots were then generated for human CS12–CS16 datasets and day 4, day 9 and day 21 μNTLS datasets using the prcomp function in the R package Stats. Pearson's correlations between cell clusters from human CS12–CS16 datasets and day 9 and day 21 μNTLS datasets were calculated using the cor function in Stats. In Fig. 3d–f and Extended Data Fig. 9a–d, neural cell data in human CS12 and CS15–CS16 datasets and day 9 and day 21 μNTLS datasets were integrated, respectively, using the reciprocal PCA approach based on 30 dimensions and 2,000 anchor features (IntegrateData, Seurat). Original annotations of human neural cells from the references are used.

Pallium and subpallium cells in D–V patterned μFBLS were compared with their counterparts in developing human brain at 5–14 p.c.w. periods[50]. To compare FB pallium cells from μFBLS and human embryonic tissues, dRG, IP-EN and nEN clusters were extracted from μFBLS data, and cortical clusters expressing *EMX1* were isolated from human FB datasets[50]. To compare FB inhibitory neurons from μFBLS and human embryonic tissues, nIN1, nIN2 and nIN3 clusters were extracted from μFBLS data, and telencephalic clusters expressing *DLX2* were isolated from human FB datasets[50]. Integration of FB pallium or subpallium cells from human brain datasets and μFBLS was achieved by using the reciprocal PCA approach based on 30 dimensions and 2,000 anchor features (IntegrateData, Seurat). PCA plots and Pearson's correlation calculations were generated based on the average expression of the top 1,000 variable genes identified from human pallium or subpallium datasets.

Re-analysis of mouse data

Raw count matrices and metadata of scRNA-seq data from mouse embryos at gastrulation (E6.5–E8.5, https://github.com/MarioniLab/EmbryoTimecourse2018/)[44] and organogenesis (E9.5–E13.5, https://oncoscape.v3.sttrcancer.org/atlas.gs.washington.EdU.mouse.rna/landing)[43] stages were re-analysed. Specifically, mouse datasets were filtered, normalized (NomalizeData) and scaled (ScaleData) following the standard Seurat workflow described above.

In Supplementary Fig. 9, cell clusters from a mouse E8.25 embryo dataset were regrouped compared with their original annotations[44]. Specifically, the neural cluster contains cells from the FB/MB/HB, SC, NC and NMP clusters in the original publication[44]. Similarly, the mesoderm cluster contains cells from the allantois, the anterior primitive streak, cardiomyocytes, the caudal mesoderm, the ExE mesoderm, the intermediate mesoderm, the mesenchyme, the paraxial mesoderm, the pharyngeal mesoderm, the somitic mesoderm and the notochord in the original publication[44]. The endoderm cluster contains cells from the def. endoderm, the ExE endoderm, the visceral endoderm, the parietal endoderm and the gut in the original publication[44]. The blood and endothelial cluster contains cells from blood progenitors 1/2, erythroid 1/2/3, endothelium and haematoendothelial progenitors in the original publication[44]. The nonneural–other cluster contains cells from the PGC and the ExE Ectoderm in the original publication[44]. Cells from mouse E10.5 and E11.5 datasets were annotated following annotations in the original publication[43].

In Supplementary Fig. 10, only neural cell data were extracted from mouse datasets for re-analysis. Specifically, onlyFB/MB/HB, SC and NMP clusters in the mouse E8.25 dataset were extracted. The FB/MB/HB cluster was further subclustered into FB, MB and HB clusters using FindSubClusters in Seurat. In mouse E10.5 and E11.5 datasets, cells from the NT and the NC trajectories were extracted. Normalization, Scaling, PCA, UMAP and cluster analyses were then performed following the standard Seurat workflow to cluster cells into FB, MB, IsO, HB, SC, RP, FP, NC, neuron and oligodendrocyte precursor cell clusters. Annotations of cell clusters are based on expression of canonical lineage marker genes.

Cross-species comparison

To compare scRNA-seq datasets of mouse embryos with those of μNTLS, mouse gene names from raw scRNA-seq data were first mapped to human orthologue gene names using the ensemble R package

biomaRt_2.42.0. In Supplementary Fig. 8, data of neural cells from mouse E7.75–E8.5 datasets were integrated with day 4 μNTLS data using the reciprocal PCA approach based on 30 dimensions and 2,000 anchor features (IntegrateData, Seurat). Using the same approach, neural cell data from mouse E9.5–E12.5 datasets were integrated with day 9 and day 21 μNTLS data. The top 1,000 variable genes in mouse E7.75–E8.5 and E9.5–E12.5 datasets were then identified, with their average expression among all cells in each related sample (for PCA analysis) or in each related cell cluster (for correlation analysis) calculated. In Supplementary Fig. 9, whole mouse embryo E8.25, E10.5 and E11.5 datasets and day 4, day 9 and day 21 μNTLS data were integrated, respectively, using the reciprocal PCA approach based on 30 dimensions and 2,000 anchor features (IntegrateData, Seurat). In Supplementary Fig. 10, neural cell data from mouse E8.25, E10.5 and E11.5 datasets and day 4, day 9 and day 21 μNTLS data were integrated, respectively, using the reciprocal PCA approach based on 30 dimensions and 2,000 anchor features (IntegrateData, Seurat).

Subclustering of FB, SC, neuron and NC clusters

For subcluster analysis of FB and neuron clusters, cells in each cluster were extracted from the day 21 μNTLS dataset. The top 2,000 highly variable genes were identified for each cluster using the FindVariableFeatures. FB and neuron clusters in day 9 or day 21 μNTLS data were then projected onto the UMAP of telencephalon and neuron clusters from CS12 or CS15–CS16 human embryo data (reference data)[42], respectively, and annotated based on reference data using MapQuery.

For subcluster analysis of cells associated with the SC, in addition to cells in the SC cluster, cells in the RP and FP clusters that express *HOX4–HOX13* were extracted from integrated datasets of day 4, day 9 and day 21 μNTLS. The data were then processed following the default setups in Seurat. The average expression of canonical markers associated with different D–V domains of the SC was calculated using AddModuleScore.

For subcluster analysis of the NC cluster, cells in the NC cluster were extracted from integrated datasets of day 4, day 9 and day 11 μNTLS. Cells that express the dorsal NT marker *PAX7* in day 4 μNTLS data were also extracted. Extracted cells were then analysed using Seurat, similar to subclustering analysis of the SC cluster.

Trajectory inference and pseudotime analysis of cranial NC cells and μFBLS

The R package Slingshot was used for trajectory inference (https://github.com/kstreet13/slingshot)[66]. Slingshot identifies global lineage structure with a cluster-based minimum spanning tree and fitted simultaneous principal curves to describe lineage development. For trajectory inference of *HOX*⁻ cranial NC cells, the cells were extracted from integrated day 4, day 9 and day 11 NC datasets based on their negative expression of any HOX family genes. Subclusters of *HOX*⁻ cranial NC cluster identified using UMAP in Seurat were used as input to Slingshot. The premigratory NC subcluster was arbitrarily assigned as the starting cell state. For trajectory inference of day 40 D–V patterned μFBLS, dRG and vRG clusters were assigned as starting cell states. To identify DEGs along pseudotime, a test for significant associations between gene expression and pseudotime was conducted using associationTest. To visualize gene expression dynamics, the expression levels of selected genes were first fitted onto principal curves and then plotted as a function of pseudotime using plotSmoothers. Smoothened expression patterns of all DEGs were plotted along pseudotime as heatmaps using predictSmooth and pheatmap.

Batch-to-batch comparison of μNTLS

To compare transcriptome profiles of day 9 μNTLS generated from two different batches, scRNA-seq data of day 9 μNTLS from the two batches were filtered and processed based on the same criteria before their integration using the reciprocal PCA approach based on 30 dimensions and 2,000 anchor features (IntegrateData, Seurat). Scaling, PCA and UMAP analyses were performed using Seurat on the integrated dataset. Cell clusters were identified using FindClusters. Mutual information (MI) score, which represents the dependence between clusters and the individual, was calculated using the R package MPMI[4]. The *Z* score, which represents the divergence of the MI score from its mean score expected at random, was calculated by creating background distributions for each dataset by permuting cluster assignments and re-calculating the MI score 1,000 times[4]. A dot plot was generated using DotPlot, and a heatmap was plotted based on relative expression (*Z* score) of the top 20 gene signatures to distinguish each cell cluster under comparison.

Statistics

All experiments were conducted in at least three biological replicates, except scRNA-seq assays, which were performed in one independent experiment for day 4 and day 21 μNTLS and day 40 μFBLS and in two independent experiments for day 9 μNTLS. Sample sizes are indicated in the figure legends. For comparisons between two datasets, *P* values were calculated using two-sided Student's *t*-test (Origin). For comparisons between multiple datasets, *P* values were calculated using one-way analysis of variance followed by Tukey's multiple comparison test (Origin). No statistical methods were used to predetermine sample size. Sample were randomly allocated to different experimental groups. Investigators were not blinded to allocation during experiments and outcome assessment.

Reporting summary

Further information on research design is available in the Nature Portfolio Reporting Summary linked to this article.

Data availability

Data supporting findings of this study are available within the article and its Supplementary Information. scRNA-seq data supporting this results of this study have been deposited into the Gene Expression Omnibus (GEO) database with accession number GSE194225. Mouse embryo scRNA-seq data are from the GEO (GSE87038 and GSE119945). Human embryo scRNA-seq data are from GEO (GSE157329). Developing human brain scRNA-seq data are from the Linnarsson Laboratory GitHub site. Source data are provided with this paper.

Code availability

Custom R, Python and Matlab scripts are used in this work. They are not central to the conclusions of the paper. These codes are available from the corresponding author upon request.

51. Muncie, J. M. et al. Mechanical tension promotes formation of gastrulation-like nodes and patterns mesoderm specification in human embryonic stem cells. *Dev. Cell* **55**, 679–694 (2020).
52. Kumar, N. et al. The lineage-specific transcription factor CDX2 navigates dynamic chromatin to control distinct stages of intestine development. *Development* **146**, dev172189 (2019).
53. Bayerl, J. et al. Principles of signaling pathway modulation for enhancing human naive pluripotency induction. *Cell Stem Cell* **28**, 1549–1565 (2021).
54. Cong, L. et al. Multiplex genome engineering using CRISPR/Cas systems. *Science* **339**, 819–823 (2013).
55. Chen, Y. et al. Engineering human stem cell lines with inducible gene knockout using CRISPR/Cas9. *Cell Stem Cell* **17**, 233–244 (2015).
56. Hermann, M. et al. Binary recombinase systems for high-resolution conditional mutagenesis. *Nucleic Acids Res.* **42**, 3894–3907 (2014).
57. Chu, L.-F. et al. Single-cell RNA-seq reveals novel regulators of human embryonic stem cell differentiation to definitive endoderm. *Genome Biol.* **17**, 173 (2016).
58. Cudré-Mauroux, C. et al. Lentivector-mediated transfer of Bmi-1 and telomerase in muscle satellite cells yields a Duchenne myoblast cell line with long-term genotypic and phenotypic stability. *Hum. Gene Ther.* **14**, 1525–1533 (2003).
59. Li, X. et al. Desktop aligner for fabrication of multilayer microfluidic devices. *Rev. Sci. Instrum.* **86**, 075008 (2015).

60. Watanabe, K. et al. A ROCK inhibitor permits survival of dissociated human embryonic stem cells. *Nat. Biotechnol.* **25**, 681–686 (2007).
61. Serra, D. et al. Self-organization and symmetry breaking in intestinal organoid development. *Nature* **569**, 66–72 (2019).
62. Butler, A., Hoffman, P., Smibert, P., Papalexi, E. & Satija, R. Integrating single-cell transcriptomic data across different conditions, technologies, and species. *Nat. Biotechnol.* **36**, 411–420 (2018).
63. La Manno, G. et al. RNA velocity of single cells. *Nature* **560**, 494–498 (2018).
64. Jin, S. et al. Inference and analysis of cell–cell communication using CellChat. *Nat. Commun.* **12**, 1088 (2021).
65. Aibar, S. et al. SCENIC: single-cell regulatory network inference and clustering. *Nat. Methods* **14**, 1083–1086 (2017).
66. Street, K. et al. Slingshot: cell lineage and pseudotime inference for single-cell transcriptomics. *BMC Genomics* **19**, 477 (2018).
67. Delile, J. et al. Single cell transcriptomics reveals spatial and temporal dynamics of gene expression in the developing mouse spinal cord. *Development* **146**, dev173807 (2019).

Acknowledgements We thank A. Tsakiridis, V. Wilson, A. Martinez Arias, B. Allen, J. M. Parent, S. O'Shea, D. M. Wellik, A. M. Tidball, D. M. Martin and Y. Zhai for their comments; J. N. Lakins and V. M. Weaver for providing the Brachyury–mNeonGreen human ES cell reporter line; M. Povolotski for helping with PCR genotyping; and staff at the Michigan Medicine Microscopy Core for training and support in microscopy imaging, the Michigan Orthopaedic Research Laboratories Histology Core for support in cryosectioning, the Michigan Advanced Genomics Core for scRNA-seq service, and the Michigan Lurie Nanofabrication Facility for support in microfabrication. This work is supported by the Michigan-Cambridge Collaboration Initiative (J.F.), the University of Michigan Mcubed Fund (J.F.), the 21st Century Jobs Trust Fund received through the Michigan Strategic Fund from the State of Michigan (Grant CASE-315037; J.F.), a University of Michigan Mid-career Biosciences Faculty Achievement Recognition Award (J.F.), the Dr. Miriam and Sheldon G. Adelson Medical Research Foundation (G.-L.M.), the National Science Foundation of the United States (I-Corps 2112458 and CBET 1901718 to J.F.), and the National Institutes of Health of the United States (R21 NS113518, R01 GM143297 and R01 NS129850 to J.F.; R21 NS127983 to J.F. and O.R.; R35 NS097370 and RF1 MH123979 to G.-L.M.; and R35 NS116843 to H.S.). N.K. is partially supported by the Uehara Memorial Foundation and International Medical Research Foundation of Japan. O.R. is the incumbent of the Berstein–Mason Professorial Chair of Neurochemistry at the Weizmann Institute of Science.

Author contributions X.X. and J.F. conceived and initiated the project. X.X. designed, performed and quantified most experiments, including scRNA-seq data analyses and interpretation. Y.S.K. generated the *TBXT*::T2A-Cre lineage tracing human ES cell line. A.-I.P.-A. generated the *TBXT* KO human ES cell line. R.O. assisted in developing the μFBLS culture protocol and performed iDISCO whole-mount immunostaining of μFBLS. N.K. and R.Y.T. generated H2B-GFP *CDX2* KO human ES cells. Y.-H.T. and J.R.S. provided the *CDX2* KO human ES cell line. R.Z.Y. developed Matlab scripts for image processing and independently repeated experiments. Y.Z. helped with scRNA-seq data analyses. S.S. helped with chemical perturbation assays. Y.L., F.C.K.W., A.S., G.-L.M., H.S. and O.R. helped with data interpretation and experimental designs. X.X. and J.F. wrote the manuscript. J.F. supervised the study. All authors edited and approved the manuscript.

Competing interests The University of Michigan, Ann Arbor, has filed a patent application describing microfluidic devices and methods for the development of NT-like tissues and neural spheroids (PCT/US2021/058090), with J.F. and X.X. as co-inventors. The other authors declare no competing interests.

Additional information

Supplementary information The online version contains supplementary material available at https://doi.org/10.1038/s41586-024-07204-7.

Correspondence and requests for materials should be addressed to Jianping Fu.

Peer review information *Nature* thanks Madeline Lancaster and the other, anonymous, reviewer(s) for their contribution to the peer review of this work.

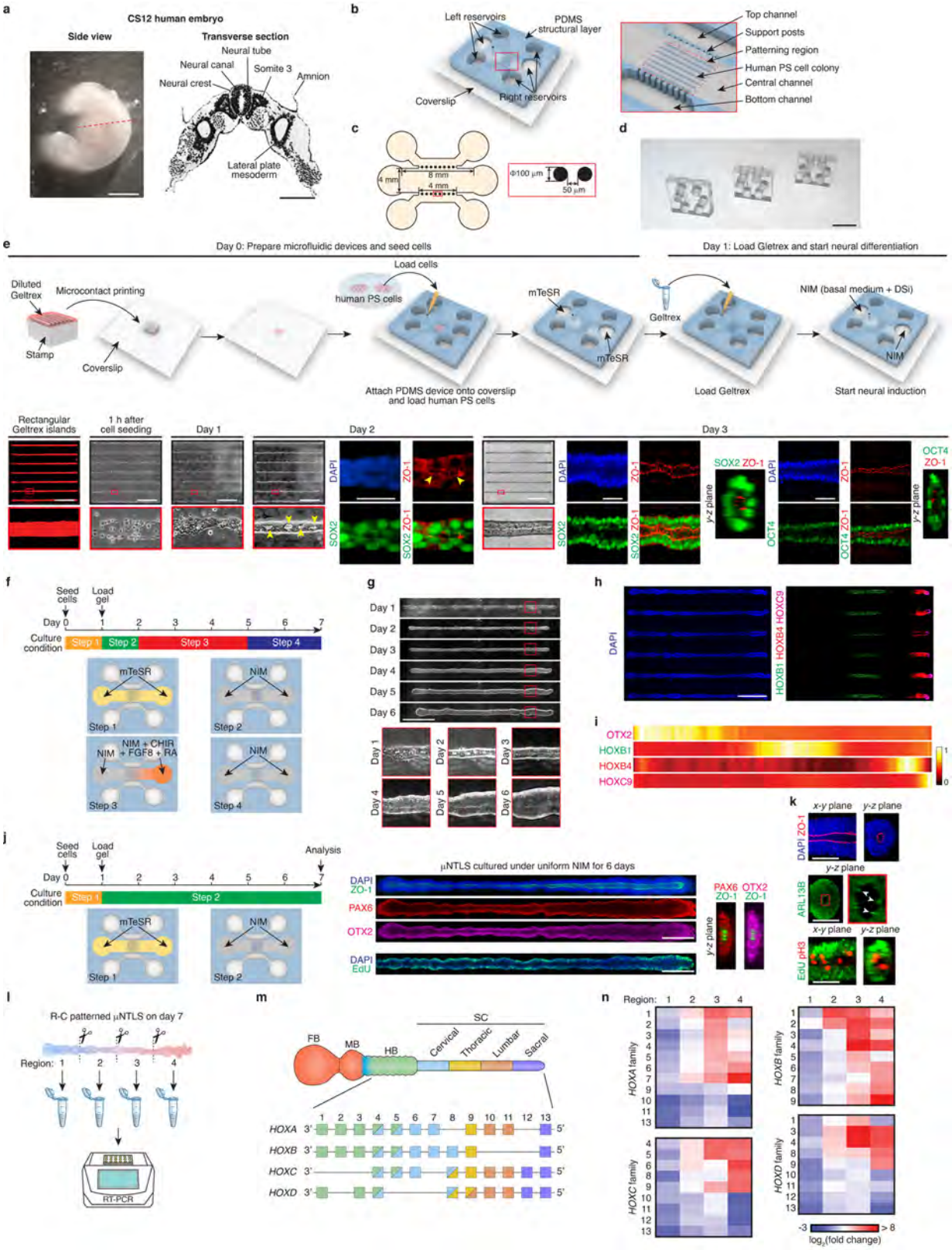

Extended Data Fig. 1 | See next page for caption.

Extended Data Fig. 1 | Development of *R-C* patterned μNTLS. a. (Left) Side view of a Carnegie Stage (CS) 12 human embryo, showing its head-to-tail length of about 4 mm. Image reproduced from ref. 42, Springer Nature Limited. During human embryogenesis, both rostral and caudal neuropores close at around CS12, leading to a completely closed NT structure at around CS12[11]. (Right) Transverse sectional image of a CS12 human embryo through somite 3, marked by the dashed red line shown on the left. Image reproduced from the Endowment for the Human Development website (https://www.ehd.org), with permission from R. F. Gasser (1975), all rights reserved. Height of NT along the *D-V* axis is about 200 μm. **b**. Schematic of microfluidic device, containing top, central, and bottom microchannels, with both ends of each channel connected with medium reservoirs. In the device center marked by a red rectangle, the three channels are separated by two linear arrays of circular support posts, which defines a patterning region in the central channel marked by a dashed red rectangle. Within the patterning region, stable gradients of chemical signals are established along the length of the central channel (R-C axis) by supplementing different concentrations of chemical factors in the two reservoirs of the central channel. Similarly, through passive diffusion from the top and bottom channels, stable gradients of dorsalizing and ventralizing factors are established perpendicular to the central channel (D-V axis). In the schematic, an array of rectangular colonies of human PS cells is formed in the patterning region. **c**. Microfluidic device design. All microchannels have a height of 150 μm. Central channel has a width of 4 mm. Circular support posts have a diameter of 100 μm and an edge-to-edge distance of 50 μm. Patterning region in the central channel is defined by a 4 mm × 4 mm square as indicated in **b**. **d**. Photograph showing microfluidic devices generated through batch fabrication. **e**. Schematics and brightfield and confocal images showing microcontact printing to generate rectangular Geltrex adhesive islands, microfluidic device assembly, cell and gel loading into the device, and lumenogenesis of human PS cell colonies to form μNTLS. Specifically, rectangular Geltrex adhesive islands (length: 4 mm; width: 100 μm) are printed onto a coverslip using microcontact printing with a polydimethylsiloxane (PDMS) stamp. A PDMS structural layer is then attached onto the coverslip with Geltrex islands aligned with the patterning region of the central channel. On day 0, dissociated single human PS cells are loaded into the central channel and allowed to adhere to Geltrex islands. One hour after cell seeding, floating human PS cells not attached to Geltrex islands are flushed away gently. On day 1, 100% Geltrex is loaded into the central channel, and a neural induction medium (NIM), comprising basal medium and dual SMAD inhibitors (DSi; see **Methods**), is added into the two medium reservoirs of the central channel. Colonies of human PS cells self-organize and undergo lumenogenesis, with small lumens, demarcated by ZO-1, emerging on day 2 (see Supplementary Video 1). These lumens grow over time and coalesce with each other. By day 3, human PS cell colonies, which still express OCT4, form an elongated tubular structure containing a single continuous, central apical lumen. Zoom-in views of some marked regions are provided. Arrowheads mark small apical lumens demarcated by ZO-1. **f**. Protocol for generating R-C patterned μNTLS. Human PS cells are seeded into the central channel on day 0 using mTeSR (Step 1). After gel loading on Day 1, culture medium in the central channel is switched to NIM (Step 2). From day 2 to day 5, CHIR99021 (CHIR, 3 μM), FGF8 (200 ng mL^{-1}) and retinoic acid (RA, 500 nM) are added into the right reservoir of the central channel in addition to NIM (Step 3). From day 5 to day 7, all caudalizing factors are removed, and only NIM is added into the two medium reservoirs of the central channel (Step 4). **g**. Representative brightfield images showing a single μNTLS on different days as indicated. Zoom-in views of a marked region are provided. **h**. Representative stitched confocal images showing an array of R-C patterned μNTLS on day 7 from a single microfluidic device stained for HOXB1, HOXB4, and HOXC9. **i**. Intensity maps showing relative mean expression levels of indicated markers as a function of relative R-C position in R-C patterned μNTLS on day 7. $n_{OTX2} = 12$, $n_{HOXB1} = 22$, $n_{HOXB4} = 22$, $n_{HOXC9} = 12$, and $n_{experiment} = 3$. **j**. (Left) Protocol for generating μNTLS with a default dorsal forebrain identity. human PS cells are seeded into the central channel on day 0 using mTeSR (Step 1). After gel loading on Day 1, culture medium is switched to NIM from Day 1 onwards (Step 2). μNTLS are analyzed on Day 7. (Right) Representative stitched confocal micrographs showing μNTLS on Day 7 stained for ZO-1, PAX6, OTX2, and EdU, as indicated. Micrographs on the right show *y-z* planes of selected regions in μNTLS. **k**. Representative confocal micrographs showing *x-y* and *y-z* planes of selected regions in R-C patterned μNTLS on day 7 stained for ZO-1, ADP-ribosylation factor-like protein 13B (*ARL 13B*), EdU, and phospho-histone H3 (pH3), respectively. Arrowheads mark ARL 13B-enriched cilia on μNTLS apical surfaces. **l**. Schematic showing dissection of R-C patterned μNTLS on day 7 using a surgical scissor into four tissue segments of equal lengths for downstream RT-qPCR analysis. **m**. Dorsal view of human NT and expression pattern of *HOX* family genes in HB and SC. Color coding of *HOX* family genes represents their expression domains along the R-C axis of NT. **n**. Heatmaps showing normalized expression of *HOX* family genes as a function of the four segments of day 7 R-C patterned μNTLS. $n = 3$ experiments. In **e**, **h**, **j** and **k**, nuclei were counterstained with DAPI. In **e**, **g**, **h**, **j** and **k**, experiments are repeated three times with similar results. Scale bars, 1 mm (side view image in **a**), 200 μm (transverse section image in **a**), 15 mm (**d**), 1 mm (whole μNTLS array images in **e**), 50 μm (zoom-in images in **e**), 800 μm (**g** and **h**), 400 μm (**j**), and 150 μm (**k**).

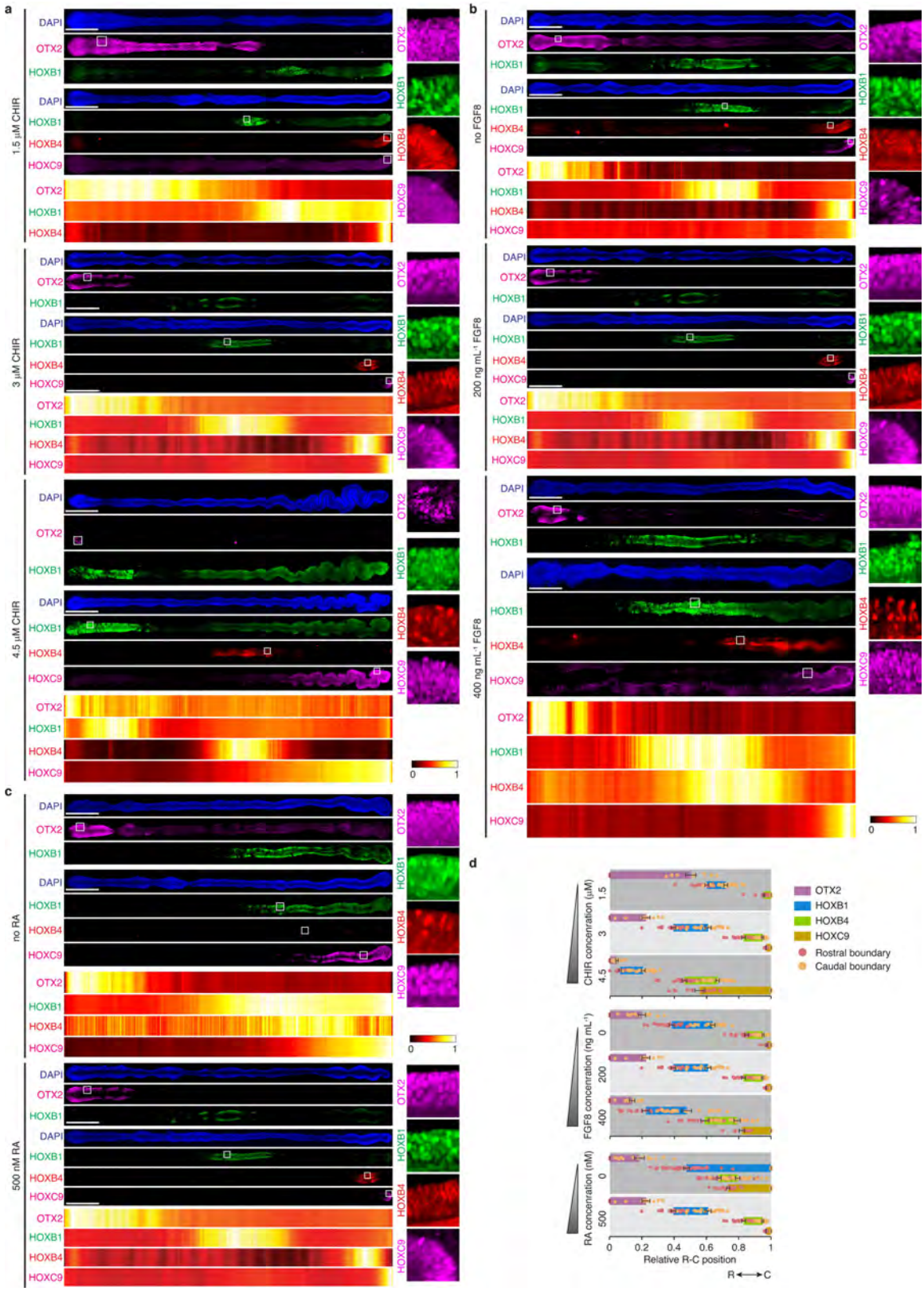

Extended Data Fig. 2 | See next page for caption.

Extended Data Fig. 2 | Effect of morphogen dosages on R-C patterning of μNTLS. a. Representative stitched confocal micrographs showing R-C patterned μNTLS on day 7 under different concentrations of CHIR as indicated, stained for OTX2, HOXB1, HOXB4, and HOXC9. Concentrations of RA and FGF8 were kept the same as 500 nM and 200 ng mL^{-1}, respectively. Zoom-in views of boxed regions are shown on the right. Intensity maps depict relative mean values of indicated markers as a function of relative R-C position in μNTLS. For 1.5 μM CHIR, $n_{OTX2} = 12$, $n_{HOXB1} = 30$, $n_{HOXB4} = 30$, $n_{HOXC9} = 18$, and $n_{experiment} = 3$; For 3 μM CHIR, $n_{OTX2} = 12$, $n_{HOXB1} = 22$, $n_{HOXB4} = 22$, $n_{HOXC9} = 12$, and $n_{experiment} = 3$; For 4.5 μM CHIR, $n_{OTX2} = 14$, $n_{HOXB1} = 28$, $n_{HOXB4} = 28$, $n_{HOXC9} = 14$, and $n_{experiment} = 3$. **b**. Representative stitched confocal micrographs showing R-C patterned μNTLS on day 7 under different concentrations of FGF8 as indicated, stained for OTX2, HOXB1, HOXB4, and HOXC9. Concentrations of CHIR and RA were kept the same as 3 μM and 500 nM, respectively. Zoom-in views of boxed regions are shown on the right. Intensity maps depict relative mean values of indicated markers as a function of relative R-C position in μNTLS. For without FGF8, $n_{OTX2} = 13$, $n_{HOXB1} = 25$, $n_{HOXB4} = 25$, $n_{HOXC9} = 12$, and $n_{experiment} = 3$; For 200 ng mL^{-1} FGF8, $n_{OTX2} = 12$, $n_{HOXB1} = 22$, $n_{HOXB4} = 22$, $n_{HOXC9} = 12$, and $n_{experiment} = 3$; For 400 ng mL^{-1} FGF8, $n_{OTX2} = 10$, $n_{HOXB1} = 20$, $n_{HOXB4} = 20$, $n_{HOXC9} = 10$, and $n_{experiment} = 2$. **c**. Representative stitched confocal micrographs showing R-C patterned μNTLS on day 7 treated with or without RA as indicated, stained for OTX2, HOXB1, HOXB4, and HOXC9. Concentrations of CHIR and FGF8 were kept the same as 3 μM and 200 ng mL^{-1}, respectively. Zoom-in views of boxed regions are shown on the right. Intensity maps depict relative mean values of indicated markers as a function of relative R-C position in μNTLS. For without RA, $n_{OTX2} = 14$, $n_{HOXB1} = 39$, $n_{HOXB4} = 39$, $n_{HOXC9} = 25$, and $n_{experiment} = 3$; For 500 nM RA, $n_{OTX2} = 12$, $n_{HOXB1} = 22$, $n_{HOXB4} = 22$, $n_{HOXC9} = 12$, and $n_{experiment} = 3$. **d**. Plot showing relative R-C positions of OTX2$^+$, HOXB1$^+$, HOXB4$^+$, and HOXC9$^+$ domains in R-C patterned μNTLS on day 7 under indicated conditions. Rostral and caudal ends of μNTLS are designated as 0 and 1, respectively. Error bars represent mean ± s.e.m. *n* values are provided in **a**-**c**. In **a**-**c**, nuclei were counterstained with DAPI. Scale bars, 400 μm.

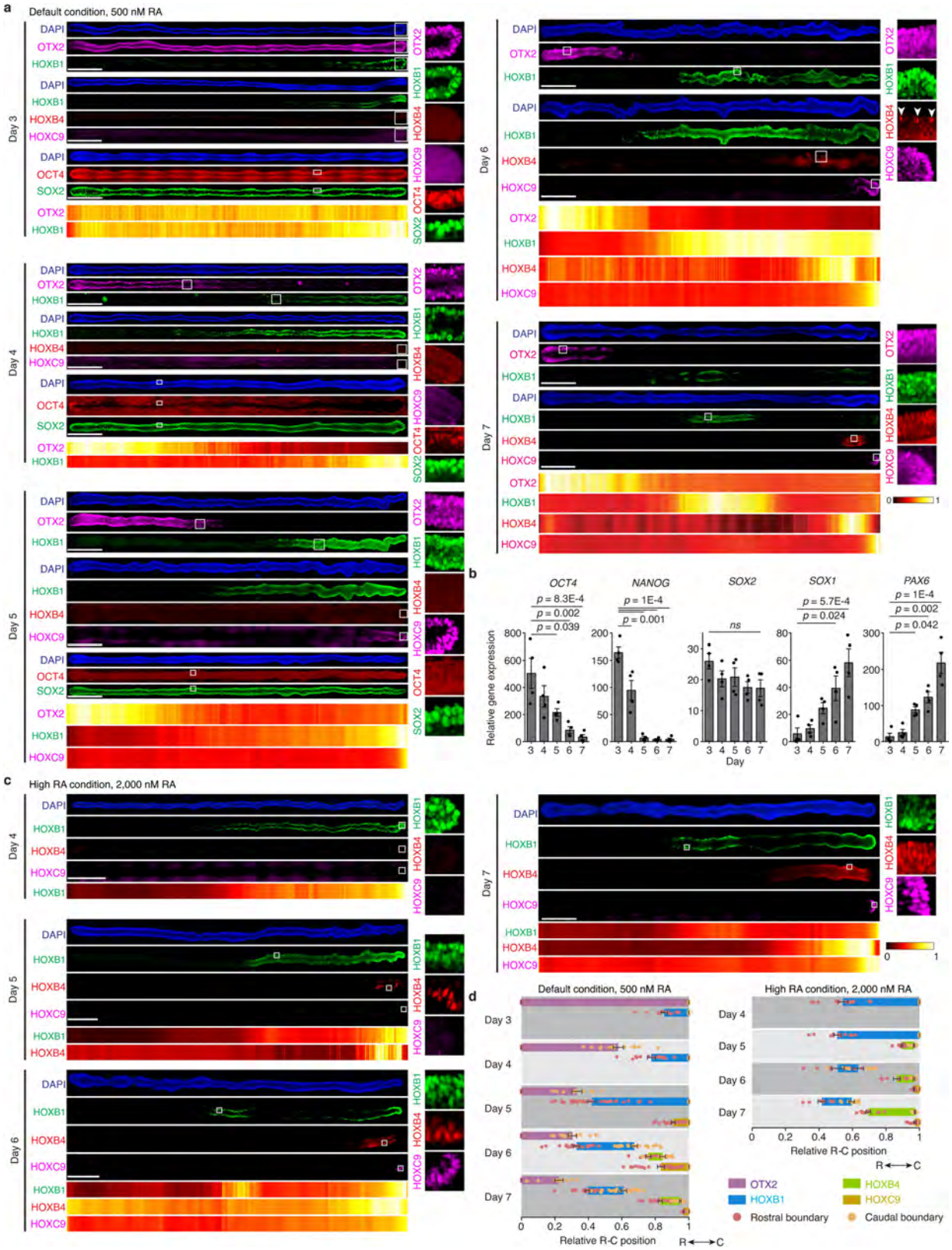

Extended Data Fig. 3 | See next page for caption.

Extended Data Fig. 3 | Dynamic HOX gene expression in R-C patterned μNTLS. a. Representative stitched confocal micrographs showing μNTLS on different days developed under default caudalizing condition (3 μM CHIR, 500 nM RA, and 200 ng mL^{-1} FGF8) stained for OTX2 and HOXB1, HOXB1, HOXB4, and HOXC9, and OCT4 and SOX2, respectively. Zoom-in views of boxed regions are shown on the right. Arrowheads mark nuclear staining of HOXB4 in day 6 μNTLS. Intensity maps depict relative mean expression levels of indicated markers as a function of relative R-C position in μNTLS. For intensity maps, on day 3, $n_{OTX2} = 15$, $n_{HOXB1} = 15$, and $n_{experiment} = 3$; on day 4, $n_{OTX2} = 15$, $n_{HOXB1} = 15$, and $n_{experiment} = 3$; on day 5, $n_{OTX2} = 10$, $n_{HOXB1} = 31$, $n_{HOXC9} = 21$, and $n_{experiment} = 3$; on day 6, $n_{OTX2} = 13$, $n_{HOXB1} = 23$, $n_{HOXB4} = 11$, $n_{HOXC9} = 27$, and $n_{experiment} = 3$; on day 7, $n_{OTX2} = 12$, $n_{HOXB1} = 22$, $n_{HOXB4} = 22$, $n_{HOXC9} = 12$, and $n_{experiment} = 3$. **b**. Plots showing expression levels of *OCT4*, *NANOG*, *SOX1/2*, and *PAX6* in R-C patterned μNTLS as a function of time. Error bars represent mean ± s.e.m. $n_{experiment} = 4$ for *OCT4*, *NANOG*, *SOX1/2*, and *PAX6*. One-way ANOVA tests were performed, followed by Tukey's multiple comparison tests to calculate *p* values. **c**. Representative stitched confocal micrographs showing μNTLS development under high RA condition (3 μM CHIR, 2,000 nM RA, and 200 ng mL^{-1} FGF8) on different days stained for HOXB1, HOXB4, and HOXC9. Zoom-in views of boxed regions are shown on the right. Intensity maps depict relative mean expression levels of indicated markers as a function of relative R-C position in μNTLS. For intensity maps, on day 4, $n_{HOXB1} = 14$ and $n_{experiment} = 3$; on day 5, $n_{HOXB1} = 13$, $n_{HOXB4} = 13$, and $n_{experiment} = 3$; on day 6, $n_{HOXB1} = 9$, $n_{HOXB4} = 9$, $n_{HOXC9} = 9$, and $n_{experiment} = 3$; on day 7, $n_{HOXB1} = 9$, $n_{HOXB4} = 12$, $n_{HOXC9} = 15$, and $n_{experiment} = 3$. **d**. Plots showing relative R-C positions of $OTX2^+$, $HOXB1^+$, $HOXB4^+$, and $HOXC9^+$ domains in R-C patterned μNTLS under default (left) and high RA (right) conditions as a function of time. Rostral and caudal ends of μNTLS are designated as 0 and 1, respectively. Error bars represent mean ± s.e.m. *n* values are provided in **a** & **c**. In **a** and **c**, nuclei were counterstained with DAPI. Scale bars, 400 μm.

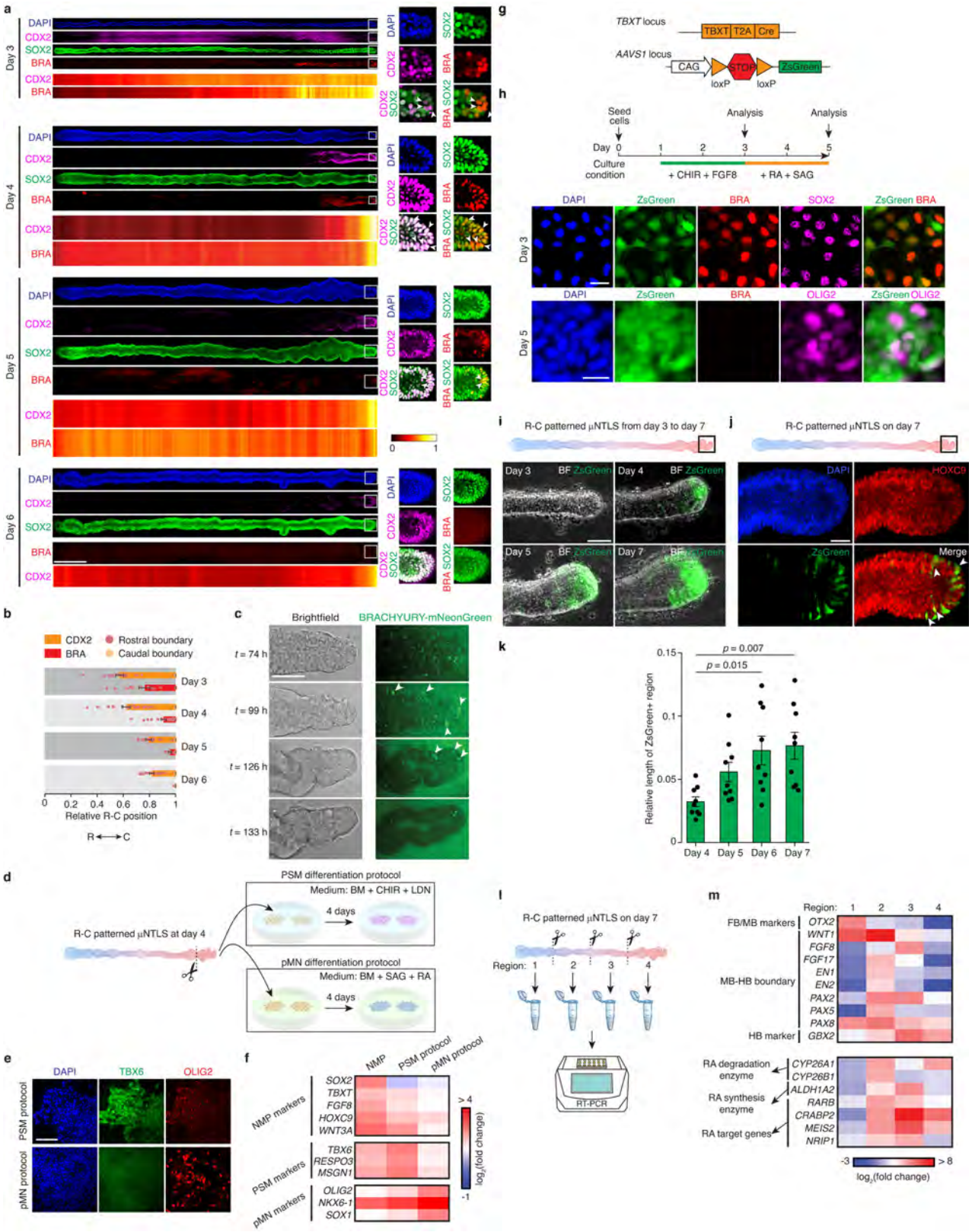

Extended Data Fig. 4 | See next page for caption.

Extended Data Fig. 4 | Development of neuromesodermal progenitors (NMPs) and secondary organizers in R-C patterned μNTLS. a. Representative stitched confocal micrographs showing μNTLS on different days stained for SOX2, CDX2, and BRACHYURY (BRA). Zoom-in views of μNTLS caudal ends are shown on the right, with arrowheads marking SOX2+BRA+ NMPs. Intensity maps depict relative mean expression levels of indicated markers as a function of relative R-C position in μNTLS. n_{colony} = 15, 20, 14, and 14 for day 3, day 4, day 5, and day 6, respectively. $n_{experiment}$ = 3. **b**. Plot showing relative R-C positions of CDX2+ and BRA+ domains in μNTLS as a function of time. Rostral and caudal ends of μNTLS are designated as 0 and 1, respectively. Error bars represent mean ± s.e.m. *n* values are provided in **a**. **c**. Live imaging with a BRACHYURY-mNeonGreen human ES cell reporter line to track dynamic BRACHYURY expression at μNTLS caudal ends. Arrowheads mark BRACHYURY-mNeonGreen$^+$ cells. Experiments were repeated three times with similar results. See Supplementary Video 3. **d**. Protocols for deriving presomitic mesodermal (PSM) and motor neuron progenitor (pMN) cells from cells isolated from caudal ends of day 4 μNTLS. Caudal regions of day 4 μNTLS were physically dissected using a surgical scissor and were re-plated and cultured under PSM or pMN differentiation protocols for another 4 days as indicated. For PSM differentiation, basal medium (BM) is supplemented with CHIR (3 μM) and LDN (500 nM). For pMN differentiation, BM is supplemented with Smoothened Agonist (SAG, SHH agonist; 1 μM) and RA (1 μM). **e**. Representative confocal micrographs showing cell colonies after 4 days of culture under PSM or pMN differentiation protocols as indicated. Cells were stained for PSM marker TBX6 and pMN marker OLIG2. Experiments were repeated three times with similar results. **f**. RT-qPCR analysis of caudal regions of day 4 R-C patterned μNTLS, which contain NMPs, and cells cultured for 4 days under either PSM differentiation protocol (PSM protocol) or pMN differentiation protocol (pMN protocol). Heatmaps show normalized expression of NMP, PSM, and pMN markers as indicated. *n* = 4 experiments. **g**. Schematic showing generation of a *TBXT*::T2A-Cre lineage tracer hESC line. **h**. (Top) Protocol for deriving NMPs from *TBXT*::T2A-Cre lineage tracer cells followed by pMN induction. *TBXT*::T2A-Cre lineage tracer cells were seeded as single cells onto culture dishes at a density of 1.5×10^4 cells cm^{-2} in mTeSR containing Y27632 (10 μM). Culture medium was switched to basal medium supplemented with CHIR (3 μM) and FGF8 (200 ng mL^{-1}) from day 1 to day 3 to promote NMP differentiation. From Day 3 to Day 5, culture medium was switched to basal medium supplemented with RA (500 nM) and SAG (500 nM) to induce pMN differentiation. (Bottom) Representative confocal micrographs showing cells on Day 3 stained for BRA and SOX2 and on Day 5 stained for BRA and OLIG2, respectively. Experiments were repeated three times with similar results. **i**. Live imaging with the *TBXT*::T2A-Cre lineage tracer to track dynamic NMP development at μNTLS caudal ends between day 3 and day 7. Experiments were repeated three times with similar results. See Supplementary Video 4. **j**. Representative confocal micrographs showing caudal ends of day 7 R-C patterned μNTLS generated from the *TBXT*::T2A-Cre lineage tracer, stained for HOXC9. White arrowheads mark ZsGreen$^+$HOXC9$^+$ cells. Experiments were repeated three times with similar results. **k**. Plot showing relative length of ZsGreen$^+$ domains in R-C patterned μNTLS as a function of time. Length of ZsGreen$^+$ domain is normalized by the total length of μNTLS. Error bars represent mean ± s.e.m. n_{colony} = 9 and $n_{experiment}$ = 3. One-way ANOVA tests were performed, followed by Tukey's multiple comparison tests to calculate *p* values. **l**. Schematic showing dissection of day 7 R-C patterned μNTLS using a surgical scissor into four tissue segments of equal lengths for downstream RT-qPCR analysis. **m**. Heatmaps showing normalized expression of FB, MB, HB, and MB-HB boundary markers and genes related to RA signaling, as a function of the four segments of day 7 μNTLS. *n* = 3 experiments. In **a**, **e**, **h** and **j**, nuclei were counterstained with DAPI. Scale bars, 400 μm (**a**), 100 μm (**c** and **e**), and 50 μm (**h**, **i** and **j**).

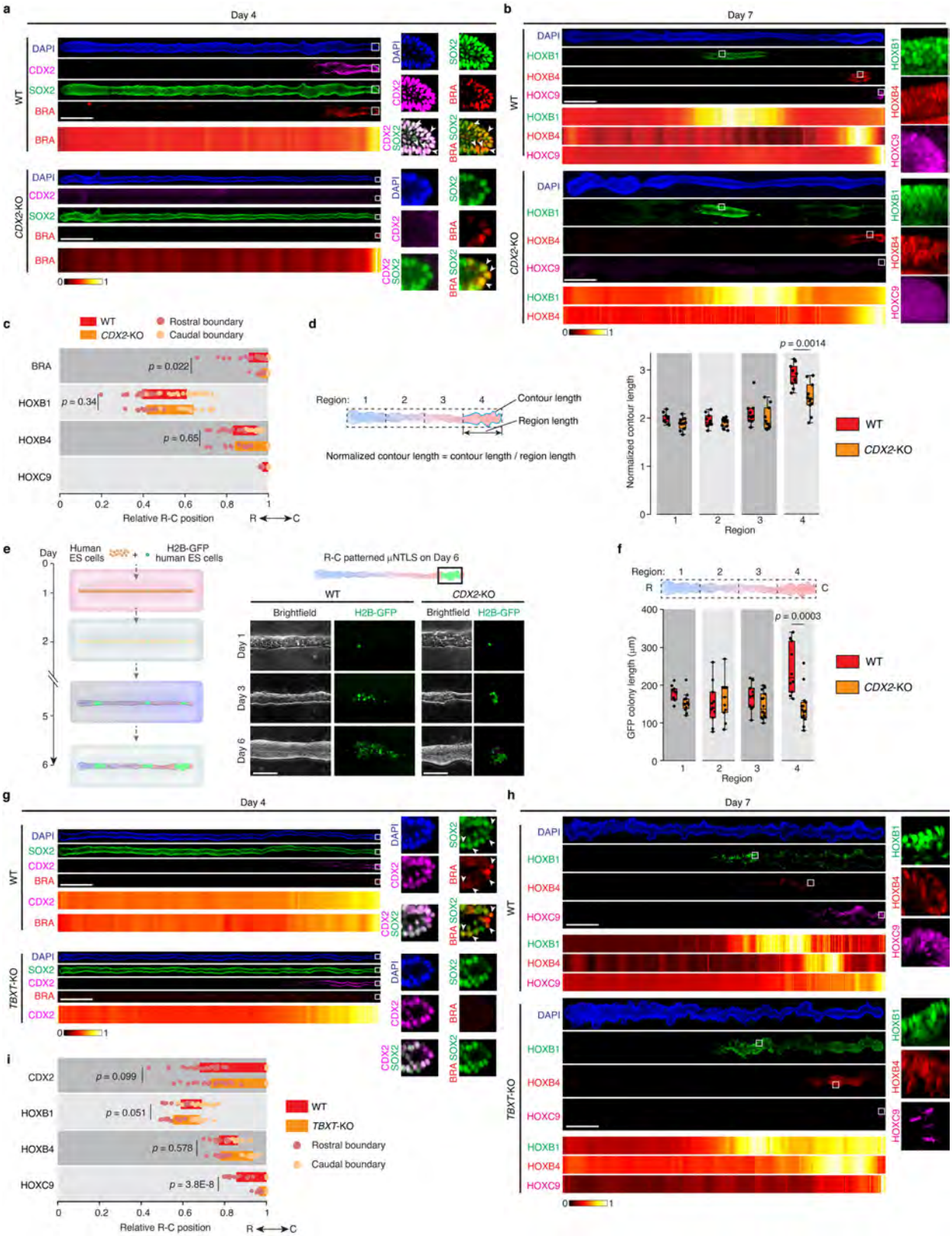

Extended Data Fig. 5 | See next page for caption.

Extended Data Fig. 5 | Roles of *CDX2* and *TBXT* in R-C patterning of μNTLS. **a**. Representative stitched confocal micrographs showing R-C patterned μNTLS on day 4, generated from wild type (WT) or *CDX2*-knockout (*CDX2*-KO) H9 human ES cell lines as indicated, stained for SOX2, CDX2, and BRACHYURY (BRA). Zoom-in views of boxed regions are shown on the right. Intensity maps depict relative mean values of indicated markers as a function of relative R-C position in μNTLS. White arrowheads mark $SOX2^+BRA^+$ NMPs. $n \geq 2$ experiments for each condition. For WT, $n_{colony} = 20$ and $n_{experiment} = 3$; for *CDX2*-KO, $n_{colony} = 14$ and $n_{experiment} = 2$. **b**. Representative stitched confocal micrographs showing R-C patterned μNTLS on day 7, generated from WT or *CDX2*-KO H9 human ES cell lines as indicated, stained for HOXB1, HOXB4, and HOXC9. Zoom-in views of boxed regions are shown on the right. Intensity maps depict relative mean values of indicated markers as a function of relative R-C position in μNTLS. $n \geq 2$ experiments for each condition. For WT, $n_{HOXB1} = 22$, $n_{HOXB4} = 22$, $n_{HOXC9} = 12$, and $n_{experiment} = 3$; for *CDX2*-KO, $n_{HOXB1} = n_{HOXB4} = n_{HOXC9} = 13$, and $n_{experiment} = 2$. **c**. Plot showing relative R-C positions of BRA+ domains in day 4 R-C patterned μNTLS and $HOXB1^+$, $HOXB4^+$, and $HOXC9^+$ domains in day 7 R-C patterned μNTLS, generated from either WT or *CDX2*-KO human ES cells as indicated. Rostral and caudal ends of μNTLS are designated as 0 and 1, respectively. Error bars represent mean ± s.e.m. *n* values are provided in **a** & **b**. Two-sided Student's *t*-tests were performed to calculate *p* values. **d**. (Left) Cartoon illustrating definition of normalized contour length, calculated as the ratio between contour length and region length. (Right) Box-and-whisker plot showing normalized contour length of μNTLS generated from WT and *CDX2*-KO human ES cells in indicated R-C regions (box: 25–75%; bar-in-box: median; whiskers: 1.5 × interquartile range). For WT, $n_{colony} = 10$ and $n_{experiment} = 2$; For *CDX2*-KO, $n_{colony} = 11$ and $n_{experiment} = 2$; Two-sided Student's *t*-tests were performed to calculate *p* values. **e**. (Left) Protocol for clonal growth assay. Single H2B-GFP human ES cells are mixed with non-fluorescent human ES cells during cell seeding at a ratio of 1:200. Length of H2B-GFP cell colonies is recorded daily. (Right) Representative brightfield and fluorescence images showing clonal growth of single WT and *CDX2*-KO H2B-GFP human ES cells in μNTLS from day 1 to day 6. Experiments were repeated three times with similar results. **f**. Box-and-whisker plot showing length of H2B-GFP cell colonies in different R-C regions of day 6 μNTLS generated from WT and *CDX2*-KO human ES cells (box: 25–75%; bar-in-box: median; whiskers: 1.5 × interquartile range). Only clonal growth from a single H2B-GFP human ES cell is included for quantification. For WT, $n_{colony} = 10, 11, 10$, and 10 for Region 1, 2, 3, and 4, respectively, and $n_{experiment} = 2$; For *CDX2*-KO, $n_{colony} = 12, 11, 14$, and 14 for Region 1, 2, 3, and 4, respectively, and $n_{experiment} = 2$. Two-sided Student's *t*-tests were performed to calculate *p* values. **g**. Representative stitched confocal micrographs showing day 4 R-C patterned μNTLS generated from WT or *TBXT*-KO WIBR3 human ES cells as indicated, stained for SOX2, CDX2, and BRA. Zoom-in views of boxed regions are shown on the right. Arrowheads mark $SOX2^+BRA^+$ NMPs. Intensity maps depict relative mean values of indicated markers as a function of relative R-C position in μNTLS. For WT, $n_{colony} = 20$ and $n_{experiment} = 3$; For *TBXT*-KO, $n_{colony} = 18$ and $n_{experiment} = 3$. **h**. Representative stitched confocal micrographs showing day 7 *R-C* patterned μNTLS generated from WT or *TBXT*-KO WIBR3 human ES cells as indicated, stained for HOXB1, HOXB4, and HOXC9. Zoom-in views of boxed regions are shown on the right. Intensity maps depict relative mean values of indicated markers as a function of relative R-C position in μNTLS. For WT, $n_{colony} = 14$ and $n_{experiment} = 2$; for *TBXT*-KO, $n_{colony} = 12$ and $n_{experiment} = 2$. **i**. Plot showing relative R-C positions of CDX2+ domain in day 4 R-C patterned μNTLS and $HOXB1^+$, $HOXB4^+$, and $HOXC9^+$ domains in day 7 R-C patterned μNTLS, generated from either WT or *TBXT*-KO human ES cells. Rostral and caudal ends of μNTLS are designated as 0 and 1, respectively. Error bars represent mean ± s.e.m. *n* values are provided in **g** & **h**. Two-sided Student's *t*-tests were performed to calculate *p* values. In **a**, **b**, **g** and **h**, nuclei were counterstained with DAPI. Scale bars, 400 μm (**a**, **b**, **g** and **h**) and 200 μm (**e**).

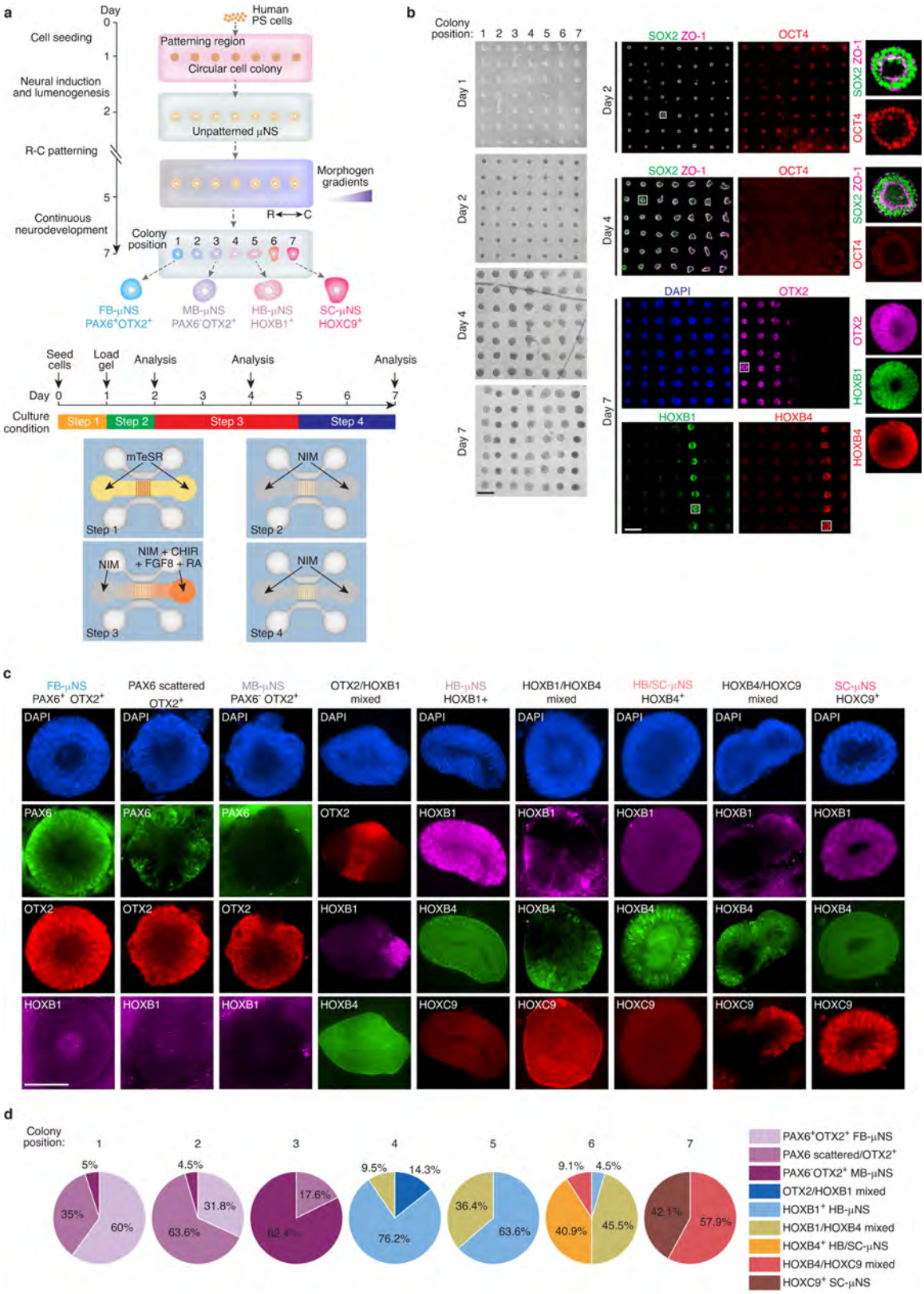

Extended Data Fig. 6 | See next page for caption.

Extended Data Fig. 6 | Development of region-specific μNS. a. Protocol for generating region-specific μNS. Human PS cells are seeded into the central channel on day 0 using mTeSR (Step 1). After gel loading on Day 1, culture medium of the central channel is switched to NIM (Step 2). From Day 2 to Day 5, CHIR (3 μM), FGF8 (200 ng mL^{-1}), and RA (500 nM) are added into the right reservoir of the central channel in addition to NIM, to induce caudalization of μNS (Step 3). From day 5 to day 7, all caudalizing factors are removed, and only NIM is added into the two medium reservoirs of the central channel (Step 4). Tissues are analyzed at different time points as indicated. **b**. Representative stitched brightfield (left) and confocal (right) micrographs showing a regular array of μNS in the patterning region on indicated days. μNS on day 2 and day 4 was stained for OCT4, SOX2, and ZO-1. On day 7, they were stained for OTX2, HOXB1, and HOXB4. Zoom-in views of boxed regions are shown on the right. Experiments were repeated three times with similar results. **c**. Representative confocal micrographs showing μNS on day 7 stained for PAX6, OTX2, HOXB1, HOXB4, and HOXC9 as indicated. Experiments were repeated three times with similar results. **d**. Pie charts showing percentages of different types of μNS at different locations of the patterning region on day 7. $n = 3$ experiments. In **b** and **c**, nuclei were counterstained with DAPI. Scale bars, 400 μm (**b**) and 100 μm (**c**).

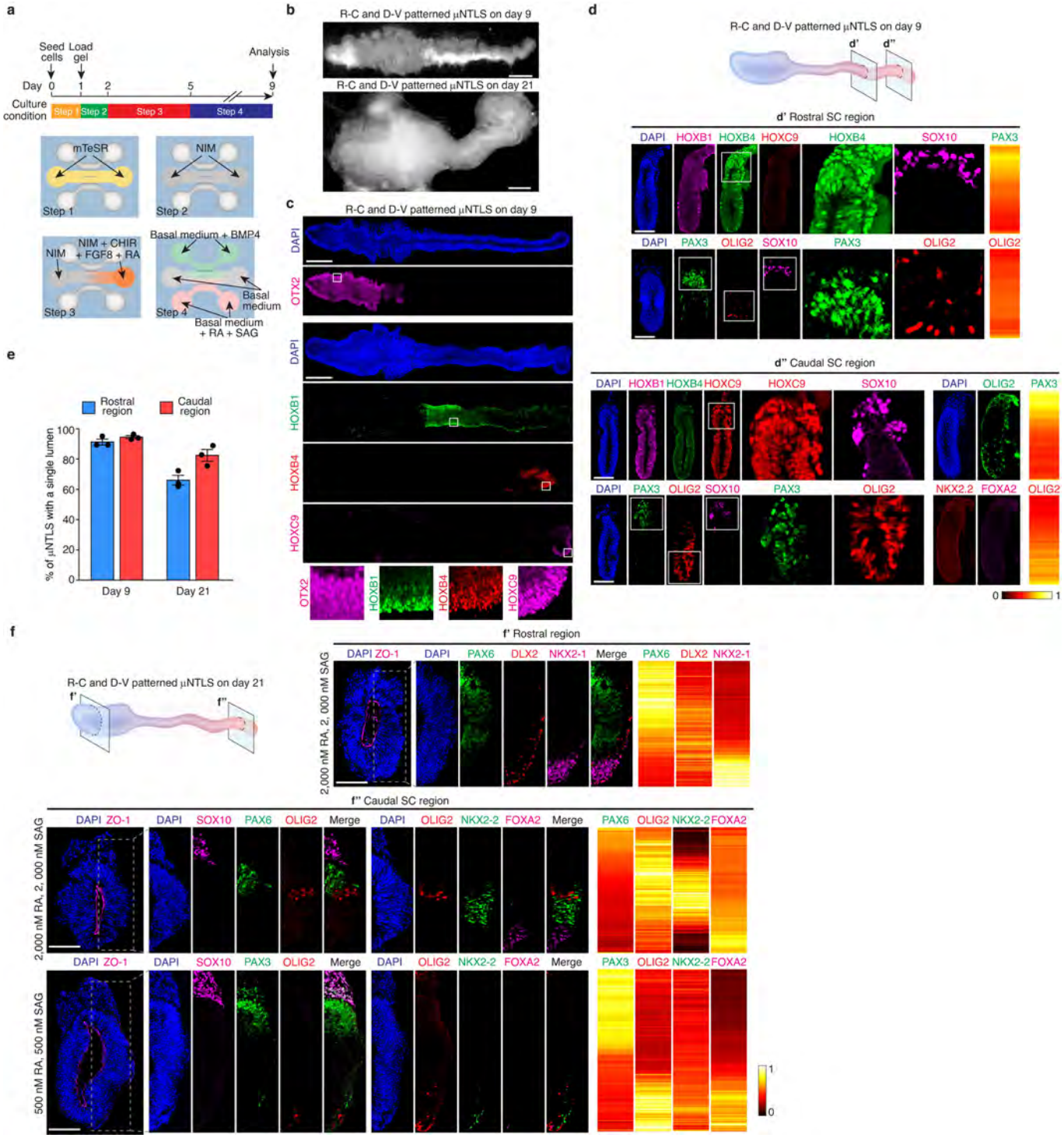

Extended Data Fig. 7 | See next page for caption.

Extended Data Fig. 7 | Development and characterization of R-C and D-V patterned μNTLS. a. Protocol for generating R-C and D-V patterned μNTLS. Human PS cells are seeded into the central channel on day 0 using mTeSR (Step 1). After gel loading on day 1, culture medium in the central channel is switched to NIM (Step 2). From day 2 to day 5, CHIR (3 μM), FGF8 (200 ng mL^{-1}), and RA (500 nM) are added into the right reservoir of the central channel in addition to NIM, to induce caudalization and R-C patterning of μNTLS (Step 3). From day 5 to day 9, BMP4 (25 ng mL^{-1}) and RA (500 nM) / smoothened agonist (SAG, 500 nM), unless otherwise specified, are added into the top and bottom channels, respectively, to induce *D-V* patterning of μNTLS. **b**. Representative brightfield images showing R-C and D-V patterned μNTLS on day 9 and day 21 as indicated. Experiments were repeated five times with similar results. **c**. Representative stitched confocal micrographs showing R-C and D-V patterned μNTLS on day 9 stained for OTX2, HOXB1, HOXB4, and HOXC9. Zoom-in views of boxed regions are shown on the bottom. Experiments were repeated five times with similar results. **d**. Representative confocal micrographs showing transverse sections of rostral (**d'**) and caudal (**d"**) SC regions of day 9 R-C and D-V patterned μNTLS as indicated, stained for HOXB1, HOXB4, HOXC9, SOX10, PAX3, OLIG2, NKX2.2, and FOXA2. Zoom-in views of boxed regions are included. Intensity maps depict relative mean values of indicated markers as a function of relative D-V position in μNTLS. For rostral SC regions, $n_{PAX3} = 20$, $n_{OLIG2} = 24$, and $n_{experiment} = 5$. For caudal SC regions, $n_{PAX3} = 22$, $n_{OLIG2} = 38$, and $n_{experiment} = 5$. **e**. Plot showing percentages of μNTLS containing a single lumen in their rostral and caudal regions on day 9 and day 21 as indicated. Error bars represent mean ± SEM. $n_{experiment} = 3$. **f**. Representative confocal micrographs showing transverse sections of rostral (**f'**) and caudal (**f"**) regions of day 21 R-C and D-V patterned μNTLS cultured under different conditions as indicated, stained for ZO-1, PAX6, DLX2, NKX2-1, SOX10, PAX3, OLIG2, NKX2-2, and FOXA2. From day 2 to day 5, CHIR (3 μM), FGF8 (200 ng mL^{-1}) and RA (500 nM) are added into the right reservoir of the central channel to induce R-C patterning of μNTLS. From day 5 to day 9, BMP4 (25 ng mL^{-1}) and RA (500 nM or 2,000 nM) / smoothened agonist (SAG, 500 nM or 2,000 nM) are added into the top and bottom channels, respectively, to induce D-V patterning of μNTLS. Zoom-in views of boxed regions are included. Intensity maps depict relative mean values of indicated markers as a function of relative D-V position in μNTLS. For 2,000 nM RA / 2,000 nM SAG condition, $n_{PAX6\text{-}rostral} = 20$, $n_{DLX2} = 20$, $n_{NKX2\text{-}1} = 20$, $n_{PAX6\text{-}caudal} = 21$, $n_{OLIG2} = 40$, $n_{NKX2\text{-}2} = 19$, $n_{FOXA2} = 19$, and $n_{experiment} = 5$; for 500 nM RA / 500 nM SAG condition, $n_{PAX3} = 20$, $n_{OLIG2} = 41$, $n_{NKX2\text{-}2} = 21$, $n_{FOXA2} = 21$, and $n_{experiment} = 5$. In **c**, **d**, and **f**, nuclei were counterstained with DAPI. Scale bars, 400 μm (**b** and **c**) and 100 μm (**d** and **f**).

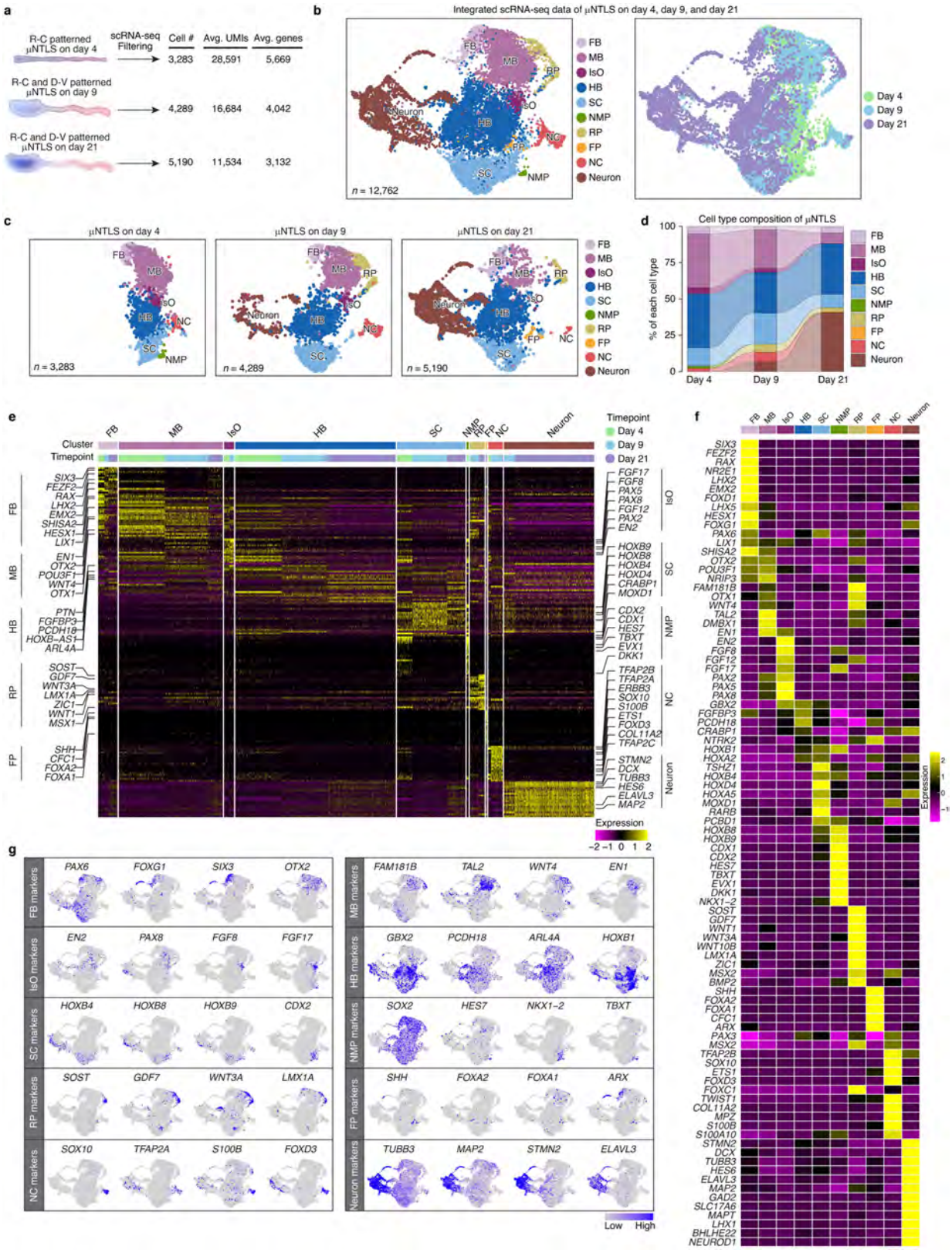

Extended Data Fig. 8 | See next page for caption.

Extended Data Fig. 8 | Characterization of μNTLS using single-cell RNA-sequencing (scRNA-seq). a. scRNA-seq assay design. R-C patterned μNTLS on day 4 and R-C and D-V patterned μNTLS on day 9 and day 21 were dissociated into single cells before the cells were sequenced using 10× Genomics and Illumina HiSeq 6000 (see Methods). Single-cell transcriptome data of day 4, day 9 and day 21 μNTLS were then integrated and analyzed. The number of cells from each sample after data filtering, average UMI counts, and average detected genes are listed. **b**. UMAP of integrated single-cell transcriptome data of day 4, day 9 and day 21 μNTLS, color-coded according to cell identity annotations (left) or time points (right). *n* indicates total cell number combined from all three time points. FB, forebrain; MB, midbrain; IsO, isthmic organizer; HB, hindbrain; SC, spinal cord; NMP, neuromesodermal progenitors; RP, roof plate; FP, floor plate; NC, neural crest. **c**. UMAP of single-cell transcriptome data of day 4, day 9, and day 21 μNTLS, separated from integrated UMAP plots in **b**. *n* indicates cell numbers at each time point. **d**. Alluvial plot showing percentages of cells for each cell cluster in μNTLS on day 4, day 9, and day 21. **e**. Heatmap of relative expression (*Z*-score) of top-20 gene signatures distinguishing each cell cluster. All genes are listed in Supplementary Table 1. **f**. Heatmap of average relative expression (*Z*-score) of selected genes among indicated cell clusters. **g**. Feature plots showing expression of selected genes associated with indicated cell cluster annotations in UMAP plots of integrated datasets from day 4, day 9, and day 21 μNTLS.

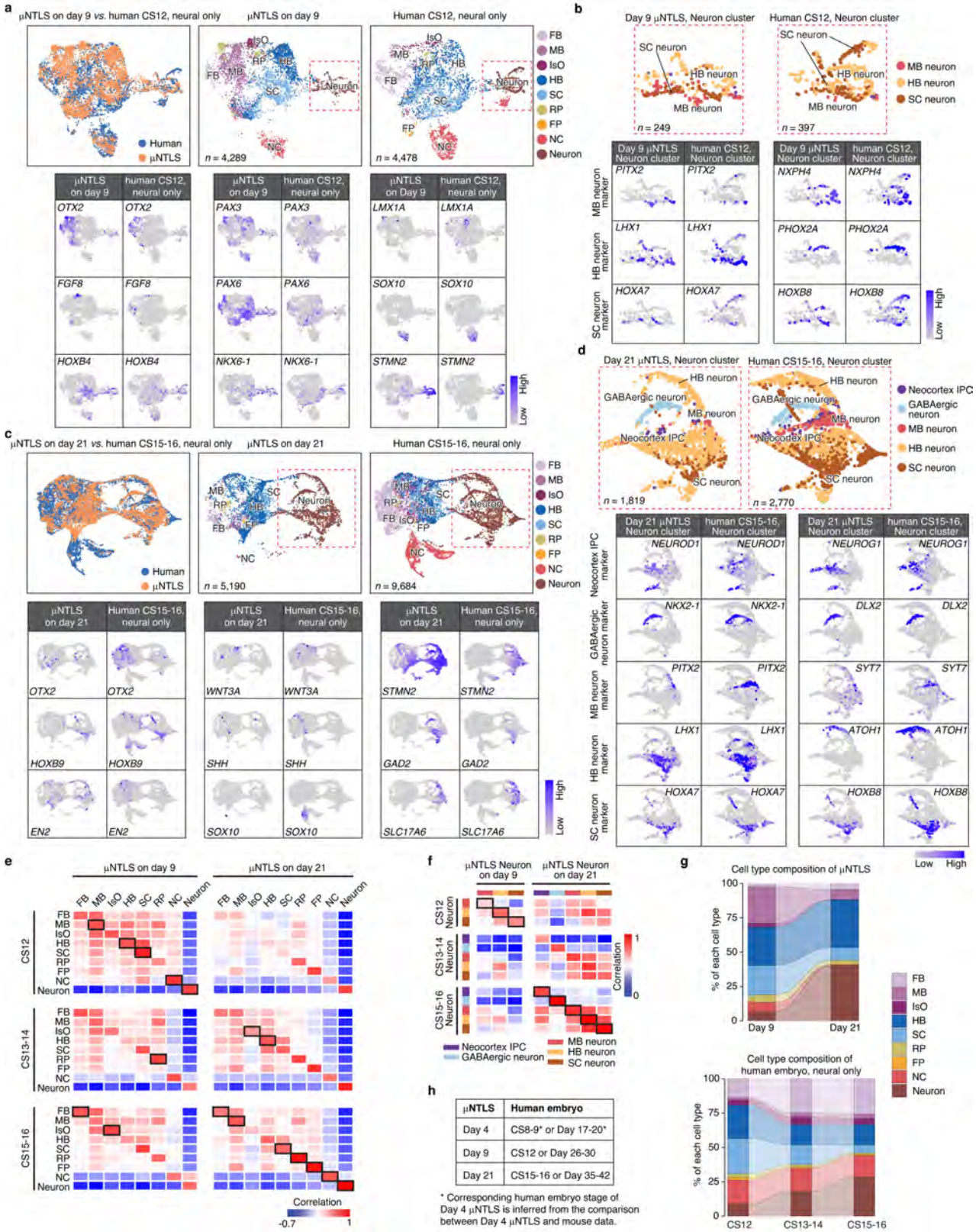

Extended Data Fig. 9 | See next page for caption.

Extended Data Fig. 9 | Transcriptomic comparison between μNTLS and neural cells from human embryonic tissues. a. (Top left) UMAP showing integrated data from day 9 μNTLS and neural cells in Carnegie Stage (CS) 12 human embryos[42]. (Top middle & right) UMAP plots of day 9 μNTLS data and CS12 human neural cell data, separated from the integrated UMAP plot, as indicated. *n* indicates cell numbers. (Bottom) Feature plots comparing expression of key marker genes between day 9 μNTLS and neural cells in CS12 human embryos. **b**. (Top) UMAP plots of Neuron clusters in day 9 μNTLS and CS12 human embryo datasets. Neuron cluster in day 9 μNTLS dataset is projected onto the Neuron cluster in CS12 human embryo dataset and is annotated following the human reference data[42] (see Methods). *n* indicates cell numbers. (Bottom) Feature Plots comparing expression of key marker genes between Neuron clusters in day 9 μNTLS and CS12 human embryos. **c**. (Top left) UMAP showing integrated data from day 21 μNTLS and neural cells in CS15-16 human embryos[42]. (Top middle & right) UMAP plots of day 21 μNTLS data and CS15-16 human neural cells, separated from the integrated UMAP plot, as indicated. *n* indicates cell numbers. (Bottom) Feature plots compare expression of key marker genes between day 21 μNTLS and neural cells in CS15-16 embryos. **d**. (Top) UMAP plots of Neuron clusters in day 21 μNTLS and CS15-16 human embryo datasets. Neuron cluster in day 21 μNTLS dataset is projected onto the Neuron cluster in CS15-16 human embryo dataset and is annotated following the human reference data[42] (see Methods). *n* indicates cell numbers. (Bottom) Feature Plots comparing expression of key marker genes between Neuron clusters in day 21 μNTLS and CS15-16 human embryos. **e**. Pearson's correlation analysis of cell clusters in day 9 and day 21 μNTLS with neural clusters in CS12-16 human embryo datasets[42]. Black boxes highlight the highest correlation coefficients in each column. Correlation coefficients between indicated μNTLS and human clusters are calculated based on variable genes identified from human neural cell clusters (Supplementary Table 1). **f**. Pearson's correlation analysis of Neuron subclusters in day 9 and day 21 μNTLS with Neuron subclusters in CS12-16 human embryo datasets[42]. Black boxes highlight the highest correlation coefficients in each column. Correlation coefficients between indicated μNTLS and human clusters are calculated based on variable genes identified from human neural cell clusters. **g**. Alluvial plots showing percentages of cells for each cell cluster in day 9 and day 21 μNTLS (top) and human embryos at CS12, CS13-14 and CS15-16 (bottom). **h**. day 4, day 9, and day 21 μNTLS show closest transcriptome similarities with human neural cells at CS8-9 (day 17–20), CS12 (day 26–30), and CS15-16 (day 35–42), respectively[42]. Note that corresponding human embryo stage of day 4 μNTLS is inferred from the comparison between day 4 μNTLS and mouse data[44] (See Supplementary Figs. 8–10).

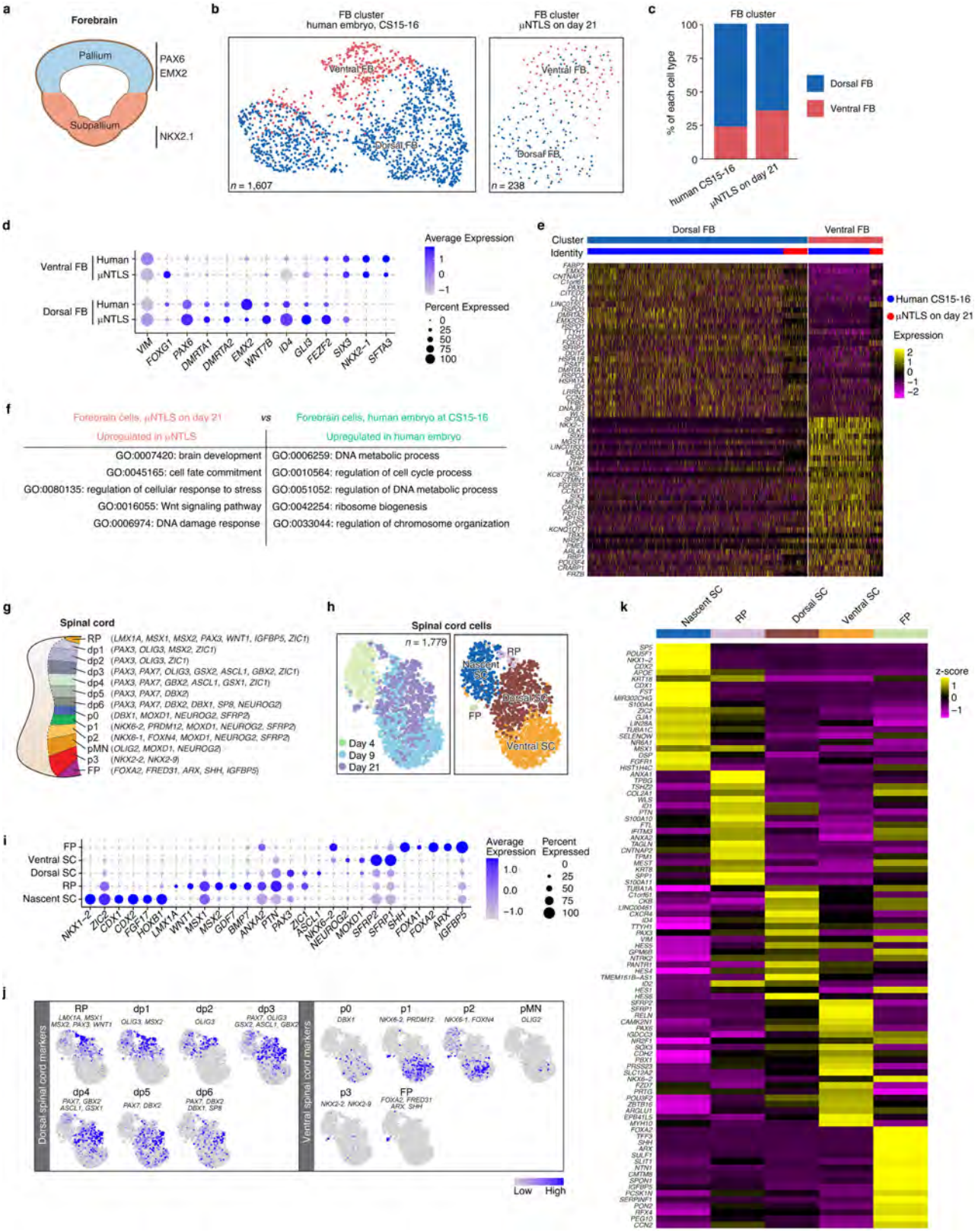

Extended Data Fig. 10 | See next page for caption.

Extended Data Fig. 10 | Analysis of Forebrain (FB) cluster and Spinal cord (SC)-related cells in μNTLS. a. D-V patterning of FB, leading to formation of dorsal pallium and ventral subpallium domains. Pallium is marked by *PAX6* and *EMX2* expression, whereas subpallium is marked by *NKX2-1*. **b**. UMAP plots of FB clusters in CS15-16 human embryo data (left) and day 21 μNTLS data (right). FB cluster in day 21 μNTLS data is annotated following human reference data[42] (see Methods). **c**. Stacked bar plots showing percentages of cells for each FB subcluster in CS15-16 human FB cluster and day 21 μNTLS FB cluster. **d**. Dot plot showing expression of key marker genes across different cell subclusters in day 21 μNTLS FB cluster and CS15-16 human embryo FB cluster as indicated. Dot sizes and colors indicate proportions of cells expressing corresponding genes and their averaged scaled values of log-transformed expression, respectively. **e**. Heatmap showing relative expression (*Z*-score) of top-30 gene signatures calculated from CS15-16 human FB cells in both CS15-16 human FB cluster and day 21 μNTLS FB cluster as indicated. For gene signature information, see Supplementary Table 1. **f**. Enrichment of Gene Ontology (GO) terms in DEGs upregulated in day 21 μNTLS FB cells or CS15-16 human FB cells as indicated. For detailed information about DEGs and GO terms, see Supplementary Table 1. **g**. In vivo, dorsal SC gives rise to roof plate (RP) and six neuronal progenitor domains (dp1-dp6), whereas ventral SC generates floor plate (FP) and five neuronal progenitor domains (pMN and p0-p3). These domains express distinct combinations of transcription factors. Markers listed on the right for each domain are identified from scRNA-seq data of mouse SC between E9.5 - E13.5[67]. **h**. UMAP of SC-related cells from integrated dataset of day 4, day 9, and day 21 μNTLS, color-coded according to time points (left) or subcluster identity annotations (right). *n* indicates cell number. Note that cells from SC cluster as well as those from RP and FP clusters that express *HOX4-13* genes have been included in analyses in **h**-**k**. **i**. Dot plot showing expression of key marker genes across subclusters of SC-related cells as indicated. Dot sizes and colors indicate proportions of cells expressing corresponding genes and their averaged scaled values of log-transformed expression, respectively. **j**. Feature plots showing average expression of indicated markers associated with each SC progenitor domain in UMAP plots of SC-related cells. **k**. Heatmap of average relative expression (*Z*-score) of top-20 gene signatures distinguishing each cell subcluster in SC-related cells. For gene signature information, see Supplementary Table 1.

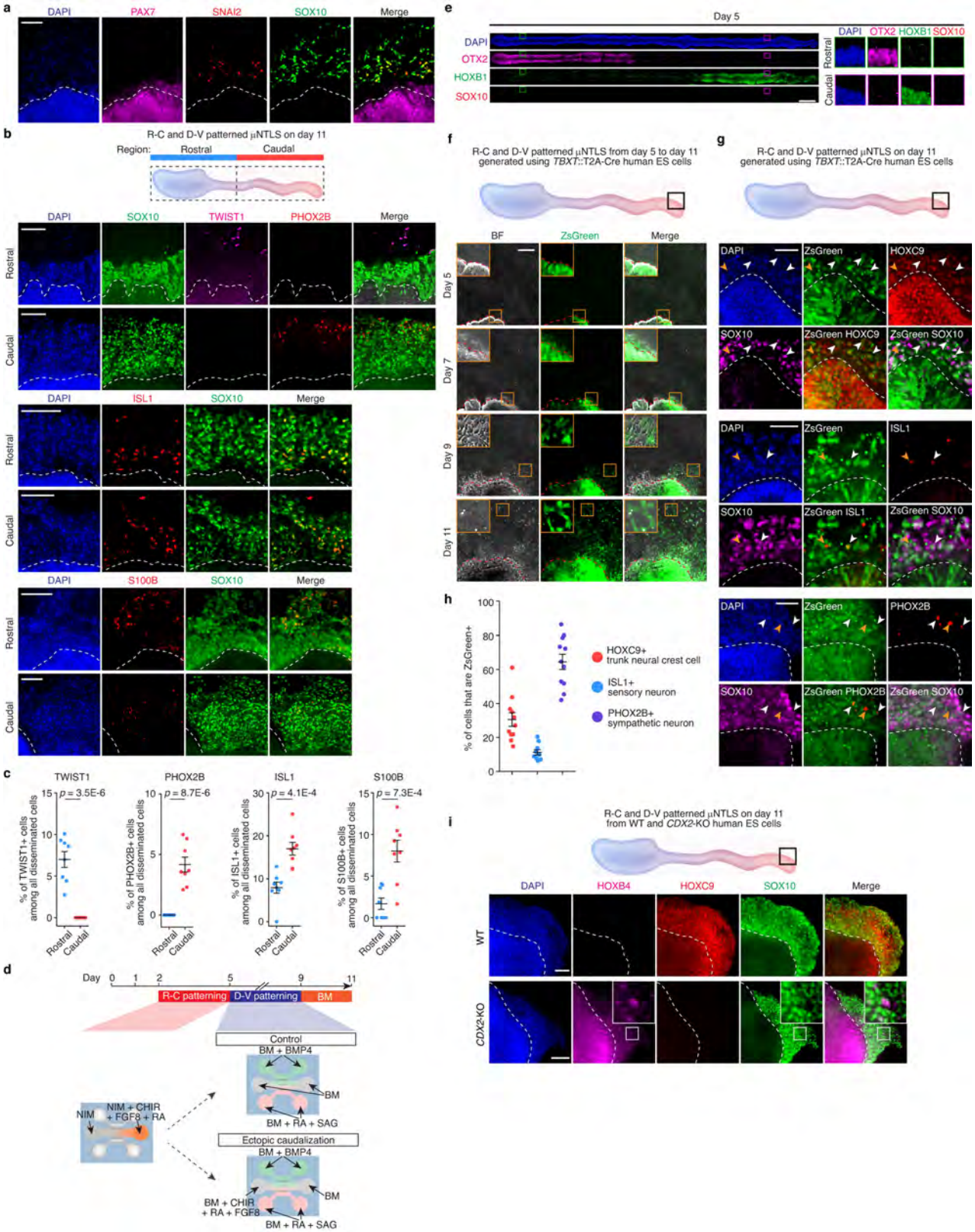

Extended Data Fig. 11 | See next page for caption.

Extended Data Fig. 11 | Characterization of neural crest (NC) development in μNTLS. a. Representative confocal micrographs showing NC cells from R-C and D-V patterned μNTLS on day 11 stained for PAX7, SNAI2, and SOX10. Dashed lines mark dorsal boundaries of μNTLS. Experiments were repeated twice with similar results. **b**. Representative confocal micrographs showing NC cells and their derivatives in rostral and caudal regions of R-C and D-V patterned μNTLS on day 11, stained for SOX10, TWIST1, PHOX2B, ISL1, and S100B. Dashed lines mark dorsal boundaries of μNTLS. Experiments were repeated three times with similar results. **c**. Plots showing percentages of TWIST1$^+$, PHOX2B$^+$, ISL1$^+$, and S100B$^+$ cells among all disseminated cells in rostral and caudal halves of μNTLS. Error bar represents mean ± s.e.m. $n_{TWIST1} = n_{PHOX2B} = n_{ISL1} = n_{S100B} = 8$ and $n_{experiment} = 2$. Two-sided Student's *t*-tests were performed to calculate *p* values. **d**. Protocol for generating control R-C and D-V patterned μNTLS and ectopic caudalization of μNTLS. From day 2 to day 5, CHIR (3 μM), FGF8 (200 ng mL^{-1}), and RA (500 nM) are supplemented into the right reservoir of the central channel in addition to NIM to induce caudalization and R-C patterning of μNTLS. From day 5 to day 9, BMP4 (25 ng mL^{-1}) and RA (500 nM) / smoothened agonist (SAG, 500 nM) are supplemented into the top and bottom channels, respectively, to induce D-V patterning of μNTLS. For ectopic caudalization of μNTLS, caudalizing factors CHIR (3 μM), FGF8 (200 ng mL^{-1}), and RA (500 nM) are added together into the left reservoir of the center channel from day 5 to day 9. Culture medium in all reservoirs is then switched back to fresh basal medium (BM) from day 9 to day 11 to allow for further development of NC cells. **e**. Representative stitched confocal micrographs showing day 5 μNTLS cultured following the protocol in **d**, stained for OTX2, HOXB1, and SOX10. Zoom-in views of boxed regions are shown on the right. Experiments were repeated three times with similar results. **f**. Live imaging with the *TBXT*::T2A-Cre lineage tracer to track progenies of NMPs during the development of R-C and D-V patterned μNTLS from day 5 to day 11 (see Supplementary Video 6). Only caudal ends of μNTLS are monitored as indicated. Dashed lines mark dorsal boundaries of μNTLS. Zoom-in views of boxed regions are shown. Experiments were repeated three times with similar results. **g**. Representative confocal micrographs showing caudal ends of R-C and D-V patterned μNTLS generated from the *TBXT*::T2A-Cre lineage tracer, stained on day 11 for SOX10, HOXC9, ISL1, and PHOX2B. Dashed lines mark dorsal boundaries of μNTLS. White arrowheads mark ZsGreen$^+$ NC cells, and yellow arrowheads mark ZsGreen$^-$ NC cells. Experiments were repeated twice with similar results. **h**. Plot showing percentages of ZsGreen$^+$ cells among all HOXC9$^+$ trunk NC cells, ISL1$^+$ sensory neurons, or PHOX2B$^+$ sympathetic neurons. $n_{HOXC9} = 11$, $n_{ISL1} = 9$, $n_{PHOX2B} = 11$, and $n_{experiment} = 2$. Error bars represent mean ± s.e.m. **i**. Representative confocal micrographs showing NC cells in caudal regions of R-C and D-V patterned μNTLS on day 11 generated from wild type (WT) and *CDX2*-KO human ES cell lines, stained for indicated markers. Dashed lines mark dorsal boundaries of μNTLS. Zoom-in views of boxed regions are shown. Experiments were repeated twice with similar results. In **a**, **b**, **e**, **g** and **i**, nuclei were counterstained with DAPI. Scale bars, 100 μm (**a**, **b**, and **i**), 200 μm (**e** and **f**), and 50 μm (**g**).

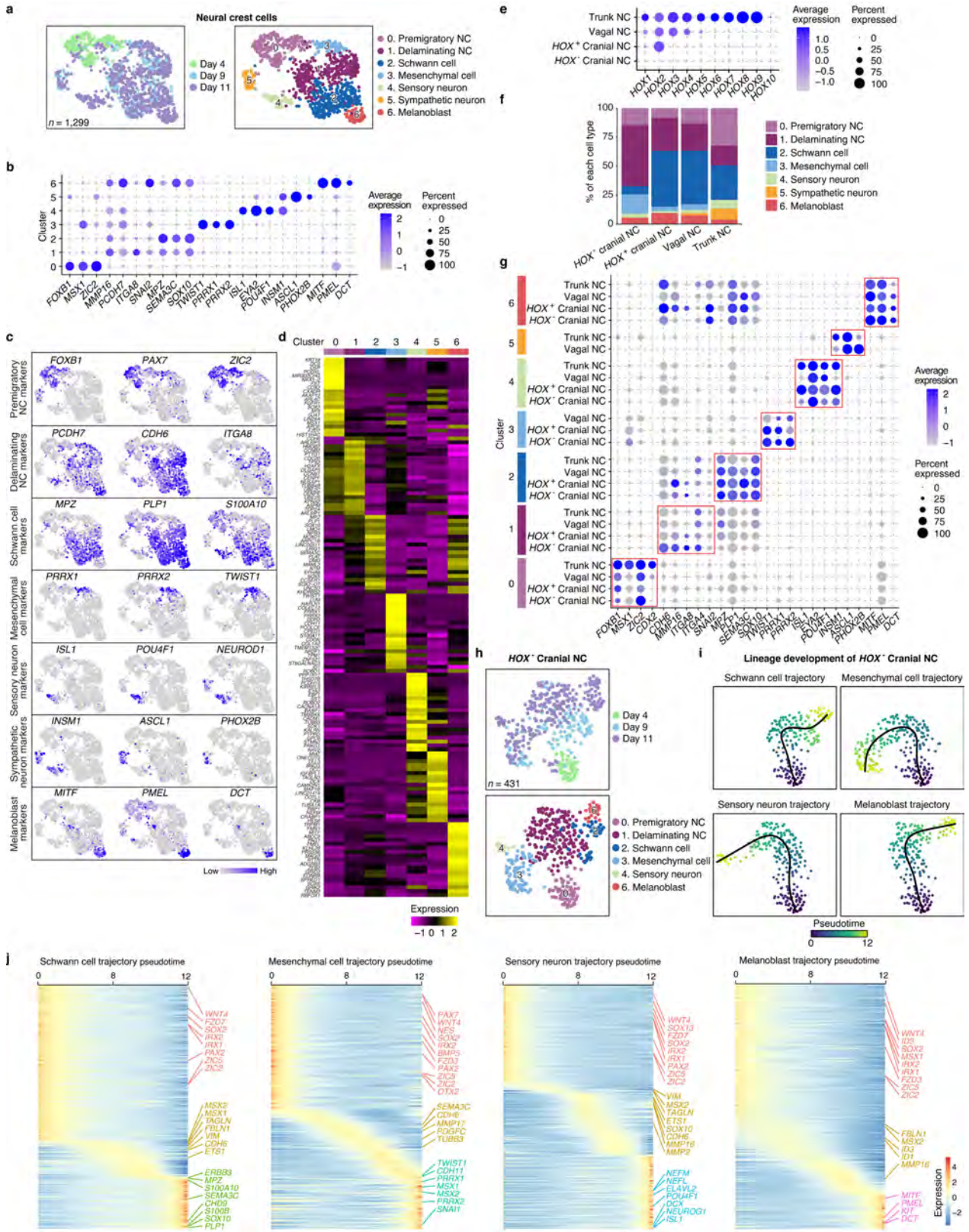

Extended Data Fig. 12 | See next page for caption.

Extended Data Fig. 12 | Subclustering analysis and trajectory inference of NC cluster in μNTLS. a. UMAP of NC cluster from integrated dataset of day 4, day 9, and day 11 μNTLS, color-coded according to time points (left) or cell subcluster identity annotations (right). Seven cell subclusters are identified, including Premigratory NC (Cluster 0), Delaminating NC (Cluster 1), Schwann cell (Cluster 2), Mesenchymal cell (Cluster 3), Sensory neuron (Cluster 4), Sympathetic neuron (Cluster 5), and Melanoblast (Cluster 6). *n* indicates cell number. **b**. Dot plot showing expression of key marker genes across all NC subclusters as indicated. Dot sizes and colors indicate proportions of cells expressing corresponding genes and their averaged scaled values of log-transformed expression, respectively. **c**. Feature plots showing expression of selected markers associated with indicated cell subclusters in UMAP plots of NC cluster. **d**. Heatmap of average relative expression (*Z*-score) of top-20 gene signatures distinguishing each cell subcluster in NC cluster. For gene signature information, see Supplementary Table 1. **e**. Dot plot showing expression of *HOX* genes in *HOX*$^-$ cranial NC, *HOX*$^+$ cranial NC, vagal NC, and trunk NC. *HOX*$^-$ cranial NC doesn't express any *HOX* genes. *HOX*$^+$ cranial NC expresses *HOX* paralogous group (PG) 1-2 but not *HOX* PG 3-13. Vagal NC expresses *HOX* PG 3-5 but not *HOX* PG 6-13. Trunk NC expresses *HOX* PG 6-9 but not *HOX* PG 10-13. Dot sizes and colors indicate proportions of cells expressing corresponding genes and their averaged scaled values of log-transformed expression, respectively. **f**. Stacked bar plot showing cellular compositions in *HOX*$^-$ cranial, *HOX*$^+$ cranial, vagal, and trunk NC cells, as indicated. **g**. Dot plot comparing expression of key marker genes in *HOX*$^-$ cranial NC, *HOX*$^+$ cranial NC, vagal NC, and trunk NC across different NC clusters as indicated. Dot sizes and colors indicate proportions of cells expressing corresponding genes and their averaged scaled values of log-transformed expression, respectively. **h**. UMAP of *HOX*$^-$ cranial NC cells separated from NC cluster shown in **a**, color-coded according to time points (top) or cell subcluster identity annotations (bottom). Six cell subclusters are identified, including Premigratory NC (Cluster 0), Delaminating NC (Cluster 1), Schwann cell (Cluster 2), Mesenchymal cell (Cluster 3), Sensory neuron (Cluster 4), and Melanoblast (Cluster 6). *n* indicates cell number. **i**. UMAP of cell subclusters of *HOX*$^-$ cranial NC cells associated with lineage developments of Schwann cell, Mesenchymal cell, Sensory neuron, and Melanoblast, color-coded according to pseudotime. Solid lines represent principal curves of each lineage. Pseudotime values are computed by projecting each single cell onto principal curves. **j**. Heatmap of smoothened expression of all differentially expressed genes (DEGs) along pseudotime of Schwann cell, Mesenchymal cell, Sensory neuron and Melanoblast lineage development trajectories in *HOX*$^-$ cranial NC cells. Selected genes are highlighted. A gene is considered significant when adjusted *p*-value based on FDR is <0.05 (see Methods). For DEG information, see Supplementary Table 1.

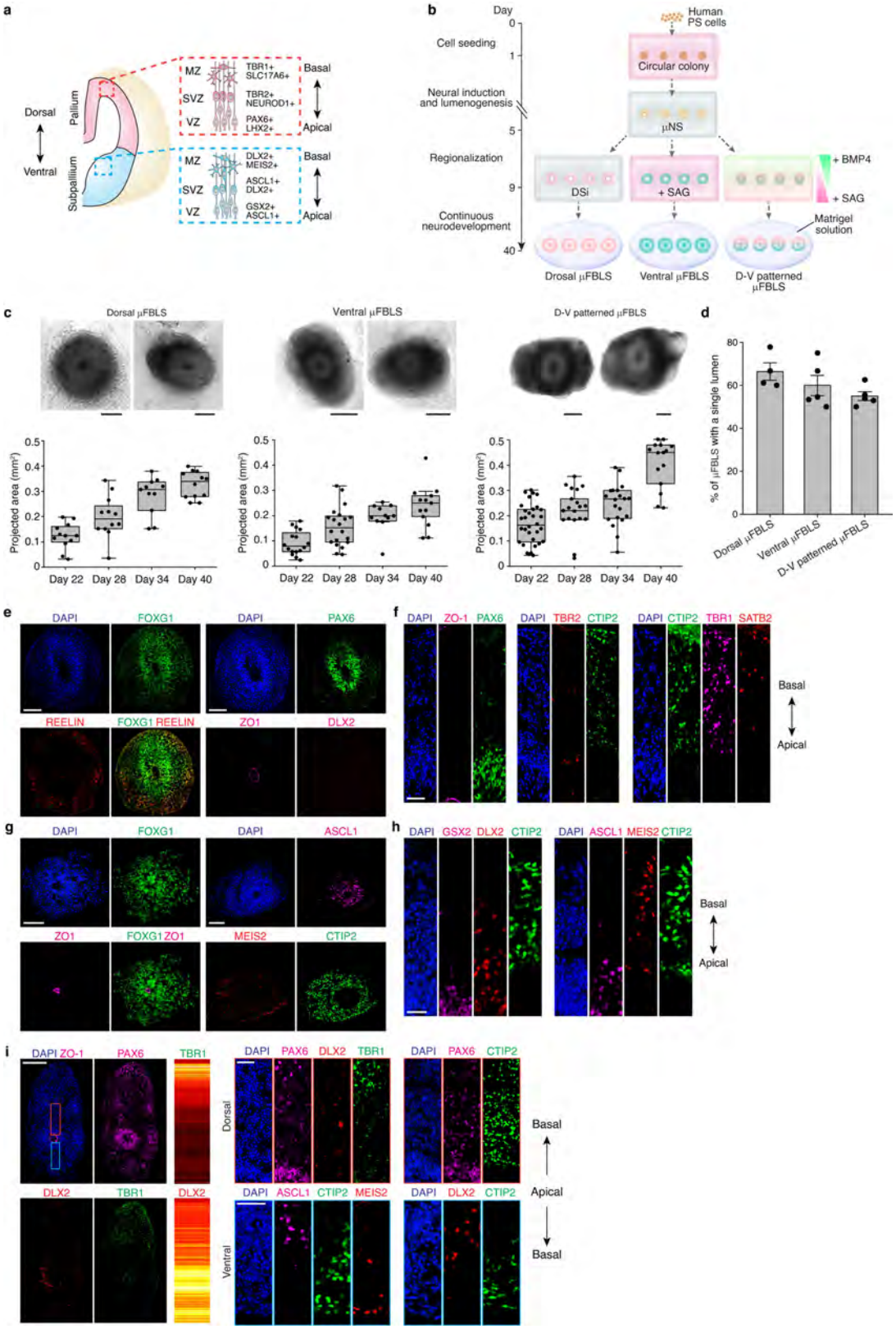

Extended Data Fig. 13 | See next page for caption.

Extended Data Fig. 13 | Development of microfluidic forebrain-like structure (μFBLS). a. Transverse view of forebrain, with dorsal pallium and ventral subpallium. Both pallium and subpallium can be divided into ventricular zone (VZ), subventricular zone (SVZ) and marginal zone (MZ) from the apical to basal surface. Different domains in pallium and subpallium express distinct combinations of transcription factors as indicated. **b**. Protocol for generating μFBLS. Human PS cells are seeded into the central channel on day 0 using mTeSR, and Geltrex is loaded into the central channel on day 1 to provide 3D culture environment. After gel loading on day 1, culture medium is switched to NIM from day 1 to day 5 to induce neural differentiation. From day 5 to day 9, to generate dorsal μFBLS, NIM are added into all reservoirs connecting the three channels; to generate ventral μFBLS, smoothened agonist (SAG, 500 nM) is supplemented into NIM in all reservoirs; to generate D-V patterned μFBLS, BMP4 (25 ng mL^{-1}) and SAG (500 nM) are supplemented into basal medium in the top and bottom channels, respectively. After regionalization of μFBLS in the microfluidic device, PDMS structural layers are detached manually from the coverslip on day 9, with μFBLS remaining on PDMS structural layers. μFBLS on PDMS structural layers are continuously cultured in basal medium supplemented with insulin (2.5 μg mL^{-1}) and 1% Matrigel till day 40 (See Methods). **c**. (Top) Representative brightfield images showing dorsal, ventral and D-V patterned μFBLS on day 40 as indicated. (Bottom) Box-and-whisker plots showing projected areas of dorsal (left), ventral (middle) and D-V patterned (right) μFBLS on indicated days (box: 25–75%; bar-in-box: median; whiskers: 1.5 × interquartile range). n_{dorsal} = 12, 12, 11, and 12 on day 22, day 28, day 34, and day 40, respectively; $n_{ventral}$ = 16, 20, 11, and 13 on day 22, day 28, day 34, and day 40, respectively; $n_{D\text{-}V}$ = 32, 19, 20, and 15 on day 22, day 28, day 34, and day 40, respectively. $n_{experiment}$ = 3. **d**. Plot showing percentages of dorsal, ventral, and D-V patterned μFBLS on day 40 with a single lumen. $n_{experiment}$ = 4, 5, and 5 for dorsal, ventral, and D-V patterned μFBLS, respectively. Error bars represent mean ± s.e.m. **e**. Representative confocal micrographs showing sections of dorsal μFBLS on day 40, stained for FOXG1, REELIN, ZO-1, PAX6, and DLX2. Experiments were repeated three times with similar results. **f**. Representative confocal micrographs showing sections of dorsal μFBLS on day 40 stained for ZO-1, PAX6, TBR1/2, CTIP2, and SATB2. Experiments were repeated three times with similar results. **g**. Representative confocal micrographs showing sections of ventral μFBLS on day 40, stained for FOXG1, ZO-1, ASCL1, MEIS2, and CTIP2. Experiments were repeated three times with similar results. **h**. Representative confocal micrographs showing sections of ventral μFBLS on day 40, stained for GSX2, DLX2, CTIP2, ASCL1, and MEIS2. Experiments were repeated three times with similar results. **i**. Representative confocal micrographs showing sections of D-V patterned μFBLS on day 40, stained for ZO-1, PAX6, TBR1, DLX2, ASCL1, CTIP2 and MEIS2. Zoom-in views of boxed regions are shown on the right. Intensity maps depict relative mean values of indicated markers as a function of relative D-V position in μFBLS. Experiments were repeated three times with similar results. In **e**-**i**, nuclei were counterstained with DAPI. Scale bars, 200 μm (**c**, **e** and **i** (left)), 50 μm (**f** and **i** (zoom-in images)), 100 μm (**g**), and 30 μm (**h**).

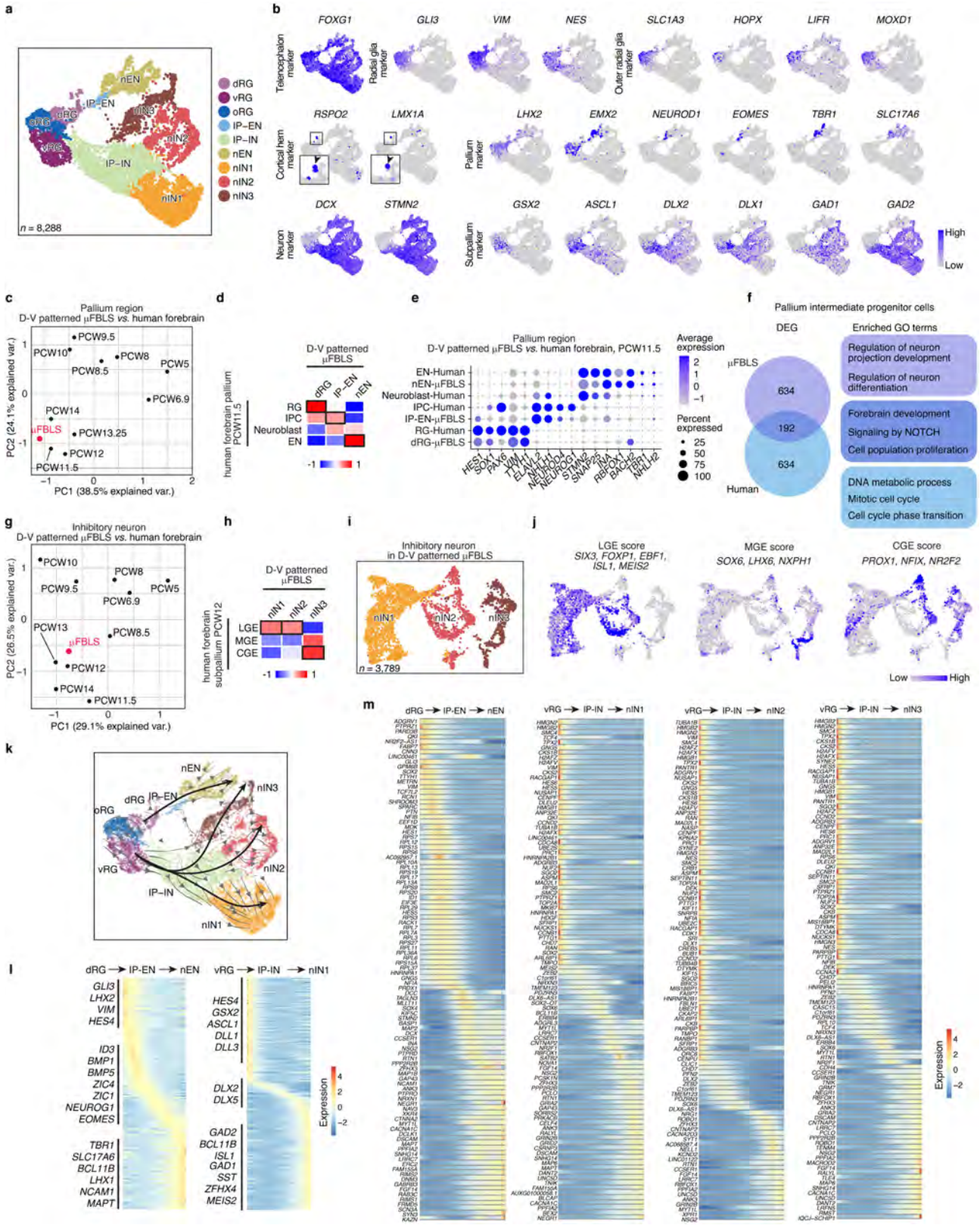

Extended Data Fig. 14 | See next page for caption.

Extended Data Fig. 14 | Single-cell transcriptome analysis of D-V patterned μFBLS. a. UMAP of single-cell transcriptome data of day 40 D-V patterned μFBLS, color-coded according to cell identity annotations. Nine cell clusters are identified, including dorsal radial glia (dRG), ventral radial glia (vRG), outer radial glia (oRG), excitatory intermediate progenitor(IP-EN), inhibitory intermediate progenitor (IP-IN), newborn excitatory neuron (nEN), and newborn inhibitory neuron 1 / 2 / 3 (nIN1, nIN2 and nIN3). *n* indicates cell number. **b**. Feature plots showing expression of selected markers associated with indicated cell identities in UMAP plots of single-cell transcriptome data of day 40 D-V patterned μFBLS. Zoom-in views of boxed regions are shown. Arrowheads mark cortical hem-like cells showing notable expression of *RSPO2* and *LMX1A*. **c**. Principal component analysis (PCA) of pallium cells in day 40 D-V patterned μFBLS relative to published data of pallium cells in human forebrain at different timepoints as indicated[50]. Pallium cells in μFBLS include dRG, IP-EN, and nEN clusters isolated from D-V patterned μFBLS dataset. Reference cortical clusters expressing *EMX1* are isolated from human brain datasets[50]. **d**. Pearson's correlation analysis of pallium cells (dRG, IP-EN, and nEN clusters) in day 40 D-V patterned μFBLS with pallium cells in PCW11.5 human brain dataset[50]. Black boxes highlight the highest correlation coefficients in each column. Original annotations of human brain cells from the reference dataset are used here (RG or radial glia / IPC or intermediate progenitor cell / Neuroblast / EN or excitatory neuron). Correlation coefficients between paired μFBLS and human clusters are calculated based on variable genes identified from human pallium cell clusters. **e**. Dot plot comparing expression of key marker genes in different cell clusters of day 40 μFBLS and PCW11.5 human pallium cells as indicated. Dot sizes and colors indicate proportions of cells expressing corresponding genes and their averaged scaled values of log-transformed expression, respectively. **f**. Venn diagram of differentially expressed genes (DEGs) between intermediate neural progenitor cells (IPC) from day 40 μFBLS and PCW11.5 human pallium cells, with 192 shared genes including some commonly used IPC markers (*TBR2*, *NEUROD4* and *NEUROG1*). Enriched Gene Ontology (GO) terms in each compartment of the Venn diagram are shown on the right. For information about DEGs and GO terms, see Supplementary Table 1. **g**. Principal component analysis (PCA) of inhibitory neurons in day 40 D-V patterned μFBLS relative to published data of inhibitory neurons from human forebrain at different timepoints as indicated[50]. Inhibitory neurons in μFBLS include nIN1, nIN2 and nIN3 clusters isolated from D-V patterned μFBLS dataset. Inhibitory neurons from human forebrain include telencephalic clusters expressing *DLX2* and are extracted from original human brain datasets[50]. **h**. Pearson's correlation analysis of inhibitory neuron clusters in day 40 D-V patterned μFBLS with those in PCW12 human brain dataset[50]. Original annotations of human brain cells from the references are used here (LGE or lateral ganglionic eminence; MGE or medial ganglionic eminence; CGE or caudal ganglionic eminence). Correlation coefficients between paired μFBLS and human cell clusters are calculated based on variable genes identified from human inhibitory neuron clusters. **i**. (Left) UMAP projection of scRNA-seq data of inhibitory neurons from day 40 D-V patterned μFBLS (nIN1 / 2 / 3), with cell identity annotations indicated. **j**. Feature plots showing expression of LGE-, MGE- and CGE-associated inhibitory neuron markers in inhibitory neurons from day 40 D-V patterned μFBLS. **k**. UMAP of single-cell transcriptome data of day 40 D-V patterned μFBLS, color-coded according to cell identity annotations. Grey arrows indicate predicted future cell states calculated using RNA velocity algorithm scVelo. Black arrows indicate lineage trajectories constructed using Slingshot. One excitatory neuron trajectory (dRG → IP-EN → nEN) and three inhibitory neuron trajectories (vRG → IP-IN → nIN1, vRG → IP-IN → nIN2, and vRG → IP-IN → nIN3) are constructed. **l**. Heatmap of smoothened expression of all differentially expressed genes (DEGs) along the pseudotime of nEN and nIN1 lineage development trajectories. Selected genes are listed on the left. A gene is considered significant when adjusted *p*-value based on FDR is <0.05 (see Methods). For DEG information, see Supplementary Table 1. **m**. Heatmap of smoothened expression of top-100 DEGs along the pseudotime of nEN, nIN1, nIN2, and nIN3 lineage development trajectories. A gene is considered significant when adjusted *p*-value based on FDR is <0.05 (see Methods). For DEG information, see Supplementary Table 1.

nature portfolio

Corresponding author(s): Jianping Fu

Last updated by author(s): Jan 18, 2024

Reporting Summary

Nature Portfolio wishes to improve the reproducibility of the work that we publish. This form provides structure for consistency and transparency in reporting. For further information on Nature Portfolio policies, see our Editorial Policies and the Editorial Policy Checklist.

Statistics

For all statistical analyses, confirm that the following items are present in the figure legend, table legend, main text, or Methods section.

n/a	Confirmed	
☐	☒	The exact sample size (*n*) for each experimental group/condition, given as a discrete number and unit of measurement
☐	☒	A statement on whether measurements were taken from distinct samples or whether the same sample was measured repeatedly
☐	☒	The statistical test(s) used AND whether they are one- or two-sided *Only common tests should be described solely by name; describe more complex techniques in the Methods section.*
☐	☒	A description of all covariates tested
☐	☒	A description of any assumptions or corrections, such as tests of normality and adjustment for multiple comparisons
☐	☒	A full description of the statistical parameters including central tendency (e.g. means) or other basic estimates (e.g. regression coefficient) AND variation (e.g. standard deviation) or associated estimates of uncertainty (e.g. confidence intervals)
☐	☒	For null hypothesis testing, the test statistic (e.g. *F*, *t*, *r*) with confidence intervals, effect sizes, degrees of freedom and *P* value noted *Give P values as exact values whenever suitable.*
☒	☐	For Bayesian analysis, information on the choice of priors and Markov chain Monte Carlo settings
☒	☐	For hierarchical and complex designs, identification of the appropriate level for tests and full reporting of outcomes
☐	☒	Estimates of effect sizes (e.g. Cohen's *d*, Pearson's *r*), indicating how they were calculated

Our web collection on statistics for biologists contains articles on many of the points above.

Software and code

Policy information about availability of computer code

Data collection	Microscopy images were acquired using Olympus DSUIX81 spinning-disc confocal microscope, Nikon X1 Yokogawa spinning-disc confocal microscope, Nikon A1SI point scanning confocal microscope, Zeiss Axio Observer Z1, or Labomed TCM 400 microscope. Single cell sequencing was performed using 10× Genomics Chromium system.
Data analysis	Image analysis was performed using Fiji 1.5.3 and Matlab R2019b. Statistical analysis was performed using Origin 2021. scRNA-seq analysis was performed using Cell Ranger Single-Cell Software Suite (v.3.1.0, 10× Genomics), Seurat 3.0, Slingshot 3.18, CellChat 1.5.0 in R 4.0.4, scVelo 0.2.4 and Scenic 1.1.2 in Python 3.8, and David bioinformatics resources 6.8.

For manuscripts utilizing custom algorithms or software that are central to the research but not yet described in published literature, software must be made available to editors and reviewers. We strongly encourage code deposition in a community repository (e.g. GitHub). See the Nature Portfolio guidelines for submitting code & software for further information.

Data

Policy information about availability of data

All manuscripts must include a data availability statement. This statement should provide the following information, where applicable:

- Accession codes, unique identifiers, or web links for publicly available datasets
- A description of any restrictions on data availability
- For clinical datasets or third party data, please ensure that the statement adheres to our policy

Data availability

Data supporting findings of this study are available within the article and its Supplementary Information files. scRNA-seq data supporting this study's results are

deposited at Gene Expression Omnibus (GEO) with accession number GSE194225. Mouse embryo scRNA-seq data are from GEO (GSE87038 and GSE119945). Human embryo scRNA-seq data are from GEO (GSE157329). Developing human brain scRNA-seq data are from Linnarsson Lab GitHub site. All Source Data for graphs included in the paper are available in the online version of the paper.

Code availability
Custom R, Python, and MATLAB scripts are used in this work. They are not central to the conclusions of the paper. These codes are available from the corresponding author upon request.

Field-specific reporting

Please select the one below that is the best fit for your research. If you are not sure, read the appropriate sections before making your selection.

☒ Life sciences ☐ Behavioural & social sciences ☐ Ecological, evolutionary & environmental sciences

For a reference copy of the document with all sections, see nature.com/documents/nr-reporting-summary-flat.pdf

Life sciences study design

All studies must disclose on these points even when the disclosure is negative.

Sample size	All experiments were conducted with at least two independent experiments and multiple biological replicates. The numbers of uNTLS, uNS and uFBLS in each experiments were used to account of data consistency. Sample sizes were determined as sufficient since they led to similar results. Sample size for single cell RNA-Seq was determined when the main cell lineages were captured.
Data exclusions	Due to intrinsic inhomogeneity of Geltrex, some Geltrex leaked into top or bottom channels after loading. Such experiments were excluded from data analysis. No similar platform has been previously reported, thus the criteria were established specifically for this platform.
Replication	Reported results were repeated and confirmed for at least two independent experiments. Key experimental findings were reliably reproduced by two investigators involved in this work.
Randomization	Samples were randomly allocated to different experimental groups. However, no particular randomization method was used in this work.
Blinding	Blinding is not applicable to data collection because the investigator is aware of sample and treatment allocations while setting up the experiments.

Reporting for specific materials, systems and methods

We require information from authors about some types of materials, experimental systems and methods used in many studies. Here, indicate whether each material, system or method listed is relevant to your study. If you are not sure if a list item applies to your research, read the appropriate section before selecting a response.

Materials & experimental systems

n/a	Involved in the study
☐	☒ Antibodies
☐	☒ Eukaryotic cell lines
☒	☐ Palaeontology and archaeology
☒	☐ Animals and other organisms
☒	☐ Human research participants
☒	☐ Clinical data
☒	☐ Dual use research of concern

Methods

n/a	Involved in the study
☒	☐ ChIP-seq
☒	☐ Flow cytometry
☒	☐ MRI-based neuroimaging

Antibodies

Antibodies used	SOX2 Stemgent 09-0024, CDX2 Biogenex MU392AUC, TBXT Thermo Fisher Scientific PA5-46984, OTX2 Proteintech 13497-1-AP, HOXB1 R&D Systems AF6318, HOXB4 DSHB I12 anti-Hoxb4, HOXC9 Abcam ab50839, ZO-1 Thermo Fisher Scientific 33-9100, ARL13B Rb Proteintech 17711-1-AP, pH3 Abcam ab183626, PAX6 Santa Cruz Biotech sc-81649, OCT4 Santa Cruz Biotech sc-5279, TBX6 Thermo Fisher Scientific AF4744-SP, SOX10 R&D Systems AF2864, PAX3 R&D Systems MAB2457, PAX7 DSHB PAX7, OLIG2 Abcam ab109186, NKX6-1 DSHB F55A12, FOXA2 R&D Systems AF2400, NKX2-2 DSHB 74.5A5, NKX2-1 Abcam ab133737, DLX5 Santa Cruz Biotech sc-398150, MAP2 Sigma Aldrich M1406-.2ML, TUJ1 BioLegend MRB-435P, SNAI2 Cell Signaling 9585, S100B Thermo Fisher Scientific MA1-25005, TWIST1 Cell Signaling 31174, PHOX2B Santa Cruz sc-376997, ISL1 DSHB 39.4D5, CTIP2 Abcam ab18465, TBR2 Abcam ab23345, TBR1 Abcam ab31940, SATB2 Abcam ab51502, MEIS2 Santa Cruz sc-81986, GSX2 Millipore-Sigma ABN162, ASCL1 Abcam ab211327, FOXG1 Abcam ab18259, REELIN MBL international Corporation D233-3, Donkey raised secondary antibodies Fisher

A10036, A21202, A21208, A10040, A21447.
The antibody information (including species, application, and catalog number) has been provided in Supplementary Table 4.

Validation

All the 13497-1-APantibodies have been validated by the companies from which they were offered. Details of the validation statements,
antibody profiles and relevant citations can be found on the manufacturer's website.
SOX2 (09-0024): https://www.reprocell.com/antibodies-and-staining-kits-c10/stemab-sox2-antibody-affinity-purified-rabbit-antimouse-human-p266
SOX2 (09-0024) antibody was validated by the manufacturer using mouse ES cells. More than 30 citation
CDX2 (MU392AUC,): http://store.biogenex.com/us/applications/ihc/controls/controls/anti-cdx-2-clone-cdx2-88.html
CDX2 (MU392AUC,) antibody was validated by the manufacturer using colonic epithelial cells. more than 30 citations.
TBXT (PA5-46984): https://www.thermofisher.com/antibody/product/Brachyury-Antibody-Polyclonal/PA5-46984
TBXT (PA5-46984) antibody was validated by the manufacturer using mouse notochord tissues and human mesoderm-like cells. More than 52 citations.
OTX2 (13497-1-AP): https://www.ptglab.com/products/OTX2-Antibody-13497-1-AP.htm
OTX2 antibody was validated by the manufacturer using mouse embryo, human gliomas, hESCs, and Y79 cells. 15 citations.
HOXB1 Antibody: https://www.rndsystems.com/products/human-hoxb1-antibody_af6318
HOXB1 antibody was validated by the manufacturer using NTera-2 Human Cell Line.
HOXB4 antibody: https://dshb.biology.uiowa.edu/I12-anti-Hoxb4
HOXB4 antibody was validated by the manufacturer using mouse embryos. 5 citations
HOXC9 antibody: https://www.abcam.com/hoxc9-antibody-hoxca6e6-ab50839.html
HOXC9 antibody was validated by the manufacturer using HT-1080 whole cell lysate and Hela cells. 11 citations
ZO-1 antibody: https://www.thermofisher.com/antibody/product/ZO-1-Antibody-clone-ZO1-1A12-Monoclonal/33-9100
ZO-1 antibody was validated by the manufacturer by Knockdown. 476 citations
ARL13B antibody: https://www.ptglab.com/products/ARL13B-Antibody-17711-1-AP.htm
ARL13B antibody was validated by the manufacturer using MDCK cells, NIH3T3 cells, hTERT-RPE1 cells, MEFS, etc. 469 citations
pH3 antibody: https://www.abcam.com/histone-h3-phospho-s10-antibody-ab183626.html
pH3 antibody was validated by the manufacturer using Hela cells, U2OS whole cell lysate, Human gastric carcinoma tissue, etc.
PAX6 antibody: https://www.scbt.com/p/pax-6-antibody-pax6
PAX6 antibody was validated by the manufacturer using transfected 293T whole cell lysates. 17 citations
OCT4 antibody: https://www.scbt.com/p/oct-3-4-antibody-c-10
OCT4 antibody was validated by the manufacturer using mouse embryos and human adrenal gland tissue. 57 citations
TBX6 antibody: https://www.rndsystems.com/products/human-tbx6-antibody_af4744
TBX6 antibody was validated by the manufacturer using human fibrosarcoma cell line, hiPSC derived mesoderm, and embryonic mouse mesoderm. 21 citations
SOX10 antibody: https://www.rndsystems.com/products/human-sox10-antibody_af2864
SOX10 antibody was validated by the manufacturer using human melanoma tissue, hESC derived neural crest, and SK-Mel-28 Human Cell Line. 92 citations.
PAX3 antibody: https://www.rndsystems.com/products/human-mouse-pax3-antibody-274212_mab2457
PAX3 antibody was validated by the manufacturer using B16-F1 mouse melanoma cell line. 20 citations.
PAX7 antibody: https://dshb.biology.uiowa.edu/PAX7
PAX7 antibody was validated by the manufacturer using chick embryos. 112 citations
OLIG2 antibody: https://www.abcam.com/olig2-antibody-epr2673-ab109186.html
OLIG2 antibody was validated by the manufacturer using Mouse cerebrum tissue, primary hippocampal rat neurons/glia, primary mouse neurons/glia. 118 citations
NKX6-1 antibody: https://dshb.biology.uiowa.edu/F55A12
NKX6-1 antibody was validated by the manufacturer using human pancreatic islet of Langerhans. 53 citations
FOXA2 antibody: https://www.rndsystems.com/products/human-hnf-3beta-foxa2-antibody_af2400
FOXA2 antibody was validated by the manufacturer using human liver cells, human hepatocellular carcinoma cell line, hESC derived endoderm cells. 95 citations
NKX2-2 antibody: https://dshb.biology.uiowa.edu/74-5A5
NKX2-2 antibody was validated by the manufacturer using chick embryo. 205 citations
NKX2-1 antibody: https://www.abcam.com/ttf1-antibody-epr59552-ab133737.html
NKX2-1 antibody was validated by the manufacturer using Human lung adenocarcinoma tissue, Human papillary carcinoma of thyroid gland tissue, human Thyroid gland tissue. 13 citations
DLX5 antibody: https://www.scbt.com/p/dlx-5-antibody-h-4
DLX5 antibody was validated by the manufacturer using HeLa cells. 2 citations
MAP2 antibody: https://www.sigmaaldrich.com/US/en/product/sigma/m1406
MAP2 antibody was validated by the manufacturer using rat brain enriched microtubule protein preparation or rat cerebral cortex extract. 250 citations
TUJ1 antibody: https://www.biolegend.com/en-us/products/purified-anti-tubulin-beta-3-tubb3-antibody-11580?Clone=TUJ1
TUJ1 antibody was validated by the manufacturer using human brain tissue, rat brain tissue, SH-SY5Y neuroblastoma cells. 543 citations
SNAI2 antibody: https://www.cellsignal.com/products/primary-antibodies/slug-c19g7-rabbit-mab/9585
SNAI2 antibody was validated by the manufacturer using A204, SKMEL5, NIH/3T3 cells, A204 cells. 505 citations.
S100B antibody: https://www.thermofisher.com/antibody/product/S100B-Antibody-clone-SH-B4-Monoclonal/MA1-25005
S100B antibody was validated by 6 citations.
TWIST1 antibody: https://www.cellsignal.com/products/primary-antibodies/twist1-e7e2g-rabbit-mab-if-formulated/31174?site-search-type=Products&N=4294956287&Ntt=31174&fromPage=plp&_requestid=4734247
TWIST1 antibody was validated by the manufacturer using mouse embryos. 1 citation
PHOX2B antibody: https://www.scbt.com/p/phox2b-antibody-b-11
PHOX2B antibody was validated by 29 citations.
ISL1 antibody: https://dshb.biology.uiowa.edu/39-4D5
ISL1 antibody was validated by 62 citations.
CTIP2 antibody: https://www.abcam.com/products/primary-antibodies/ctip2-antibody-25b6-ab18465.html
CTIP2 antibody was validated by 718 citations.

TBR2 antibody: https://www.abcam.com/products/primary-antibodies/tbr2--eomes-antibody-ab23345.html
TBR2 antibody was validated by 474 citations.
TBR1 antibody: https://www.abcam.com/products/primary-antibodies/tbr1-antibody-ab31940.html
TBR1 antibody has been referenced in 425 publications.
SATB2 antibody: https://www.abcam.com/products/primary-antibodies/satb1--satb2-antibody-satba4b10-c-terminal-ab51502.html
SATB2 antibody has been referenced in 269 publications.
MEIS2 antibody: https://www.scbt.com/p/meis2-antibody-63-t
MEIS2 antibody has been referenced in 11 publications.
GSX2 antibody: https://www.emdmillipore.com/US/en/product/Anti-Gsh2-Antibody,MM_NF-ABN162
GSX2 antibody has been referenced in 26 publications.
ASCL1 antibody: https://www.abcam.com/products/primary-antibodies/mash1achaete-scute-homolog-1-antibody-epr19840-ab211327.html
ASCL1 antibody has been referenced in 17 publications.
FOXG1 antibody: https://www.abcam.com/products/primary-antibodies/foxg1-antibody-ab18259.html
FOXG1 antibody has been referenced in 126 publications.
REELIN antibody: https://www.mblintl.com/products/d223-3/
REELIN antibody has been referenced in 12 publications.

Eukaryotic cell lines

Policy information about cell lines

Cell line source(s)	H1 hESC (WA01, WiCell; NIH registration number: 0043), H9 hESC (WA09, WiCell; NIH registration number: 0062), WIBR3 hESC (NIH registration number: 0079), a BRACHYURY-mNeonGreen H9 hESC reporter line, a CDX2-knockout H9 hESC line, a TBXT-knockout WIBR3 hESC line, a TBXT::T2A-Cre lineage tracer H9 hESC line, and 1196a line (human induced pluripotent stem cell)
Authentication	All hPSC lines have been authenticated by original sources as well as in-house by immunostaining for pluripotency markers and successful differentiation to the three definitive germ layers
Mycoplasma contamination	All hPSC lines are tested negative for mycoplasma contamination
Commonly misidentified lines (See ICLAC register)	No commonly misidentified lines listed by ICLAC were used in this work.